AUS MRinRT 2022 Program & Abstract Booklet

Gold Sponsors

Silver Sponsors

Bronze Sponsors

Day 1: Wednesday the 7th of December

Education Session	
Session Chairs: Kate Skehan and Shivani Kumar	
9:00 – 1:00pm	
9-10:00am	Dr Richard Speight (NHS) Talk – Title TBA
10-10:15am	Q&A with Dr Richard Speight
10:15-10:30am	Laura O'Connor: Magnetic Resonance Imaging to Cone Beam Computed Tomo
10:30-10:45am	Kate Skehan: Implementation of a dedicated MRI protocol for RT planning
10:45-11:15am	**Morning Tea**
11:15-12:15pm	Dr Donald McRobbie: MRI safety first and safety second
12:15-12:30pm	Q&A with Dr Donald McRobbie
12:30-12:45pm	Min Ku: Development of a Professional Certification for Radiation Therapists Undertaking MRI
12:45-1:00pm	Shivani Kumar: Implementation of workflows for the Australian MRI Linac
1:00-2:00pm	**Lunch**

Session 1: Solving Clinical Problems	
Session Chairs: Farshad Faroudi and Sirisha Tadimalla	
2:00 – 3:00pm	
2:00-2:15pm	Leah McDermott: Plan Adaption Sanity Check for MR-Linac Adapted Treatment
2:15-2:30pm	Madiha Tai: The use of Electron Contamination Deflector
2:30-2:45pm	Elizabeth Patterson: Electron Streaming Dosimetry on the Elekta Unity MR-Linac
2:45-3:00pm	Sarah Elliott: Assessment and Shielding of Electron streams for APBI on Unity
3:00-3:15pm	Julie Burbery & Crispen Chamunyonga: Keeping Abreast of MR Technology: Developing educational opportunities
3:15-3:30pm	David Crawford: Dose Escalated Stereotactic Ablative Radiotherapy of Pancreas
3:30-4:00pm	**Afternoon Tea**

Session 2: Building Better Systems	
Session Chairs: Stuart Crozier and Laura O'Connor	
4:00 – 6:00pm	
4:00-4:15pm	David Waddington: Advanced Reconstruction with Deep Learning for ultralow field MRI
4:15-4:30pm	Esther Wong: Extended FOV Imaging on the Australian MRI Linac
4:30-4:45pm	Shanshan Shan: Motion-Corrected Image Reconstruction using and unrolling network
4:45-5:00pm	James Grover: Super-Resolution Imaging on the Australian MRI-Linac
5:00-5:15pm	Paul Liu: In Silico Demonstration of MR-Guided Multi-leaf Collimator Tracking
5:15-5:30pm	James Korte: Magnetic Resonance Biomarker Assessment Software
5:30-5:45pm	Mingyan Li: Initial imaging results using the 8-element torso coil array for the Australian MRI Linac system
5:45-6:00pm	Paul Keall: Towards MRI-Guided Proton Therapy: The ultimate Cancer Treatment
END OF CONFERENCE PROCEEDINGS FOR DAY 1	

ACPSEM CPD Endorsed Activity

ASMIRT CPD APPROVED

Day 2: Thursday the 8th of December

Session 3: International Speaker Presentations	
Session Chairs: Paul Keall and Sarah Elliott	
9:00 – 11:00am	
9:00-9:45am	Dr. Percy Lee: MRI-Guided Radiotherapy: A New Standard of Care?
9:45-10:00am	Q&A
10:00-10:45am	Dr. Neelam Tyagi: Pancreas stereotactic ablative RT on a 1.5 Tesla MRI-linac system
10:45-11:00am	Q&A
11:00-11:30am	**Morning Tea**

Session 4: Adapting to Change and Managing Motion	
Session Chairs: Peter Metcalfe and Urszula Jelen	
11:30 – 1:30pm	
11:30-11:45am	Paul Keall: ICRU Report on MRI-Guided Radiation Therapy using MRI-Linacs
11:45-12:00pm	Yu Feng Wang: Quantitative imaging biomarkers: reliable detection of treatment-related changes from measurement uncertainty
12:00-12:15pm	Maxwell Eastwood: Comparison of Adaptive and Non-Adaptive Radiation Therapy plans using deformable
12:15-12:30pm	Maddison Picton: Adaptive MR Guided Radiotherapy for Head & Neck Cancer
12:30-12:45pm	Parmoun Daghigh: Assessing Real-Time Liver Motion Monitoring on the Elekta Unity MR-Linac
12:45-1:00pm	Reza Alinaghizadeh: Motion Evaluation for the Abdomen Imaging on Elekta MR-Linac
1:00-1:15pm	Sirisha Tadimalla: Personalised liver Stereotactic body RT using MRI
1:15-1:30pm	Felicity Height: Initial Experience with Daily ART for APBI on unity
1:30-2:30pm	**Lunch**
1:45-2:30pm	ACPSEM MRI-Linac Working Group Meeting (in the conference room)

Session 5: Better and Faster Images	
Session Chairs: Brad Oborn and Yu Feng Wang	
2:30 – 4:45pm	
2:30-3:00pm	Marco Mueller: Clinical Applications of APTW CEST Imaging in Brain Cancer
3:00-3:15pm	Philip Martin: Repeatability of Quantitative MRI Radiomic in Glioblastoma
3:15-3:30pm	Dominique Mathieu: Inter-Fraction T2/Flair Variation During MRI-Guided Radiotherapy
3:30-4:00pm	**Afternoon Tea**
4:00-4:15pm	Sweet Ping Ng: Automatic Segmentation of Salivary Glands and Skeletal Muscles
4:15-4:30pm	Stephen Gibson: Seeing the Beam: First-Time Imaging of the B0 Variation
4:30-4:45pm	Elia Lombardo – Offline and Online LSTM Networks for Respiratory Motion Prediction at MR-Linacs
END OF NORMAL CONFERENCE PROCEEDINGS FOR DAY 2	

6:30pm: Conference Dinner (Hawaiian Shirt Themed)

ACPSEM CPD Endorsed Activity

ASMIRT CPD APPROVED

Day 3: Friday the 9th of December

Session 6: Dosing Up	
Session Chairs: David Waddington and Leah McDermott	
9:00 – 10:15am	
9:00-9:15am	Amrinder Chhabra: Beam Matching for Two 1.5T MR Linacs
9:15-9:30am	Alex Burton: The Current Status of MR-Linac Dosimetry Audits: An Update from the ACDS
9:30-9:45am	Brendan Whelan: Open Source Toolkit for Quantification, Reporting and Correction
9:45-10:00am	Sweet Ping Ng: Early Experience of MR-Guided Radiotherapy for Brain, Head
10:00-10:15am	Tamara Barry: New Kids on the Block: Winning and Learning - the PAH MRI Sim Service
10:15-10:45am	**Morning Tea**

Session 7: No CT Required	
Session Chairs: Peter Greer	
10:45 – 12:20pm	
10:45-11:00am	Yosef Al-Abasse: Prostate Cancer Treatment: Validation of air coils and synthetic CT images
11:00-11:15am	Jonathan Goodwin: Susceptibility based detection of gold seed fiducial markers
11:15-11:30am	Hilda Chourak: MRI-Only Radiation Therapy for Prostate Cancer:
11:30-11:45am	Peter Greer: The NINJA MRI-Only Implementation Substudy-Preliminary results
11:45-12:00pm	Laura O'Connor: Comparison of Popular SCT Generation methods for MRI
12:00-12:15pm	Urszula Jelen: Towards Simulation-Free MR-Linac Treatment Planning
12:15-12:20pm	Conference close
12:30-1:30pm	**Lunch**
END OF CONFERENCE PROCEEDINGS FOR DAY 3	

1:30-2:30pm	TROG Special Interest Group Meeting (In the conference room)

ACPSEM CPD Endorsed Activity

ASMIRT CPD APPROVED

MAGNETIC RESONANCE IMAGING TO CONE BEAM COMPUTED TOMOGRAPHY TREATMENT VERIFICATION FOR PELVIC MALIGNANCIES

Laura M O'Connor[1,2] , Alesha Quinn[1], Samuel Denley[1], Lucy Leigh[3], Jarad Martin[1], Jason A Dowling[4], Kate Skehan[1], Helen Warren-Forward[2], Peter B Greer[1,5]

[1] Department of Radiation Oncology, Calvary Mater Hospital, Edith Street, Waratah, Newcastle, NSW, Australia, 2298
[2] School of Health Sciences, University of Newcastle, University Drive, Newcastle NSW, Australia, 2308
[3] Hunter Medical Research Institute, Lot 1 Kookaburra Ct, New Lambton Heights NSW, 2305
[4] Australian E-Health Research Centre, Commonwealth Scientific and Industrial Research Organisation (CSIRO), Bowen Bridge Rd, Herston, QLD, Australia, 4029
[5] School of Information and Physical Sciences, University of Newcastle, University Drive, Newcastle, NSW, Australia, 2308

Introduction: Magnetic Resonance Imaging (MRI)-only treatment planning supersedes the conventional use of a simulation computed tomography (CT) scan for treatment planning. In the radiation therapy workflow, the treatment planning data set is also utilised for daily online image guidance. Therefore, in the absence of a planning CT scan in MRI-only workflows, image guidance solutions also need to be evaluated. The treatment planning and delivery systems are designed so that current departmental procedure uses the sCT as a reference image for image guidance on treatment. However, given the sCT is not a true anatomical image, but a synthetically generated density map for dose calculation, it should ideally not be used for image guidance. As current practice is to use CT to CBCT as image guidance, it should be determined if the substitution of MRI to CBCT for image guidance affects the accuracy of the image matching, due to the different tissue contrasts. Previous work in this area for prostate matching identified that a training package reduces the inter-user variability in MRI-CBCT matching, to align with the variability of CT-CBCT matching values[1].

This study aimed to implement an MRI treatment image guidance training package and to assess the viability of MRI to Cone Beam Computed Tomography (CBCT) based image guidance for MRI-only planning treatment workflows for a variety of pelvic treatment sites.

Materials and Methods: Planning CT and MRI were acquired in the treatment position, utilizing positioning tattoos and patient specific ancillary equipment for similar alignment of patients between the scanning modalities. An MRI image matching training package was developed by MRI radiation therapists. Ten radiation therapists, with a range of clinical experience and MRI experience, underwent the training package prior to matching assessment. The matching assessment was performed on four match regions: prostate gold seed, prostate soft tissue, rectum/anal canal and gynaecological. Each match region comprised of three CBCT matches per patient and five patients per region. The ten radiation therapists performed the CBCT image matching to CT and to MRI for all regions and recorded the match values.

Linear fixed effects modes were utilised to estimate the mean shifts (and standard error) for CT-CBCT and MRI-CBCT respectively for each area. These were adjusted for radiation therapist and MRI experience. The inter-observer errors (IOE) were also calculated (as the standard deviation of the 10 radiation therapist measures) per image, for each direction of measurement, for CT-CBCT and MRI-CBCT respectively .

Results: As shown in figure 1, the median inter-observer error for MRI-CBCT matching and CT-CBCT matching for all regions were within 2mm and 1 degree. There was no statistically significant association in inter-user variation in mean match values for radiation therapist experience levels. There was no statistically significant association in inter-user variation in mean match values for MRI experience levels for prostate soft tissue a gynaecological match regions, while there was a statistically significant difference for prostate gold seed and rectum match regions.

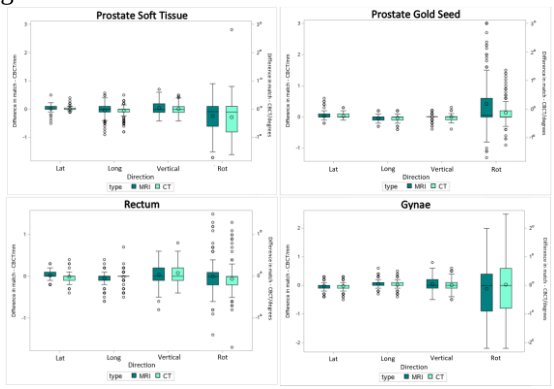

Figure 1. Box and Whisker plot comparison of MRI-CBCT and CT-CBCT match values for prostate soft tissue, prostate gold-seed, rectum and gynaecological matching sites (lateral, long and vertical (mm), rotation (º))

Conclusions: The results of this study support the concept on MRI to CBCT image guidance in a MRI-only planning workflow.

References:

1. Are cone beam CT image matching skills transferrable from planning CT to planning MRI for MR-only prostate radiotherapy? (R.L. Brooks et al.), *Br J Radiol*. **94** (1123), 20210146.

AUS MRinRT

Implementation of a dedicated MRI protocol for RT planning

Kate Skehan[1], Matthew Richardson[1], Samuel Dickson[1], Kate Martin[1], Geetha Govindarajulu[1], Swetha Sridharan[1]
[1] Calvary Mater Hospital Newcastle, kate.skehan@calvarymater.org.au

Introduction: The utilisation of dedicated MRI simulators is of high importance for RT departments. The recently published scientific reports by AAPM [1] and IPEM [2] setting out recommedations for clinical implementation of MR-Sim have further highlighted the importance of RT-specific scan protocols.

One area identified which would benefit from a dedicated MRI-Sim protocol was in gynacological cancers. Accurate anatomical identification is critical in this cohort to ensure the target is not under-treated and to limit the dose to surrounding normal tissues.[3-5]. Our departmental clinical practice was for gynaecological patients to receive two CT scans at simulation; one full bladder and one empty bladder scan with tampon in-situ. This was complimented with a full and empty bladder T2-weighted MRI scan. Diagnostic MRI exams historically have generated vaginal opacification methods to distend and delineate the vagina. This is not recommended for gynaecological RT planning as a distended vaginal volume cannot accurately be reproduced for daily treatment.

Fusion of planning CT and MRI scans led us to ponder if tampons do not reveal the true shape and extent of the anatomy [4]. We theorised a method to improve visualisation of the true extent of the vaginal vault, without deforming the natural anatomy using MRI simulation for RT planning.

Materials and Methods: We modified the diagnostic opacification technique for use in MRI simulation with the alternate goal of delineation and visualisation; without distension. The standard diagnostic 60cc of ultrasound gel, considered the correct amount for distension, was then tested in varying lesser amounts. Aquasonic 100® ultrasound transmission gel was warmed to 36°C and delivered vaginally on the MRI couch by a Radiation Oncologist using a sterile 50ml catheter tip syringe pre imaging. During testing both CT + tampon and MRI + vaginal gel simulation scans were acquired for comparative qualitative imaging.

Results: After trialling varying volumes of ultrasound gel, 10-15cc was found to be optimal for most patients. We observed with this amount of gel the superior aspect of the vaginal vault and cervix is well visualised on T2 imaging, whilst tending not to unfold the natural fornices of the collapsed vagina (Fig. 1).

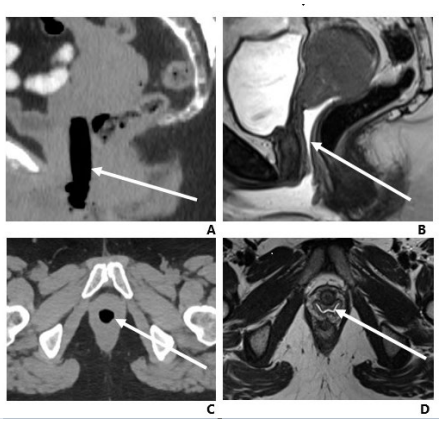

Figure 1 A 38 year old female with cervical squamous cell carcinoma. (**A)** Sagittal CT reconstruction with tampon in-situ. (**B)** Sagittal T2-weighted image with vaginal gel in-situ. (**C)** Axial CT with tampon in-situ. (**D**) Axial T2-weighted image with vaginal gel in-situ.

Conclusions: The adaption of this diagnostic technique has facilitated more accurate contouring of the natural vaginal anatomy in gynaecological cancers. We feel this is an example of the direct clinical benefits of effective communication, collaboration and expertise sharing across specialities. Close partnerships between the MR and Radiation Oncology communities is critical for utilisation, growth and improved outcomes[6].

References:

1. Glide-Hurst, C., et al., *Task Group 284 report: Magnetic resonance imaging simulation in radiotherapy: considerations for clinical implementation, optimization, and quality assurance.* Med Phys. **48**. 10.1002/mp.14695.
2. Speight, R., et al., *IPEM topical report: guidance on the use of MRI for external beam radiotherapy treatment planning.* Phys. Med, Biol, 2021 *Phys.***66** 055025
3. Eminowicz, G. and M. McCormack, *Variability of clinical target volume delineation for definitive radiotherapy in cervix cancer.* Radiother Oncol, 2015. **117**(3): p. 542-7.
4. Wu, D.H., et al., *Interobserver variation in cervical cancer tumor delineation for image-based radiotherapy planning among and within different specialties.* J Appl Clin Med PhysJournal of 2005. **6**(4): p. 106-110.
5. Lim, K., et al., *Consensus Guidelines for Delineation of Clinical Target Volume for Intensity-Modulated Pelvic Radiotherapy for the Definitive Treatment of Cervix Cancer.* Int J Radiat Oncol, 2011. **79**(2): p. 348-355.
6. Chandarana H, Wang H, Tijssen RHN, Das IJ. *Emerging role of MRI in radiation therapy.* J Magn Reson Imaging. 2018;48(6):1468-1478

AUS MRinRT

DEVELOPMENT OF A PROFESSIONAL CERTIFICATION FOR RADIATION THERAPISTS UNDERTAKING MRI

Min Ku[1], Tanya Morgan[1]

[1] Australian Society of Medical Imaging and Radiation Therapy, min.ku@asmirt.org

Introduction: The Australian Society of Medical Imaging and Radiation Therapy (ASMIRT) is the peak body representing medical radiation practitioners in Australia. Currently ASMIRT offers a broad range of certification options and are looking to increase this suite to include Magnetic Resonance (MR) certification for radiation therapists. The current certifications consist of a theoretical examination and completion of clinical examinations and provides a nationally recognised benchmark for professional practice. This presentation details the development of a professional certification from inception to implementation.

Materials and Methods: The first MRI linear accelerator (MR Linac) was installed in Australia in 2019.[1] With the progression of technology and the ability to facilitate online MR-guided adaptive radiotherapy, the need for further education for radiation therapists in MRI was critical. Furthermore, radiation therapists undertaking MRI are required to meet the regulatory authorities' Professional capabilities for medical radiation practice Domain 1: Key Capabilities 8 & 9.[2]

In June 2020, the Queensland University of Technology (QUT) commenced an on-line short course in MRI for radiation therapists.[3,4] As an extension of this program, a collaboration between QUT and ASMIRT was created to develop a novel certification to enhance the MR knowledge and skills of radiation therapists.

ASMIRT committee and reference group members, comprising MR experts and educationalists, were tasked with the development of a certification syllabus that would reflect the professional skillset of a radiation therapist performing MR imaging. The collaboration determined a consensus of syllabus content, and the subsequent development of the certification examination questions was undertaken in partnership with QUT.

The next step was to deliver a pilot examination for radiation therapist practitioners of varying clinical experience, from those a few years post undergraduate university graduation, and those that had undertaken vendor and other MRI knowledge-based training.

Organisations that currently undertake MR Simulation and MR Linac treatments were approached to advise of the pilot, and to seek volunteers to participate.

Results: A total of three organisations agreed to participate in the pilot to be held in November 2022. Participants were provided with the syllabus and information regarding the online examination process three months prior to the examination.

Surveys will be distributed post pilot certification examination.

Conclusions: The development of this novel certification will provide practitioners and employers with direction for study and educational programs. It presents a benchmark of industry-standard skill, and formal professional recognition of the ability for the MR radiation therapist.

Acknowledgements: The authors wish to thank the volunteers who participated in the pilot, ASMIRT committee and reference group members, QUT and the ASMIRT Board of Directors.

References:

1. Tan H. The past and future of adaptive radiation therapy. The Medical Republic [Internet]. The Medical Republic. 2021 [cited 2022 Oct 6]. Available from: https://medicalrepublic.com.au/the-past-and-future-of-adaptive-radiation-therapy/58734

2. Medical Radiation Practice Board of Australia (2020). MRPBA Professional capabilities for medical radiation practice https://www.medicalradiationpracticeboard.gov.au/Registration-Standards/Professional-Capabilities.aspx

3. Pollard, N, 2020, June 11. The Radiation Therapy discipline at QUT are launching an 'MRI for Radiation Therapists' course. It is fully online, designed & developed by MRI specialists. https://twitter.com/nataliepollar16/status/1270958405344038912

4. McMahon, K. (2021). Real-world expertise Spectrum Vol 28. No 1. March 2021

AUS MRinRT

IMPLEMENTATION OF WORKFLOWS FOR AUSTRALIAN MR LINAC – RADIATION THERAPY PERSPECTIVE

Shivani Kumar[1,2], Jarrad Begg[2,3], Bin Dong[1], Esther Wong[1], Doaa Elwadia[3,4], Andrew Wallis[3], Daniele Miller[3], Justin Spicer[3], Gary Liney[1], Paul Liu[5], Paul Keall[5], Trang Pham[1,2,3]

[1] Ingham Institute for Applied Medical Research, Sydney, Shivani.kumar@unsw.edu.au
[2] School of Clinical Medicine, South West Sydney Clinical School, University of New South Wales, Sydney
[3] Department of Radiation Oncology, Liverpool Hospital, Sydney [4]
[4] Discipline of Medical Imaging Science, Faculty of Medicine and Health, The University of Sydney, Sydney
[5] Image X Institute, School of Health Sciences, University of Sydney, Sydney

Introduction: MR guided radiotherapy provides opportunities to benefit patients through advanced imaging. However successful implementation of MRI in RT requires workflow modifications, comprehensive training and collaboration across departments.[1-3] The volume of information and planning can be challenging. Current workflows for the two commercially available system require considerations regarding appropriate patient selection, treatment planning, immobilization and plan adaption criteria. While there is vendor support for training and commissioning there is a steep earning curve to implement and successfully execute MR guided radiotherapy (MRgRT). For the Australian MR Linac (Aus MRL) this process is even more complex and challenging. This work will focus on describing the radiation therapist perspective of clinical development and implementation of MRgRT workflow for the Aus MRL.

Methods: The learning curve for the Aus MRL has different complexities and challenges as we move towards patient treatment. The Aus MRL[4] is a split bore inline configuration with 1 tesla magnet and 6MV beam. The bespoke nature of the machines meant we've had to develop the system including tabletop design, immobilisation, imaging workflows and treatment verification and records. The radiation therapy team provided input in the design, working in close collaboration with the medical physicist, MRI physicists, MRI radiographers, imaging scientists and engineer and radiation oncologist.

Results:
MR safety training and risk assessment was prioritised as the first task to be developed and completed by all staff involved in the project. This training was done as an extension to existing MRI simulator safety training at Liverpool Cancer Therapy Centre. The patient workflow from simulation to treatment was developed and tested taking into consideration the Aus MRL requirements. Workflows such as simulation procedure had to be developed to accommodate for the couch top design and bore size limitations. MRI sequences were optimised for the purposes of radiotherapy target visualisation, matching, and real-time monitoring. Soft tissue image matching and verification workflow was developed. To ensure competency and confidence with the proposed workflows, end to end workflow was simulated including introduction of known errors that may have an impact on the accuracy of treatment delivery. This allowed the team to develop familiarisation with the process and identify process improvement following each end-to-end session.

Conclusion: While the development and implementation of the radiation therapy workflow for Aus MRL was challenging, this process has allowed radiation therapists to gain an in depth understanding of MRgRT. This knowledge and hands on experience of developing a tailored workflow would not have been feasible on a commercial MRgRT system implementation. Having radiation therapist involved in the design process also provided valuable knowledge from patient perspective that can be overlooked in a technical setting.

References:

1. Corradini, S., Alongi, F., Andratschke, N., Azria, D., Bohoudi, O., Boldrini, L., ... & Belka, C. (2021). ESTRO-ACROP recommendations on the clinical implementation of hybrid MR-linac systems in radiation oncology. Radiotherapy and Oncology, 159, 146-154.
2. Snyder, J. E., St-Aubin, J., Yaddanapudi, S., Boczkowski, A., Dunkerley, D. A., Graves, S. A., & Hyer, D. E. (2020). Commissioning of a 1.5 T Elekta Unity MR-linac: a single institution experience. Journal of Applied Clinical Medical Physics, 21(7), 160-172.
3. Kashani, R., Victoria, J. R., Yang, D., Zhao, T., Green, O. L., Rodriguez, V. L., ... & Olsen, J. R. (2015). Commissioning and Clinical Implementation of the First Online Adaptive MR Image Guided Radiation Therapy Program. International Journal of Radiation Oncology, Biology, Physics, 93(3), S18-S19.
4. Keall, P. J., Barton, M., & Crozier, S. (2014, July). The Australian magnetic resonance imaging–linac program. In Seminars in radiation oncology (Vol. 24, No. 3, pp. 203-206). WB Saunders.

AUS MRinRT

PLAN ADAPTION SANITY CHECK FOR MR-LINAC ADAPTED TREATMENT

Leah McDermott[1], Rob Behan[1], Reza Alinaghi Zadeh[1], Sandie Fisher [1]

[1] ONJ Centre Austin Health Heidelberg Melbourne, leah.mcdermott@austin.org.au

Introduction: The MR Linac introduces daily adapted MR-based treatment planning into the clinic. This requires a novel and complex workflow with associated training/skills development and quality assurance challenges. This work describes an integrated software tool that provides a plan adaption sanity check (PASC) of treatment parameters for the MR Linac (Unity 1.5T, Elekta, Crawley UK). The tool records QA and other treatment information in a single database for all patients. The aim was to create a well organised and automated data registry for patient treatment verification, trend analysis, clinical trial data collection and treatment efficiency and consistency.

Material and Methods: The tool was developed using a Python script (Python v3.8; IDE Spyder v4.1.5). It combines data directly read from MOSAIQ v2.83 (Elekta, Crawley UK) and the treatment planning system (TPS) Monaco v5.51 (Elekta, Crawley UK). Following extensive testing, data from 38 patients was recorded from August 2021 to October 2022. At the outset of the clinical workflow of each fraction, the patient is opened in PASC and previous fraction data is available to review or a new fraction is created. The user enters single-click time-stamp data at specific time points during treatment from patient entry to exit. Comments about the patient's position, image fusion and plan adaption are entered, as well as the patient's music preferences. Once the treatment plan has been approved and sent to MOSAIQ, the beam data for 1) reference plan, 2) adapted plan and 3) delivery plan (MOSAIQ) are loaded into PASC. Per field treatment plan parameters (monitor units, segments and gantry angles) are compared between all beam data sets, with values outside preset difference-ranges highlighted and flagged for review. All MR scan types and times acquired are listed, as well as plan rescaling and isocentre shifts, plotted for all fractions to date.

Results: Tests showed PASC can easily alert the treatment team to discrepancies exceeding pre-set limits between the reference and adapted beam data, and ensure the adapted and delivery plans are identical. Alerts are also raised for unexpected differences in isocentre shifts and MR details. During testing, simulated discrepancies were introduced to validate PASC automated checking process. Analysis of clinical trends in iso-shifts showed average posterior drop of 3.5mm over 30 fractions, but L-R and C-C directions were stable. This was due to a range of causes, including changes in patient weight, hair and cushion support over time. With the PASC tool, the efficiency for plan checks including data transfer and recording treatment information has been improved by 50% and manual entry errors have been minimised. Seemingly trivial recording of patient music preferences also has positive benefits for both staff and patients.

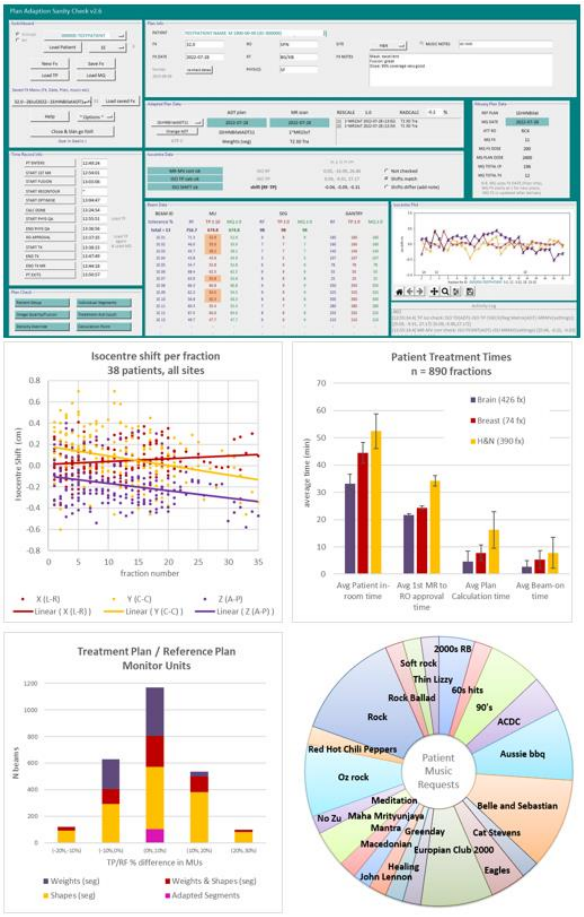

Figure 1. PASC interface and the types of treatment statistics available from the database

Conclusions: The PASC tool can be used to perform rapid and comprehensive validation of adapted plan delivery based on MR-guided treatment where time for QA is limited. The fast and structured recording of QA data and other plan information in a registry the department with a vast wealth of data for efficiency, dose and treatment optimisation.

AUS MRinRT

THE USE OF ELECTRON CONTAMINATION DEFLECTOR FOR REDUCING SKIN DOSE IN HIGH FIELD INLINE MRI-LINAC

Madiha Tai[1], Peter E. Metcalfe[1,2], Bradley M. Oborn[1]
[1] Centre for Medical Radiation Physics, University of Wollongong, Wollongong, NSW, mt660@uowmail.edu.au
[2] Ingham Institute for Applied Medical Research, Liverpool, NSW

Introduction: Studies have suggested the use of inline magnetic field for favourable dosimetry in Mr-Linac [1] [2] [3]. However, in the presence of the inline magnetic field, electron contamination is concentrated and more focused within the beam which increases the overall skin dose [4] [5] [6]. In this work, we aim to model the skin dose for Australian MRI-Linac system and investigate the efficiency of electron contamination deflector (ECD) coupled with helium bag for reducing the skin dose.

Materials and Methods: The 3D magnetic field model of 1T MRI-Linac was designed in COMSOL. The magnetic field maps were then imported to Geant4 Monte Carlo geometry which included Linatron (6MV), Multi Leaf Collimators (MLCs) and a 30cm x 30cm x 30cm water phantom. Simulations were performed with source to surface distance of 2469mm for field sizes 1cm x 1cm, 3cm x 3cm and 5cm x 5cm. Central axis percentage depth dose and surface skin dose were measured at 70µm depth by using high resolution scoring voxels of 10µm. Simulations were also performed with ECD and then with ECD coupled with helium bag for each field sizes with their corresponding magnetic field map.

Results: As shown in Figure 1, Figure 2 and Figure 3, the highly focused electron contamination produced by x-ray beam in MRI-Linatron increases the skin dose up to 133% for the field size 1cm x 1cm, 196% for 3cm x 3cm and 264% for 5cm x 5cm. By using the combination of ECD and helium bag, skin dose can be reduced to 54% for field size 1cm x 1cm, 73% for 3cm x 3cm and 96% for 5cm x 5cm. Initial data shows promising results in reducing the skin dose by 59% for 1cm x 1cm, 62% for 3cm x 3cm and 63% for 5cm x 5cm field size.

Conclusion: Modelling results indicate the use of electron contamination deflector along with a helium bag would produce promising results in reducing the surface skin dose.

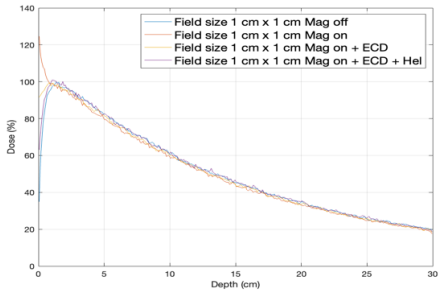

Figure 1. Percentage depth dose for field size 1cm x 1cm.

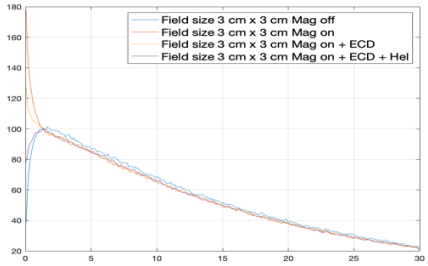

Figure 2. Percentage depth dose for field size 3cm x 3cm.

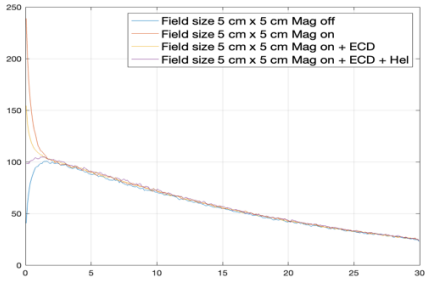

Figure 3. Percentage depth dose for field size 5cm x 5cm.

References:

1. S A Naqvi, X A Li, S W Ramahi, J C Chu and S J Ye, "Reducing loss in lateral charged particle equilibrium due to air cavities present in x-ray irradiated media by using longitudinal magnetic fields," *Med. Phys.*, vol. 28, no. 4, p. 603 – 611, 2001
2. S W Ramahi, S A Naqvi and J Chu, "Achieving a smaller penumbra region for better planning in conformal radiotherapy by using a longitudinal magnetic field," in *Annual International Conference of the IEEE Engineering in Medicine and Biology 117 Society*, 2000.
3. Y Chen, A F. Bielajew, D. W. Litzenberg, J M Moran and F. D. Becchetti, "Magnetic confinement of electron and photon radiotherapy dose: A Monte Carlo simulation with a nonuniform longitudinal magnetic field.," *Med. Phys.*, vol. 32, no. 12, p. 3810 – 125 3818, 2005.
4. B. M. Oborn, S. Kolling, P. E. Metcalfe, S. Crozier, D. W. Litzenberg and P. J. Keall, "Electron contamination modeling and 154 reduction in a 1 T open bore inline MRI-linac system.," *Med. Phys.*, vol. 41, no. 5, pp. 051708-1 – 051708-15, 2014.
5. B. M. Oborn, P. E. Metcalfe, M. J. Butson, A. B. Rozenfeld and P. J. Keall, "Electron contamination modeling and skin dose in 6MV longitudinal field MRIgRT: impact of the MRI and MRI fringe field.," *Med. Phys.*, vol. 39, no. 2, p. 874 – 890, 2012.
6. M. Tai, E. Patterson, P. E. Metcalfe, A. B. Rosenfeld and B. M. Oborn, "Skin Dose Modeling and Measurement in a High Field In-line MRI-Linac System.," *Front. Phys.*, vol. 10, 2022.

AUS MRinRT

ELECTRON STREAMING DOSIMETRY ON THE ELEKTA UNITY MR-LINAC WITH MULTIPLE DOSIMETERS

E. Patterson[1,2], P. Metcalfe[1,3,4], J. Baines[5, 6], M. Powers[5,6]
ep958@uowmail.edu.au (presenting author)
[1] Centre of Medical and Radiation Physics, University of Wollongong, Wollongong, NSW, Australia
[2] GenesisCare, Sydney, New South Wales, Australia
[3] Illawarra Health Medical Research Institute, University of Wollongong, Wollongong, NSW, Australia
[4] Ingham Institute for Applied Medical Research, Liverpool, NSW, Australia
[5] Townsville Cancer Centre, Townsville Hospital and Health Service, Townsville, QLD, Australia
[6] College of Science and Engineering, James Cook University, Townsville, QLD, Australia

Introduction

For megavoltage (MV) photon radiation treatments in the presence of a transverse magnetic field, the Lorentz force influences secondary electron motion and can lead to out-of-field dose (OFD) away from the treatment area[1,2]. This phenomenon is known as electron streaming and is dependent on the field strength and direction of the external magnetic field (B_0) relative to the beam direction, treatment field size, and the electron's initial direction of motion[1]. Electron streams are generated from photon interactions in the air column, anterior imaging coil, and at sites where the beam either enters or exits a patient[2-5]. This work aims to quantify OFD resulting from electron streaming in an Elekta Unity magnetic resonance (MR)-linac using multiple dosimeters and the Monaco treatment planning system (TPS).

Method

A solid water slab of 5.0 cm thickness was centred at isocentre and aligned 45° to an incident beam of field size 10×10 cm^2 delivered from gantry 90.0º. Entrance and exit electron streaming doses were measured ±20.0 cm from the isocentre. Dose was measured on the surface of 5.0 cm thick solid water slabs arranged parallel to the beam direction. Electron streaming OFD was measured using a MO*Skin*™ detector, EBT3 film, nanoDot optically stimulated luminescence dosimeters (OSLD), and a PTW 60019 microDiamond. These dosimeters have previously been used for MR-linac dosimetry[5-8]. The MO*Skin*™, OSLD, and microDiamond were separately positioned at the centre of the projected electron streaming dose distribution, as determined using RTQA2 film. The experimental set-up was modelled in the TPS using a 0.1 cm grid spacing and 0.2 % statistical uncertainty per control point. TPS determined OFD was compared to experimental measurements. Reported film and TPS data correspond to the dose at the centre of the projected electron streaming dose distribution. All doses are reported as a percentage of the maximum deliverable dose, D_{max}, for a 10×10 cm^2 beam in a water phantom with a source surface distance (SSD) of 133.5 cm.

Results

Figure 1 shows the measured and TPS calculated electron streaming dose for a 10×10 cm^2 beam exiting an angled solid water slab. OFD of 39.5 %, 37.7 %, 28.8 %, 25.6 %, and 29.8 % was determined using the MO*Skin*™, film, OSLD, microDiamond, and Monaco TPS, respectively. MO*Skin*™ and film doses were 32.6 % and 26.5 % greater than the TPS, respectively. Streaming doses were sensitive to volume averaging between the different detectors and the TPS.

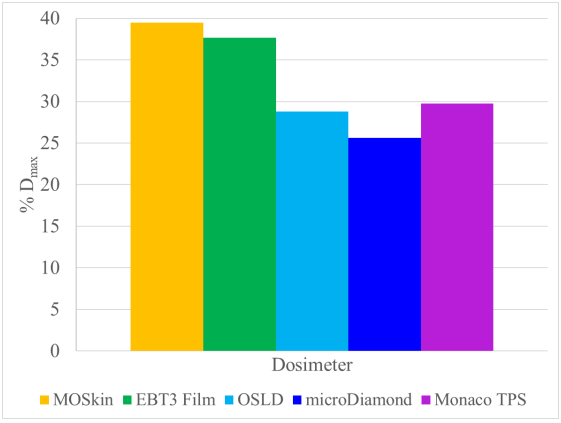

Figure 1. Measured and simulated exit electron streaming doses recorded 20 cm away from the isocentre.

Conclusion

For surface dosimetry, a thin sensitive volume positioned with an effective point of measurement (EPOM) near the surface, is ideal. For in-vivo dosimetry, volume averaging and the TPS dose grid spacing parameters, are important factors to consider to avoid underreporting electron streaming dose to a patient surface.

References:

1. J. M. Park et al.: Strahlenther. Onkol. 194, 50 (2018)
2. V. N. Malkov et al.: Phys. Med. Biol. 64, 115029 (2019)
3. V. N. Malkov et al.: Med. Phys. 46, 1467 (2019)
4. S. L. Hackett et al.: Phys. Med. Biol. 63, 095001. (2018)
5. M. Powers et al.: Front. Phys. 10, 293 (2022)
6. N. F. Roberts et al.: Med. Phys. 46, 5780 (2019)
7. A. Kim et al.: Phys. Med. Biol. 65, 045012. (2020)
8. S. J. Woodings et al.: Phys. Med. Biol. 63, 5 (2018)

AUS MRinRT

ASSESSMENT AND SHIELDING OF ELECTRON STREAMS FOR APBI ON UNITY

Sarah Elliott, Sandra Fisher, Felicity Height, Benjamin Harris, Michael Chao, Farshad Foroudi, Sweet Ping Ng

ONJCWRC, Department of Radiation Oncology, Austin Health, Heidelberg, Victoria, sarah.elliott@austin.org.au

Introduction: Electron streams may be generated during breast treatments on the MR linac (1,2,3) and result in out of field dose deposition. This work reports the management of bolus shields for our first accelerated partial breast irradiation (APBI) patients on Unity to reduce this unwanted dose to the arm, chin/nose and abdomen.

Materials and Methods: Patients with localised breast cancer meeting eligibility for APBI were enrolled on the prospective FIRM study.

Prior to each treatment, the electron streaming effect (ESE) was evauated in the reference plan using Monaco for Unity v5.51.11. To visualise the location and extent of the ESE, a box structure was created in Monaco to encompass the entire patient plus the surrounding air, extending to (but within) the anterior coil. This structure was assigned as the external contour for calculation purposes. The final approved plan was recalculated and display isodose levels were modified to clearly show the electron streams outside the patient contour, the patient's anatomy receiving dose as well as an estimate of the dose level. Monaco measurement tools were utilised to determine the exact placement of bolus pieces to shield the electron streaming dose to the patient, without perturbing the treatment fields.

Previous in-house phantom work had shown that 1cm thickness of bolus provided shielding of electron steams generated with an APBI plan. To confirm the correct placement and adequate shielding thickness of bolus on our patients, Gafchromic EBT3 film was placed on top of and underneath the bolus shields for one fraction for each patient. Film analysis was performed with RIT v6.7.64.

Results: Four patients were treated between April and August 2023, with a prescription dose of 30Gy in 5 fractions using step and shoot IMRT on Unity. Three patients had right-sided tumors and one patient a left-sided tumor. The number of beams in the treatment plans ranged from 6 and 15, the planning target volumes ranged from 123 to 290cc and the total monitor units in the adapt-to-position plans ranged from 918 to 1141.

	Measured dose (Gy)			
Patient number	**1**	**2**	**3**	**4**
Arm on bolus	3.5	1.0	7.5	4.6
Arm under bolus	<0.5	<0.5	<0.5	<1.0
Chin/nose on bolus	3.5	2.0	0.5	3.5
Chin/nose under bolus	<0.5	<0.5	<0.5	<1.0
Abdo on bolus	na	2.5	0.5	0.5
Abdo under bolus	na	<0.5	<0.5	<0.5

Figure 1. Maximum total dose from film measurements

Film measurements (in total dose) are tabulated in Figure 1 and show that bolus effectively reduces the dose from electron streams to the arm, chin, nose or abdomen to <1.0Gy per fraction for all patients.

Furthermore, film wrapping of the ipsilateral arm has shown well defined electron streams (Figure 2) and the arm may receive significant dose if not shielded. The Monaco beam model incorporates the magnetic field and appears to model out-of-field dose accurately (3) and reliably for determining appropriate placement of bolus on the patient (Figure 2).

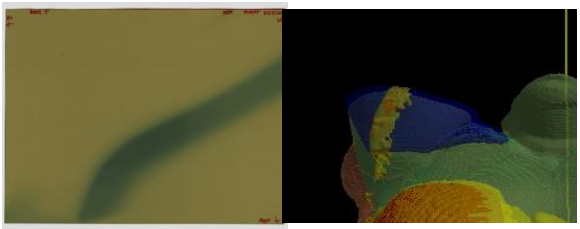

Figure 2. Electron stream captured on a piece of film wrapped around the ipsilateral arm (left) and Monaco 3D render with isodose display (right) for patient 3 (total dose isodose color brown 7Gy, yellow 3.8Gy).

The daily MR images show bolus shields and can provide verification of placement during patient set-up and treatment.

Conclusions: Assessment of ESE is required for APBI patients on Unity. The process outlined in this work ensures comprehensive evaluation of the out of field dose to the patient's anatomy using Monaco, which can guide bolus placement during treatment. Anatomy requiring shielding depends on the individual patients anatomical shape as well as the lateral/off axis distance, depth and volume of the tumor. Further work will explore these dependencies.

References:

1. Partial breast irradiation with the 1.5T MR-Linac: First patient treatment and analysis of electron return and stream effects (M. Nachbar et al.), *Radiotherapy and Oncology* **45**, 30-35 (2020).
2. Air-electron stream interactions during magnetic resonance IGRT (J. Park et al), *Strahlenther Onkol* **194,** 50-59 (2018)
3. Analysis of the electron-stream effect in patients treated with partial breast irradiation using the 1.5T MR-linear accelerator (C. De-Colle et al), *Clincal and Translational Radiaiton Oncology* **27,** 103-108 (2021)

AUS MRinRT

KEEPING ABREAST OF MR TECHNOLOGY; DEVELOPING EDUCATIONAL OPPORTUNITIES FOR CURRENT AND FUTURE RADIATION THERAPISTS

Julie Burbery[1,2] Julie.burbery@qut.edu.au , Crispen Chamunyonga[1,2] crispen.chamunyonga@qut.edu.au, Peta Rutledge[1], peta.rutledge@qut.edu.au

[1] School of Clinical Sciences, Radiation Therapy Discipline, Queensland University of Technology
[2] Centre for Biomedical Technologies, Queensland University of Technology, Brisbane, QLD, 4000, Australia,

Introduction: The utilisation of Magnetic Resonance (MR) technology in radiation therapy through dedicated MR simulation (MR-SIM) and MR-Linac technology is increasing. In Australia and New Zealand, five (5) MR- Linacs are already in clinical use. The greatest challenge highlighted in the literature is the training and education of Radiation Therapists (RTs) to ensure the safe and effective operation of MR technology.[1-3] This presentation discusses how the educational gap is being addressed by the Queensland University of Technology (QUT) in the undergraduate radiation therapy program and through the provision of continuing professional education (CPE) modules.

Methods: In 2019, professionals including Radiation therapists, Radiographers, Medical Physicists and a Radiologist were involved in the development of a comprehensive CPE program at QUT which commenced in June 2020.

Results: The successful implementation of the CPE program is providing an avenue for upskilling radiation therapy practitioners nationally and internationally. The program is currently offered through an online platform where RT practitioners undertake the didactic components. Under Phase 1, eight (8) modules were developed to address MR physics, safety, quality assurance (QA), imaging protocols, image interpretation, multi-modality image registration and the use of contrast in MR imaging and there is an opportunity to undertake a practical module at the Herston Imaging Research Facility (HIRF). Phase 2 modules will focus on MR Linac technology.

Developments in the undergraduate radiation therapy program include the incorporation of both didactic elements with practical consolidation. This is aimed at ensuring that graduates have ample opportunities to meet the needs of a changing clinical environment, practice standards and professional requirements. As such, alignment with the current MRPBA professional capabilities[4] which identify the knowledge, skills and attributes required by practitioners who use MR technology was a key consideration. The program is providing opportunities for RT students to develop knowledge which can be applied in many areas such as multi-modality image registration for planning, adaptive therapy and image-guided radiation therapy.

Conclusion: In the current era of technological advancements, the provision of educational opportunities for the current RT and future radiation therapy workforce in the use of MR technology is paramount. However, ongoing development is necessary, requiring collaborative initiatives and support from industry, clinical departments, vendors, MR experts and professional bodies.

Acknowledgements: The authors wish to thank the professionals who provided expertise in the development of the content for the QUT MRI for RT CPE program modules and the Herston Imaging Research Facility, Brisbane for support with the use of MR technology for practical sessions.

References:

1. Eccles CL, Campbell M. Keeping Up with the Hybrid Magnetic Resonance Linear Accelerators: How Do Radiation Therapists Stay Current in the Era of Hybrid Technologies? Journal of medical imaging and radiation sciences 2019;50 2:195-8.

2. Chin S, Eccles CL, McWilliam A, et al. Magnetic resonance-guided radiation therapy: A review. J Med Imaging Radiat Oncol 2020;64:163-77.

3. Glide-Hurst CK, Paulson ES, McGee K, et al. Task group 284 report: magnetic resonance imaging simulation in radiotherapy: considerations for clinical implementation, optimization, and quality assurance. Medical Physics 2021;48:e636-e70.

4. Professional Capabilities of Medical Radiation Practice. 2020. (Accessed 16 February 2020, at http://www.medicalradiationpracticeboard.gov.au/Registration/Professional-Capabilities.aspx.)

AUS MRinRT

DOSE ESCALATED STEREOTACTIC ABLATIVE RADIOTHERAPY OF PANCREAS ON MR-LINAC

D Crawford[1], V Batumalai[1,2], M Picton[1], C Pagulayan[1], C Tran[1], L Mckenzie[1], U Jelen[1], N Dunkerley[1], T Twentyman[1], M Jameson[1,2], J de Leon[1]

[1] GenesisCare, New South Wales, Australia
[2] School of Clinical Medicine, Faculty of Medicine and Health, UNSW Sydney, Australia

Introduction: Standard radiotherapy approaches delivering 40-60Gy in 1.8-2Gy per fraction add minimal to no survival benefit over chemotherapy alone for patients with unresectable locally advanced pancreatic cancer (LAPC) [1]. Ablative doses of greater than 100Gy biological-effective dose (BED_{10}) are likely needed to achieve local tumour control and improve overall survival (OS) [2], however often exceeding the tolerance of the surrounding normal tissues. Magnetic resonance-guided adaptive radiotherapy (MRgART) allow delivery of stereotactic ablative body radiotherapy (SABR) techniques more effectively with improved OS [3]. We present our early experience of dose escalated SABR of pancreas treated with MRgART on a 1.5T MR-Linac.

Materials and Methods: Ten patients with LAPC were treated with MRgART on the Unity MR-Linac (Elekta AB, Stockholm, Sweden) between December 2021 and August 2022. All patients were prescribed 5 fractions delivered on alternate days to a total dose of 50Gy (BED_{10} $100Gy_{10}$). The clinical target volume (CTV) was defined as gross tumour volume and paraaortic nodal regions covering coeliac axis to superior mesenteric artery, and was uniformly expanded by 3mm to create the planning target volume (PTV). A 3-5mm expansion of the organs at risks (OAR) was performed to create planning risk volumes (PRV). Any overlapping portion of the PTV by the PRVs was constrained to 33Gy to meet OAR constraints, and the remainder (PTV_{high}) was dose-escalated to 50Gy. For treatment, adapt-to-shape strategy was employed for each fraction where the daily MR image was recontoured to adapt to the anatomy of the day. Plan reoptimisation was performed to meet dose constraints or improve target coverage; priority was to ensure that OAR constraints were met over target coverage.

Results: The median age was 65 years (range: 50-80 years), and 6 patients were male. The CTV D_{99} coverage was ideal/acceptable in 88% of total fractions, while the PTV D_{99} coverage was ideal/acceptable in 72% fractions. Ablative dose was delivered to most target volumes as demonstrated by the median PTV_{high} D_{90} dose of 43.4 Gy (Table 1). Figure 1 illustrates an example of differences in CTV and PTV coverage for 3 adapted fractions due to interfraction OAR changes for one of the patient. The median time from patient setup to treatment delivery completion was 50 minutes (range, 29-67 minutes) for all patients.

Table 1: Target volume coverage for daily adaptive plan for all patients

Target	Daily adaptive plan	
	Median (Range)	Mean ± SD
CTV D_{99}	35.5 (26.3-50.0) Gy	35.6 ± 4.6 Gy
CTV Mean	51.5 (45.2-58.7) Gy	52.3 ± 2.8 Gy
PTV D_{99}	27.2 (15.6-37.4) Gy	26.8 ± 3.9 Gy
PTV Mean	48.5 (40.4-55.0) Gy	48.7 ± 3.2 Gy
PTV_{high} D_{90}	43.4 (31.6-49.8) Gy	43.2 ± 4.0 Gy
PTV_{high} Mean	51.1 (42.7-57.5) Gy	51.1 ± 2.9 Gy

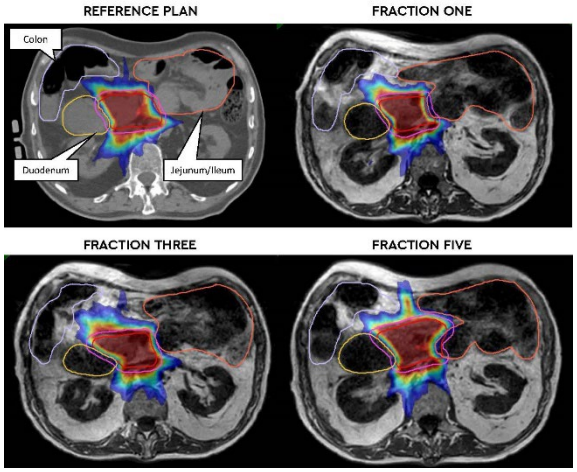

Figure 1: Differences in CTV (red) and PTV (pink) coverage between the reference plan and 3 adapted fractions due to interfraction organs at risk changes for one of the patient. Isodose is displayed from 25 to 50Gy (50-100%).

Conclusion: We have shown that dose escalated SABR treated with MRgART is dosimetrically feasible. The median treatment time of 50 minutes was well tolerated by all patients with no interruptions. Analysis of larger patient cohort with follow-up including toxicity and patient reported outcomes is planned.

References:

1. Hammel, P., et al. Effect of chemoradiotherapy vs chemotherapy on survival in patients with locally advanced pancreatic cancer controlled after 4 months of gemcitabine with or without erlotinib: the LAP07 randomized clinical trial. JAMA, 2016. 315(17): p. 1844-1853
2. Reyngold, M., P. Parikh, and C.H. Crane, Ablative radiation therapy for locally advanced pancreatic cancer: techniques and results. Radiat Oncol, 2019. 14(1): p.1-8
3. Hassanzadeh, C., et al., Ablative Five-Fraction Stereotactic Body Radiation Therapy for Inoperable Pancreatic Cancer Using Online MR-Guided Adaptation. Adv Radiat Oncol, 2021. 6(1): p. 100506

AUS MRinRT

ADVANCED RECONSTRUCTION WITH DEEP LEARNING FOR ULTRALOW FIELD MRI

David E. J. Waddington[1], Efrat Shimron[2], Shanshan Shan[1,3], Neha Koonjoo[4] and Matthew S. Rosen[4,5,6]
[1] Image X Institute, Faculty of Medicine and Health, The University of Sydney, AU, david.waddington@sydney.edu.au
[2] Department of Electrical Engineering and Computer Sciences, UC Berkeley, Berkeley, CA, USA
[3] School of Biomedical Engineering, Shanghai Jiao Tong University, Shanghai, China
[4] A. A. Martinos Center for Biomedical Imaging, Charlestown, MA, USA
[5] Harvard Medical School, 25 Shattuck St., Boston, MA, USA
[6] Department of Physics, Harvard University, Cambridge, MA, USA

Introduction: Portable MRI scanners that operate at very low magnetic fields are increasingly being deployed in clinical settings. However, the intrinsic low signal-to-noise ratio (SNR) of these low-field MRI scanners often necessitates many signal averages, and therefore, excessively long acquisition times. Advanced reconstruction strategies based on deep learning could dramatically shorten acquisition times in low-field MRI when combined with undersampling. Here, we compare leading data-driven[1] and model-driven[2] deep learning frameworks to gold-standard compressed sensing (CS) for the reconstruction of ultralow field MRI data.

Materials and Methods: Phantom experiments were performed on a 6.5 mT MRI scanner with a quadrature head coil and a brain-shaped phantom.[3] A 3D Cartesian balanced-steady state free precession (bSSFP) sequence with TR/TE = 22/11 ms and matrix size 64 x 75 x 25 (Readout x Phase Encode 1 x Phase Encode 2) was used for acquisition with 256 signal averages. K-space was retrospectively 4× undersampled in the phase-encode dimensions with a Poisson-disc (PD) mask. Human data were prospectively acquired with a 2× undersampled PD mask and 40 signal averages (~7 min. acquisition).

Data-driven AUTOMAP[1] and model-driven Unrolled Optimization[2] reconstruction networks were implemented as described in Refs 4 and 5, respectively. A training corpus consisting of 50,000 brain image/k-space pairs was derived from the human connectome project (HCP) database. K-space data were undersampled with PD masks at the desired reduction factors (R=2 or 4) and networks were trained for up to 300 epochs. To reconstruct 3D data, a 1D FFT was applied along the fully-sampled readout dimension and trained networks were applied to the resulting hybrid k-space to reconstruct volumes slice-by-slice.

For CS reconstruction, sensitivity maps were calculated with ESPIRiT, and L1-wavelet CS reconstruction was performed using SigPy.[4]

For phantom experiments, the normalized root-mean-square error (NRMSE) and structural similarity (SSIM) reconstruction metrics were calculated relative to the fully-sampled ground-truth acquisition.

Results: Reconstructions of 4× undersampled phantom data are shown in Figure 1a. Reconstruction with AUTOMAP yielded the highest/best structural similarity metric, while CS reconstruction gave the lowest/best NRMSE metric. CS and unrolling network images demonstrate sharper reconstructed edges. Human brain images prospectively acquired with PD undersampling (R=2) and reconstructed via AUTOMAP are shown in Figure 1b.

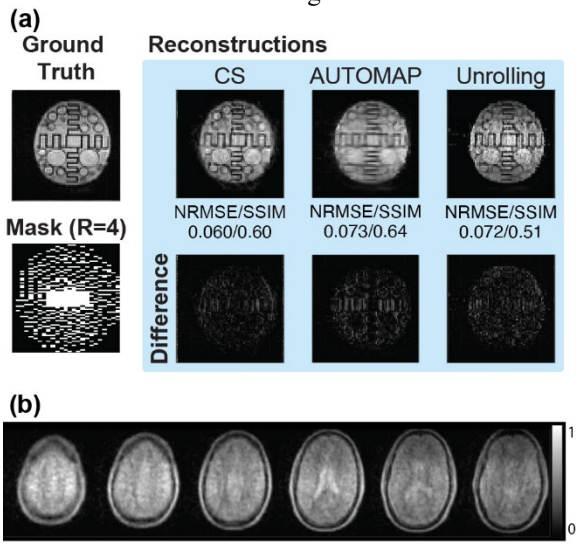

Figure 1: (a) Comparison of image reconstruction accuracy for Compressed Sensing (CS), AUTOMAP, and Unrolling Network techniques with R=4. **(b)** AUTOMAP reconstruction of an R=2, sub-7-minute scan of the human brain at 6.5 mT. The central 6 slices are shown.

Conclusions: Undersampling is an effective means to shorten long MR acquisitions. Our findings demonstrate that AUTOMAP can improve structural similarity, as compared to CS, when reconstructing undersampled data. Prospective deployment of PD undersampling will enable the clinical utility of deep learning reconstruction to be tested on low-field MRI scanners. These results will inform the development of faster imaging strategies for portable MRI.

Acknowledgements: D.E.J.W. is supported by a Cancer Institute NSW Early Career Fellowship 2019/ECF1015. The work presented herein was funded in part by the Advanced Research Projects Agency-Energy (ARPA-E), U.S. Department of Energy, under Award Number DE-AR0000823.

References:

1. Zhu et al., *Nature*, **555**, 487-492 (2018).
2. Zhang et al. *IEEE CVPR*, 1828-1837 (2018).
3. Sarracanie M et al., *Sci Rep*., **5,** 15177 (2015).
4. Koonjoo et al., *Sci Rep.,* 8248 (2021).
5. Shan et al., *arXiv*, 2205.10993 (2022).
6. Ong F et al., ISMRM Ann. Meeting, 4819 (2019).

AUS MRinRT

EXTENDED FOV IMAGING ON THE AUSTRALIAN MRI LINAC (AMRL)

Esther Wong[1], Bin Dong[2], Gary Liney[3]

[1] Esther Wong
[2] Bin Dong
[3] Gary Liney

Introduction:

The split bore of the AMRL presents significant imaging limitations due to gradient and magnetic field distortions. The accepted level of residual distortion will determine the isocentric imaging volume that can be acquired. In the design of the AMRL this was specified to be a maximum of 30 cm. While, the non linearity of the gradients are predictable and remedied easily, the non uniformity of the B0 field is much more significant, more difficult to measure and is dependent on many things including image sequence. Furthermore, high order shim coils used in clinical scanners to optimise B0 uniformity are not present on this system.

This study examines the extent and control of B0 uniformity on the AMRL using pixel-by-pixel measurements of a phantom. It then goes on to demonstrate a method of obtaining greatly extended imaging volumes by utilising the computer controlled couch movement together with acquisitions of smaller distortion free sub-volumes. This is demonstrated with phantoms and a volunteer. The concatenation of such volumes provides an elegant way of obtaining distortion free images up to 80 cm in length.

Materials and Methods:

Part a)B0-field mapping

Phase images with echo times of 10ms and 17.2ms were acquired in a 25cm spherical phantom. These were taken in each plane and at several distances both with and without shimming. B0-field maps were generated from the phase difference (via SPM). The integrated body coil was used as a transceiver in all imaging.

Part b) Extended FOV

i)Extended FOV with phantoms

Four bottles were placed in a straight line along the AMRL couch. The bottles were imaged repeatedly with FOV=20cm (determined from part a). In total 6 datasets were acquired with centre frequency adjusted and the table incremented 15 cm prior to each image. A baseline image with FOV = 40cm was also acquired for comparison.

ii) Extended FOV with volunteer

The same method was repeated on a volunteer to acquire 5 datasets in both sagittal and coronal planes. The method was tested both with and without overlapping sub volumes. Images were stitched together automatically using in-house software (Python), using known distances and offsets to obtain a single 80cm FOV image.

Results:

Part a)B0 field mapping

Table 1 comparison of homogeneity at DSV 10cm and 20cm with and without shim

	10cm DSV		20cm DSV	
	Without shim (ppm)	With shim (ppm)	Without shim (ppm)	With Shim (ppm)
0cm	0.27	0.26	0.73	0.72
20cm	0.20	0.22	0.71	0.72
40cm	0.22	0.23	0.76	0.76
60cm	0.23	0.24	0.78	0.79

Table 1 shows measurements made within the dimensions of the test object. The uniformity was within manufacturer specification (±0.47 ppm) and shimming made little difference to the values as they became worse further from the isocentre. A 20 cm distortion free FOV was chosen on this basis for subsequent tests.

Part b) Extended FOV

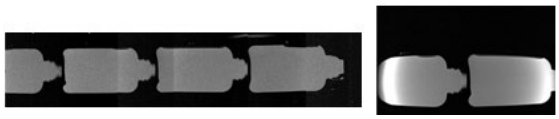

Figure 1 Illustration of the moving table method; bottles shown without distortion (left) compared to visible distortion in two bottles with 40 cm FOV on right.

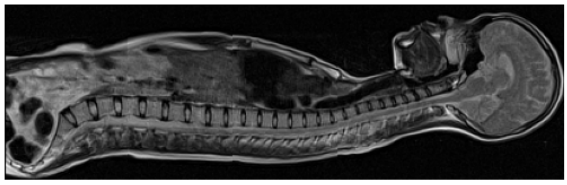

Figure 2 Whole-body image of volunteer demonstrating a seamless and distortion free 80 cm length FOV.

Figure 1 shows a comparison of the extended imaging method (left), in comparison to a 40cm FOV which shows severe distortions. ***Figure 2*** shows the volunteer image using the same technique with 5cm overlapping between images, showing excellent SNR and uniformity even at the edges of the sections. Similar image quality was observed with no overlap reducing the total acquisition time.

Conclusion: Two methods have been developed to measure, correct or avoid B0 distortion. B0 mapping may be useful when shimming alone is insufficient or larger bandwidths (low SNR) are not warranted. The acquisition of contiguous distortion free volumes shows great potential for whole body treatment guidance not currently available on other commercially available MRL systems, and without known limitations of coil arrays.

AUS MRinRT

MOTION-CORRECTED IMAGE RECONSTRUCTION USING AN UNROLLING NETWORK ON AN MRI-LINAC

Shanshan Shan[1,2], Yang Gao[3], Paul Liu[1,2], Tess Reynolds[1], Bin Dong[2], Hongfu Sun[3], Mingyan Li[3], Gary Liney[2], Feng Liu[3], Paul Keall[1,2], David Waddington[1,2]

[1]Image X Institute, Faculty of Medicine and Health, The University of Sydney, Australia
shanshan.shan@sydney.edu.au.

[2]Department of Medical Physics, Ingham Institute for Applied Medical Research, Australia.

[3]School of Information Technology and Electrical Engineering, University of Queensland, Australia.

Introduction: With superior soft-tissue contrast, MRI-Linacs aim to provide real-time tumour tracking for adaptive radiotherapy treatment, which promises more accurate and conformal tumour treatments [1]. However, respiratory motions can cause undesired artifacts that will reduce image quality and degrade the accuracy of tumour tracking [2]. The usage of external devices (e.g., respiratory bellows and ECG) for respiratory motion estimation is challenging to quantify intrabody deformations and requires additional set-up time [3]. Here, we investigate the use of an interpretable model-driven unrolling network to rapidly reconstruct motion-corrected thorax images and extract respiratory signals for accurate and real-time tumor tracking on an MRI-Linac.

Materials and Methods: During treatment, radial k-space center data was fed into the unrolling network [4] to reconstruct low-resolution dynamic motion-free images, as shown in Figure 1. Tumor positions were extracted from the low-resolution images to estimate respiratory signals, which were then used to guide tumor tracking. After treatment, all k-space data was retrospectively gated according to the estimated respiration and high-resolution motion-corrected images were reconstructed from the unrolling network for intrafraction treatment verification. The unrolling network was implemented in Pytorch with an architecture consisting of four blocks, which starts with a data fidelity calculation, followed by nonlinear transforms with a soft-thresholding operation. Datasets of 3000 training thorax images and 450 validation images from ten volunteers were encoded with a golden-angle radial acquisition to generate raw k-space data. Our deep-learning-reconstruction approach was validated with a digital CT/MRI breathing XCAT (CoMBAT) phantom and experimentally with a motion phantom on an MRI-Linac.

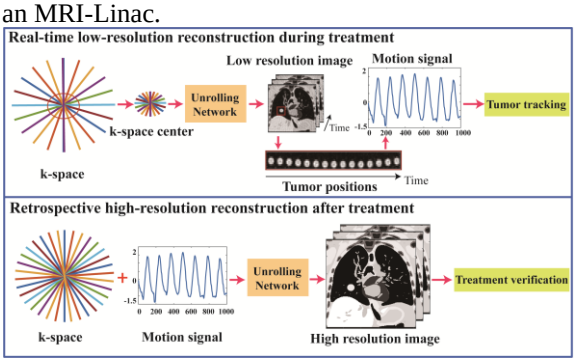

Figure 1: Rapid Motion-corrected Image Reconstruction Workflow.

Results: Performance of the unrolling network in reconstructing digital phantom images were shown in Figure 2. Severe image blurring was visible in ungated image, while the blurring was significantly reduced in gated image. Quantitatively, the gated image provided higher SSIM (0.93) and lower RMSE (0.02) than the ungated one (0.52/0.08). Experimental motion phantom results in Figure 3 showed that the unrolling network successfully estimated respiratory signals and sharper structural details were seen in gated image compared with the ungated one, as indicated by red arrows. The inference time of unrolling reconstruction of one image slice (size=256×256) was 50ms.

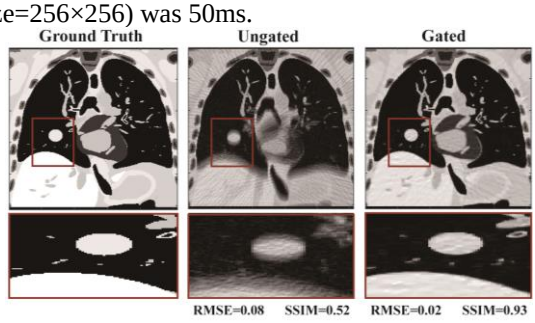

Figure 2. Performance of the unrolling network in reconstructing digital phantom images.

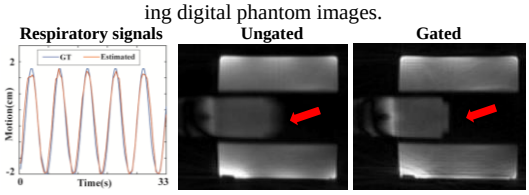

Figure 3. Performance of the unrolling network in reconstructing experimental motion phantom images.

Conclusion: We have demonstrated rapid motion-corrected image reconstruction and real-time respiration estimation from an MRI-Linac with an unrolling network. Experimental implementation promises to reduce motion artefacts and reconstruction latency for dynamic tumor tracking.

References:

1. P. J. Keall, M. Barton, and S. Crozier, "The Australian magnetic resonance imaging–linac program." pp. 203-206.

2. Bruijnen, T., Stemkens, B., Terhaard, C.H., Lagendijk, J.J., Raaijmakers, C.P. and Tijssen, R.H., 2019. Intrafraction motion quantification and planning target volume margin determination of head-and-neck tumors using cine magnetic resonance imaging. Radiotherapy and Oncology, 130, pp.82-88..

3. Jiang, W., Ong, F., Johnson, K.M., Nagle, S.K., Hope, T.A., Lustig, M. and Larson, P.E., 2018. Motion robust high resolution 3D free-breathing pulmonary MRI using dynamic 3D image self-navigator. Magnetic resonance in medicine, 79(6), pp.2954-2967.

4. Shan, S., Gao, Y., Liu, P.Z., Whelan, B., Sun, H., Dong, B., Liu, F. and Waddington, D.E., 2022. Distortion-Corrected Image Reconstruction with Deep Learning on an MRI-Linac. arXiv preprint arXiv:2205.10993.

SUPER-RESOLUTION IMAGING ON THE AUSTRALIAN MRI-LINAC

James Grover[1,2], Paul Liu[1,2], Bin Dong[2], Shanshan Shan[1,2], Brendan Whelan[1,2], Paul Keall[1,2], David Waddington[1,2]

[1] Image X Institute, Faculty of Medicine and Health, The University of Sydney, Australia
james.grover@sydney.edu.au

[2] Department of Medical Physics, Ingham Institute for Applied Medical Research, Australia

Introduction: Real-time magnetic resonance imaging guided radiation therapy (MRIgRT) has a trade-off between spatial and temporal resolution. Super-resolution increases MRI spatiotemporal resolution by up-sampling a low-resolution (LR) MRI to high-resolution (HR) reducing tracking latency. In this work, we integrate deep learning and 4× super-resolution on the Australian MRI-linac to improve real-time adaptive MRIgRT.

Methodology: We trained an Enhanced Deep Super-Resolution (EDSR) network on MRIs of the human brain and thorax[1-3]. This deep learning-based EDSR network and baseline bicubic interpolation were integrated into the Australian MRI-linac (Figure 1) using Gadgetron[4].

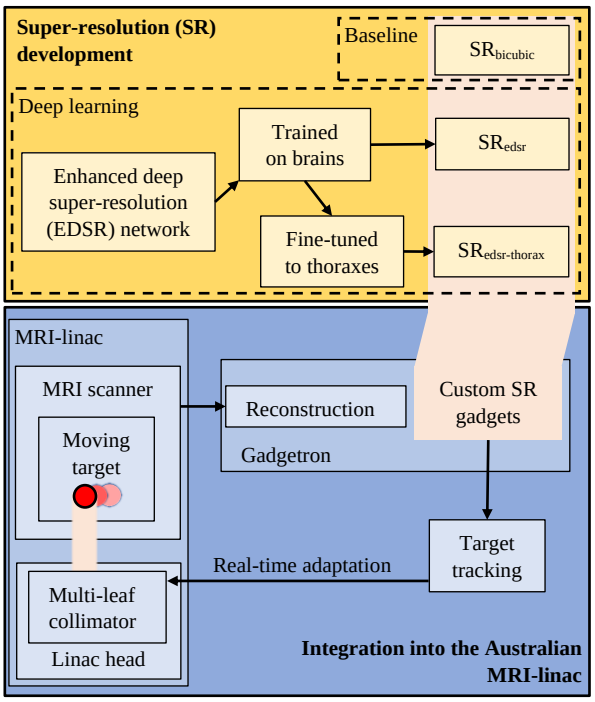

Figure 1. Overview of the work.

Volunteer and motion phantom experiments at the Australian MRI-linac were used to test this end-to-end integration. A volunteer thorax experiment was conducted to observe the effect of super-resolution on the delineation of anatomy. A long-to-acquire HR volunteer brain acquisition was down-sampled to a LR. This LR MRI was used as input to super-resolution and the resulting super-resolution MRI was directly compared to the original HR MRI through a peak signal-to-noise ratio (PSNR) and normalised root mean-squared-error (NRMSE). In a multi-leaf collimator (MLC) tracking experiment, a one-dimensional motion phantom moved to sinusoid and patient traces where the latency and latency-corrected error were subsequently calculated.

Results: In the thorax experiment, super-resolution MRIs displayed sharper anatomical features compared to LR MRIs (Figure 2).

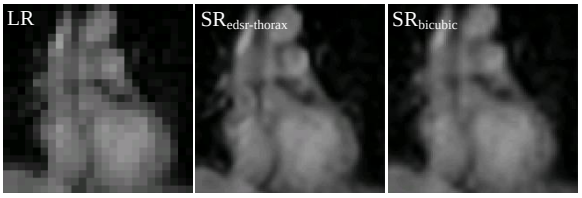

Figure 2. Super-resolution (SR) on thorax MRIs.
Cropped to cardiac region.
LR: low-resolution input.

In the brain experiment, EDSR (Figure 3) gave an approximate 7 dB PSNR boost while showing half the NRMSE compared to bicubic interpolation.

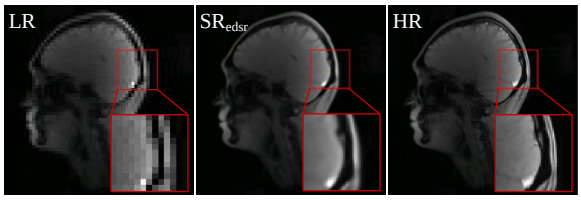

Figure 3. Super-resolution (SR) on brain MRIs.
PSNR: 33.5 dB; NRMSE: 2.1%.
LR: low-resolution input; HR: high-resolution.

In the MLC tracking experiment, super-resolution contributed only an additional 3% latency (0.35s cf. 0.36s) while reducing the latency-corrected error by over 40% (1.46mm cf. 0.82mm).

Conclusion: Super-resolution increased the spatiotemporal resolution of MRIs used in real-time adaptive MRIgRT on the Australian MRI-linac.

References:

1. B. Lim et al., *arXiv*. 1707.02921 (2017).
2. A.B. Mamonov and J. Kalpathy-Cramer, *The Cancer Imaging Archive*. (2016).
3. D. Lee et al., *Med. Phys.* **45**(3), 1009-1017 (2018).
4. M.S. Hansen and T.S. Sørensen, *Mag. Res. in Med.* **69**(6), 1768-1776 (2013).

IN SILICO DEMONSTRATION OF MRI-GUIDED MULTI-LEAF COLLIMATOR TRACKING OF MULTIPLE LUNG CANCER TARGETS

Paul Z.Y. Liu[1,2], Doaa Elwadia[2,3,4], Jarrad Begg[2,3,5], Shivani Kumar[3,5], Bin Dong[2], Daniela Miller[2,3], Justin Spicer[2,3], Andrew Wallis[2,3], Emily Hewson[1], Paul Keall[1,2], Trang Pham[2,3,5]

[1] Image X Institute, School of Health Sciences, University of Sydney, Sydney, paul.liu@sydney.edu.au
[2] Ingham Institute for Applied Medical Research, Sydney
[3] Department of Radiation Oncology, Liverpool Hospital, Sydney
[4] School of Health Sciences (Medical Imaging Discipline), Faculty of Medicine & Health, University of Sydney, Sydney
[5] School of Clinical Medicine, South West Sydney Clinical School, University of New South Wales, Sydney

Introduction: Many radiotherapy patients are treated for multiple targets made up of primary tumours, lymph nodes and metastases. As each target can move independently during treatment, large margins are needed to encompass the motion of all targets. MR-guided multi-target multi-leaf collimator (MLC) tracking is a real-time beam adaptation technique that independently accounts for the motion of each target to reduce the required size of these margins [2]. In this work, we utilise patient data collected as part of the Australian MRI-Linac Patient Imaging (AMPI) trial to simulate MR-guided multi-target MLC tracking for two lung cancer patients.

Method: Patient 1 had recurrent thymoma with a left pleural based soft tissue mass and pleural-based nodule. Patient 2 had primary two non-small cell lung cancers in the left and right upper lobes and mediastinal nodal metastases. Coronal and sagittal cineMRIs of these patients were acquired using the TRUFI sequence at 128×128 pixel resolution, 400 field-of-view with TR = 3.5ms, TE = 1.8ms and 2 Hz frame rate. The images were used as imput motion during multi-target MLC tracking simulations by performing template matching to find the position each target (Figure 1).

Both patients received VMAT as their standard treatment. To simulate multi-target tracking, the treatment plans were analysed by dividing the area of each MLC field into two segments that each irradiated a different target (Figure 2, top). During multi-target tracking, the two segments of the divided MLC field were moved independently in response to motion from the cineMRIs then recombined into a single deliverable MLC field.

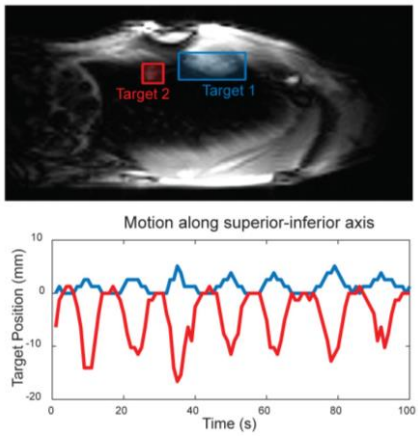

Figure 1. (Top) Example of a sagittal cineMRI for patient 1 with two target positions calculated with template matching. (Bottom) The resulting motion trace showing independent motion of these two targets.

Results: For patient 1, both targets were tracked on a single sagittal plane. For patient 2, the two primary tumours and the mediastinal node were tracked on two alternating coronal planes. Patient 1 had up to 22 mm of independent motion between the two targets and patient 2 had up to 6 mm of independent motion. Multi-target MLC tracking was shown to track both targets independently during the simulated treatments. For example, at the peak inhale position shown in Figure 2 (bottom), coverage of both planning target volumes was maintained.

Conclusion: The AMPI trial has imaged lung cancer patients with multiple targets on the Australian MRI-Linac. All targets could be clearly seen and tracked on the acquired cineMRIs. We have simulated MR-guided multi-target MLC tracking for these patients and demonstrated that coverage of these targets can be maintained in the presence of independent motion.

References:

1. Stereotactic body radiation therapy in the treatment of multiple primary lung cancers (K. Creach et al.), *Radiother Oncol* **104**:19–22 (2012)
2. First experimental investigation of simultaneously tracking two independently moving targets on an MRI-linac using real-time MRI and MLC tracking (Liu et al.), *Med Phys* **47**:6440 (2020)

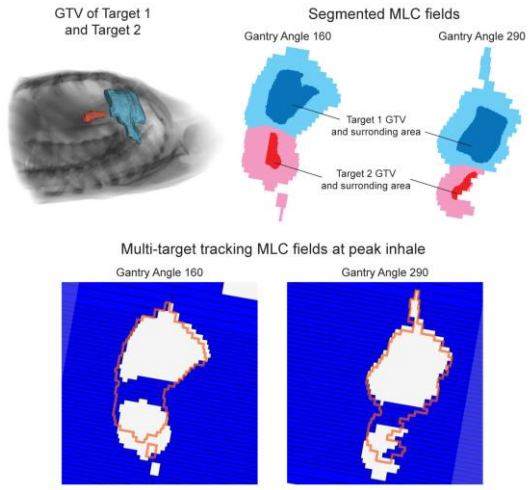

Figure 2. (Top) Gross tumour volumes (GTVs) were used to divide the MLC fields. Two examples for patient 1 are shown. (Bottom) Original MLC field (orange) and the recalculated MLC fields (blue) during multi-target tracking. From the cineMRIs, target 1 moved 5 mm superior, 4 mm anterior and target 2 moved 17 inferior, 8 mm posterior.

AUS MRinRT

MAGNETIC RESONANCE BIOMARKER ASSESSMENT SOFTWARE (MR-BIAS): AN AUTOMATED OPEN SOURCE TOOL FOR THE ISMRM/NIST SYSTEM PHANTOM

James Korte[1,2], Zachary Chin[3], Madeline Carr[4,5], Lois Holloway[4,5], Rick Franich[1,3]

[1] Peter MacCallum Cancer Centre, Department of Physical Sciences, Melbourne, james.korte@petermac.org
[2] The University of Melbourne, Department of Biomedical Engineering, Melbourne
[3] RMIT University, School of Science, Melbourne
[4] University of Wollongong, Centre for Medical Radiation Physics, Wollongong
[5] Liverpool and Macarthur Cancer Therapy Centres and Ingham Institute, Liverpool, Sydney

Introduction: Quantitative magnetic resonance imaging (qMRI) biomarkers have potential to improve treatment of oncology patients via enhanced treatment response monitoring and biological guidance during radiotherapy. The emergence of MRI simulation and on-board MRI guidance in radiotherapy provides a unique opportunity to investigate qMRI biomarkers, but care must be taken to account for variability in MRI images [1]. The ISMRM/NIST system phantom provides a reference object for characterising qMRI measurements, such as T1 relaxation mapping which is recommended for quantitative measurement of tissue permeability with dynamic contrast enhanced (DCE) MRI [2]. To analyse system phantom images there are limited open-source options [3], and often require time-consuming manual steps such as image sorting and defining regions of interest (ROIs). To address these issues, we have developed a fully automated tool to analyse system phantom images, freely available at: https://github.com/JamesCKorte/mrbias.

Materials and Methods: Magnetic Resonance BIomarker Assessment Software (MR-BIAS) automates three main tasks to analyse system phantom images (Figure 1). MRI datasets are sorted based on DICOM metadata to identify a geometric image and T1 and T2 image sets. ROIs are detected by registering the geometric image to a predefined ROI atlas. MRI parameters are estimated in the detected ROIs by fitting relaxation models to the T1 and T2 image sets. The tool is written in Python (v3.7) and supports T1 inversion recovery (T_1^{IR}), T1 variable flip angle (T_1^{VFA}) and T2 multiple spin-echo (T_2^{MSE}) data.

Inter-operator variability and efficiency was assessed by observing six participants using MR-BIAS and a semi-automated tool [3], recording time taken to analyse three MRI datasets and the variability of estimated T1 and T2 values [4]. The accuracy of MR-BIAS was compared against T1 and T2 values measured in an existing study, which used a custom script to analyse monthly phantom data (n=11) acquired on a Siemens 3T Skyra MRI simulator [5]. Accuracy was evaluated with percentage error (%bias) between estimated vales and NIST reference values over a physiological range (T_1: 121-1884 ms, T_2: 30-380 ms). A basic compatibility test of MR-BIAS on Elekta Unity 1.5T MRI data was also performed.

Results: MR-BIAS automatically analysed the three datasets with less variability than the semi-automated tool and approximately ten times faster.

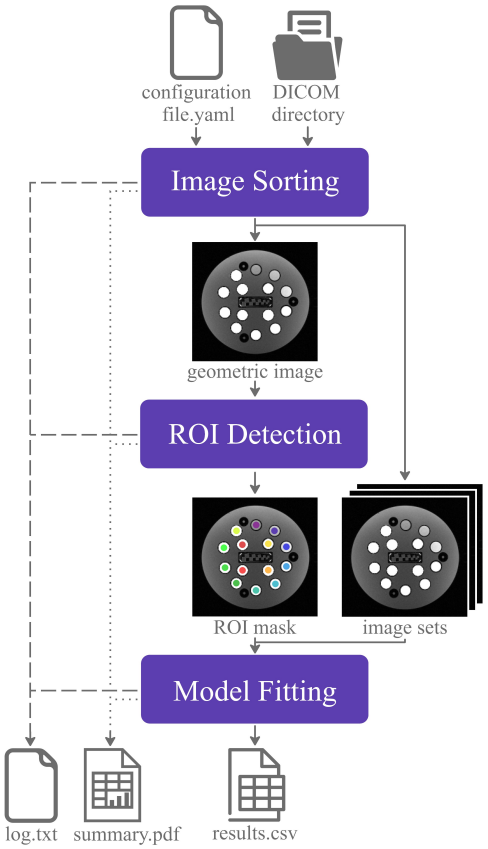

Figure 1. MR-BIAS automated workflow

On the monthly data, MR-BIAS had median accuracy across all ROIs in the physiological range for T_1^{IR} within ±6%, T_1^{VFA} within ±17.5% and T_2^{MSE} within ±14.5%. These are comparable to the custom script with a median accuracy for T_1^{IR} within ±6%, T_1^{VFA} within ±13% and T_2^{MSE} within ±14%. MR-BIAS successfully analysed data from an Elekta Unity.

Conclusions: MR-BIAS is a free automated tool that minimises operator variability and can accurately and efficiently analyse system phantom images.

References:

1. Biomarkers in MRgRT clinical trials (PJ. van Houdt et al.), *Eur J Cancer.* **153**, 64-71 (2021).
2. Consensus DCE recommendations (JL. Evelhoch), *DCE MRI in Oncology,* Springer, 109-113 (2005).
3. NIST Phantom Viewer (S. Russek et al., 2021), *https://github.com/MRIStandards/PhantomViewer.*
4. Automated qMRI measurement (Z. Chin), *Thesis for Master of Medical Physics*, RMIT (2020).
5. Longitudinal accuracy of T1 and T2 (ME. Carr et al.), *J. Appl. Clin. Med. Phys.* 1-8 (2021).

AUS MRinRT

IMAGING RESULTS USING THE 8-ELEMENT TORSO COIL ARRAY FOR THE AUSTRALIAN MRI-LINAC SYSTEM

Mingyan Li[1], Ewald Weber[1], David Waddington[2], Shanshan Shan[2], Paul Liu[2], Bin Dong[3], Paul Keall[2], Feng Liu[1], Stuart Crozier[1]

[1] School of Information Technology and Electrical Engineering, The University of Queensland, Australia
[2] Image X Institute, Faculty of Medicine and Health, The University of Sydney, Australia
[3] Ingham Institute for Applied Medical Research, Sydney, Australia

Introduction: This abstract presents the initial imaging results with using the developed 8-element torso array coils[1,2]. It can provide higher SNR and better image quality than the existing whole-body transceive coil[3]. In addition, with simultaneous multiple receive channels, the coil has fast imaging capability, an important feature to facilitate the tumour tracking during radiotherapy.

Materials and Methods: As shown in Figure 1 (a), the 8-element torso coil array has two sub arrays with 4 rectangular coils in each array[1]. The coil-patient setup is shown in (b) with sub arrays placed on anterior and posterior sides of the volunteer. The length and width of individual coil element is 300 mm and 100 mm, then the four coil elements can cover the 300 mm DSV. The coils are made with flexible coaxial cables and tuned to 42 MHz. All coils are decoupled well with the overlapping method. The measured mutual coupling among all channels (S_{xy}) are lower than -18 dB for a body-equivalent load and a human torso. A water phantom was used for SNR comparison between the whole-body coil and the developed torso coil. Volunteer images were also acquired to evaluate the *in vivo* image quality and fast imaging performance of the 8-element toros coil array.

Results: As shown in (c) and (d), although the whole-body coil can achieve better image uniformity, the SNR is lower than the torso coil. The SNR of two coils are 16.4 (whole-body coil) and 67.4 (torso coil) at the centre; 15.7 (whole-body coil) and 147.4 (torso coil) at the surface. The much higher SNR is then translated into sharper boundaries and finer detailed structures marked with red arrows in the *in vivo* image in (f). With only one third of scanning time, the image exhibited in (h) does not have any obvious aliasing artefacts when compared to the fully sampled image in (g).

Conclusions: Validated with both phantom and volunteer images, the developed 8-element torso coil has much higher SNR in both centre and surface regions compared to the existing whole-body coil. This advantage allows the coil to produce *in vivo* images with sharper boundaries between tissues, which will be beneficial for tumour contouring. With simultaneous multiple receive channels, the coil can also perform parallel imaging up to a reduction factor of 3, without seeing any obvious aliasing artefacts. This will facilitate the real-time tumour tracking during the radiotherapy.

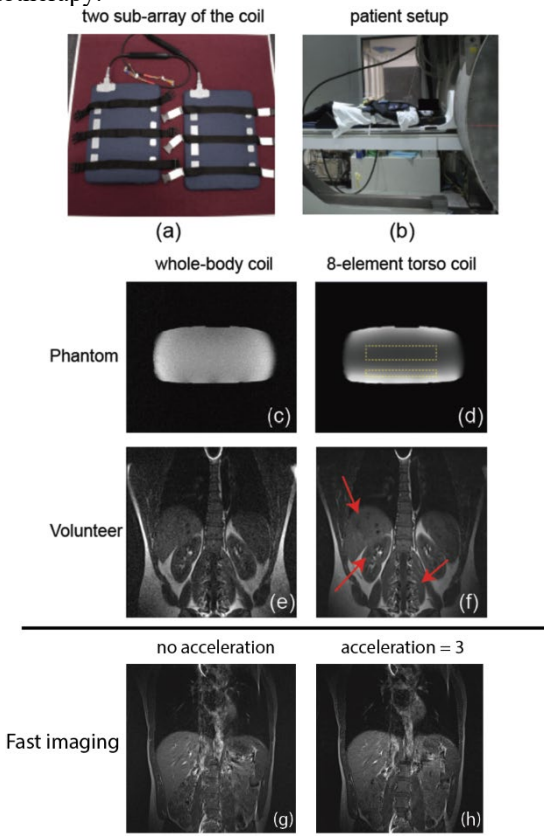

Figure 1 (a) Two sub arrays of deveopled 8-element toros coil array. (b) Coil-patient setup on the rotating couch of the MRI-Linac system. (c) and (d) Phantom images acquried with the whole-body coil and torso coil. (e) and (f) *In vivo* images acquried with the whole-body coil and torso coil. (g) and (h) In vivo images without and with acceleraiton (R=3).

References:

1. M. Li, et al., Theoretical Design and Image Reconstruction of an 8-element Receive-only Surface Coil Array for the 1.0 T Australian MRI-Linac System, *ISMRM 2020,* Paris, France
2. M. Li, et al., An 8-element torso RF coil array for the Australian inline MRI-Linac: Initial imaging results, annual meeting of *ISMRM 2022,* Toronto, Canada
3. G. P. Liney, et al., Imaging performance of a dedicated radiation transparent RF coil on a 1.0 Tesla inline MRI-linac, Phys. Med. Biol. 2018 Jun 25;63(13):135005

AUS MRinRT

TOWARDS MRI-GUIDED PROTON THERAPY: THE ULTIMATE CANCER TREATMENT?

Paul Keall,[1] Suzie Sheehy,[2] Michael Barton,[3] Trang Pham,[3] Stuart Crozier,[4] and Anatoly Rozenfeld[5]
[1] Image X Institute, University of Sydney, paul.keall@sydney.edu.au
[2] University of Melbourne
[3] Liverpool Hospital, UNSW, Ingham Institute
[4] University of Queensland
[5] CMRP, University of Wollongong

Introduction: Radiation therapy (RT) is indicated to treat half of all cancer patients.[1] Today, RT is both effective and cost-effective. However, RT can be further improved by:

- improving image guidance which has been shown in randomised trials to improve outcomes (weekly vs daily, PACE-B ref)
- implementing adaptive radiotherapy (MIRAGE ref)
- reducing treatment toxicity by reducing dose to normal tissues through proton therapy
- targeting additional focused radiation to the radioresistant, aggressive and metastatic-potential sub-volumes of the cancer.

A future RT system to maintain the strengths of RT and achieve the above improvements is MRI-guided proton therapy, arguably the ultimate cancer therapy. The aim of this research was to develop a plan to clinically realise MRI-guided proton therapy.

Material and Methods: A multidisciplinary team of world leading scientists, clinicians and entrepreneurs with unique expertise and experience to tackle this challenge was assembled. The team included members of the successive NHMRC Program Grants that designed and built the ground-breaking and globally unique Australian MRI-Linac demonstrating the capacity and expertise in the integrated MRI-guided cancer therapy device space.

The team developed a 2-phase plan, a Research Planning phase, and a Research Implementation phase, to realise MRI-guided cancer therapy.

Results: The key Research Planning phase deliverable is a comprehensive Research Plan that includes the preliminary design, partner engagement, and first site decided for a commercially attractive clinical MRI-Guided Proton Therapy system. Our preliminary design will be informed by extensive consumer, clinician, health economics and public/private provider market engagement to maximise the product-market fit, clinical applications and workflow. A multi-institutional system-wide design exercise covering the interoperability and integration of the MRI and the proton system will be undertaken. Site selection and the tenders and selection of industry partners will be completed.

The key Research Implementation phase deliverables are the construction, research and development, and clinical demonstration of the world's first clinical MRI-Guided Proton Therapy system. This system will be a viable commercial prototype, with the clinical implementation advancing science, medicine and de-risking the commercial pathway.

Conclusions: We plan to unleash the clinical potential of proton beam radiation therapy for cancer patients by building a clinical magnetic resonance imaging (MRI) guided proton therapy device. This device will be the most accurate and precise radiation therapy treatment system ever created.

Acknowledgements: Many coinvestigators, Sebastien Ybert, Helen Ball and Julia Johnson.

Reference

1. Barton et al.. *Radiother Oncol.* 2014.

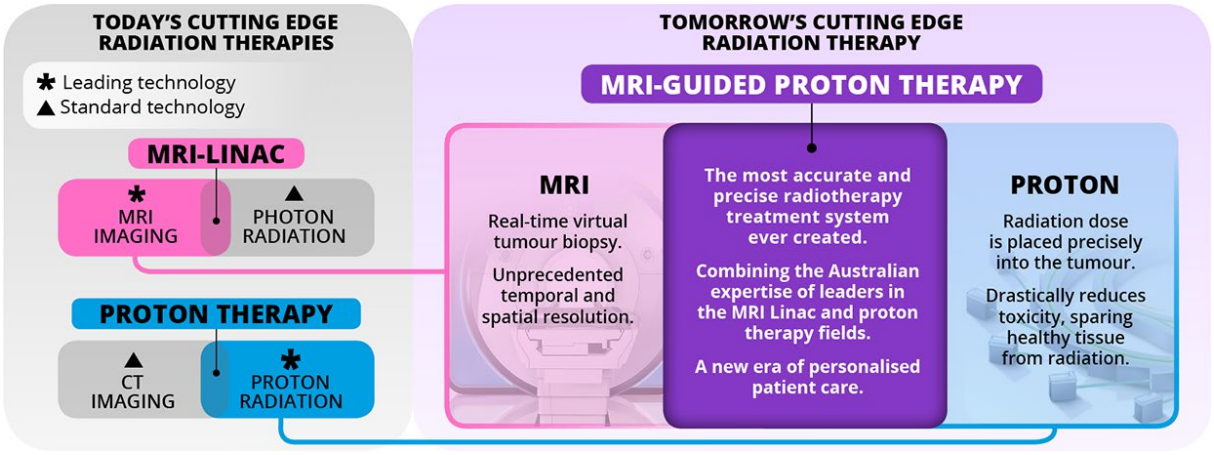

Figure 1. We plan to bring together the two most disruptive treatment devices in radiation therapy. We plan to design, build, and clinically pioneer MRI-Guided Proton Therapy.

AUS MRinRT

ICRU REPORT ON MRI-GUIDED RADIATION THERAPY USING MRI-LINACS

P Keall[1], C Glide-Hurst[2], A Tree[3], P Lee[4], B Murray[5], B Raaymakers[6], U van der Heide[7] and M Cao[8]
[1] ACRF Image X Institute, Faculty of Medicine and Health, University of Sydney, 2006 NSW Australia
[2] University of Wisconsin—Madison, Wisconsin, USA
[3] The Royal Marsden Hospital and Institute of Cancer Research, London, UK
[4] City of Hope, CA and MD Anderson Cancer Center
[5] University of Alberta/MagnetTx
[6] Utrecht Medical Center
[7] The Netherlands Cancer Institute
[8] UCLA, Los Angeles, California, USA

Introduction: The ICRU has been providing guidance for over 90 years to radiation medicine. One of the objectives of the ICRU is the development of internationally accepted recommendations. Aligned with this objective, the ICRU report on MRI-guided Radiation Therapy (MRIgRT) using MRI-Linear Accelerators was commissioned.

Materials and methods: A team with diverse country-of-origin, gender and expertise was assembled, noting that most of the MRIgRT development had been performed in high-income countries. The focus of the team was on the differences in the radiation therapy process that the addition of MRI into the treatment room brings to the patient and to the treatment team. With the number of clinical systems growing rapidly, and the increase in feature availability and automation, the authors endeavoured to focus on the top-level concepts that will likely remain relevant amidst the ongoing technological changes that accompany fast-emerging technologies. These top-level concepts include personalization of imaging, high-quality intra-treatment imaging, routine online adaptive radiotherapy, integrated intra-treatment imaging with beam gating, and integrated functional imaging capabilities. A summary of the key feature differences between MRIgRT and conventional X-ray image-guided radiation therapy (IGRT are shown in Figure 1.

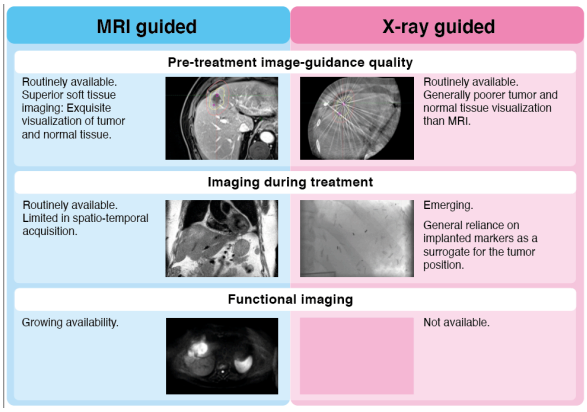

Figure 1. An illustration, using example liver cancer images, of some key differences between MRI-guided and conventional X-ray guided linear accelerator radiation therapy.

Results: The report narrative begins with an overall rationale and status of MRIgRT, followed by the clinical indications for patient MRIgRT treatments across different cancer sites. A summary of the MRI-linac interoperability challenges and an overview of the MRIgRT systems that have been developed to date is given. The MRIgRT process steps are given chronologically: treatment planning, image guidance, treatment adaptation and treatment delivery. The staff requirements, training and safety are discussed. A technical section reviews MRIgRT commissioning and dosimetry.

The recommendations span multiple MRIgRT stakeholders: administrators, newer and expert users, industry and government. A future outlook and future needs of where MRIgRT may fit into the health care system of the future, along with anticipated technological advances, are outlined.

To give new users real-world examples of MRIgRT in practice, some clinical case studies for a variety of sites and treatment complexity are given.

Conclusions: MRI-linacs are a rapidly emerging technology for radiation therapy that have undergone strong clinical adoption. MRI-linacs have higher capital, operating, staff and workflow costs than conventional X-ray guided linacs. However, MRI-linacs provide the radiation treatment team improved soft tissue discrimination and the ability to monitor patient anatomy prior to and during treatment without additional ionizing radiation risks. This additional information introduces many opportunities to improve patient outcomes. The safety (CTV-PTV) margins can be reduced, thereby reducing the likelihood and potential severity of treatment-induced side effects. MRI-linacs, particularly when coupled with online daily ART, have also enabled opportunities for hypofractionation (e.g., completing the treatment course in fewer sessions), thereby mitigating the cost and time commitment for the patient and the healthcare system. As MRI-linacs combine two devices with their own risk profiles, and they are an emerging technology, the safe implementation requires skilled teams, ongoing training, a safety-first culture, comprehensive QA programs, and clearly documented treatment workflow procedures.

Acknowledgements: Many – to be presented.

AUS MRinRT

QUANTITATIVE IMAGING BIOMARKERS: RELIABLE DETECTION OF TREATMENT-RELATED CHANGES FROM MEASUREMENT UNCERTAINTY

Yu-Feng Wang[1,2], Sirisha Tadimalla[1,3], Yu Sun[1], Lois Holloway[1,2,4], Annette Haworth[1]

[1] The University of Sydney, Sydney, Australia, ywan3672@uni.sydney.edu.au

[2] Ingham Institute for Applied Medical Research, Sydney

[3] Sydney West Radiation Oncology, Westmead Hospital, Sydney

[4]South Western Sydney Clinical School, University of New South Wales, Liverpool, NSW, Australia

Introduction: Quantitative imaging using multiparametric MRI (mpMRI) has shown potential for providing non-invasive biomarkers for post-treatment monitoring and response prediction in prostate cancer (PCa).[1, 2] The Sequential Imaging – Biofocussed Radiation Therapy (SI-BiRT) clinical trial aimed to develop quantitative imaging biomarkers (QIBs) of response to radiation therapy (RT) for PCa. Measurement uncertainties in quantitative MRI (qMRI) parameters, however, can impact their reliability in detecting treatment-related changes in longitudinal measurements.[3] Here, we present precision estimates of candidate QIBs of RT response of PCa from an in vivo test-retest study in the SI-BiRT trial to establish thresholds for reliable detection of treatment-related changes.

Methods: The mpMRI protocol consisted of T2-weighted (T2w) imaging, diffusion weighted imaging (DWI), longitudinal relaxation time (T1), and transverse relaxation time (R2*) mapping sequences. Test-retest images were acquired in 9 patients with PCa and 6 healthy volunteers on two 3T MRI scanners (MAGNETOM Prisma and Skyra respectively, Siemens Healthineers, Erlangen, Germany). qMRI parameters including the apparent diffusion coefficient (ADC), diffusion coefficient (D), perfusion fraction (f), hypoxia score (HS) were obtained from DWI, T1 and R2* were calculated, and radiomic feature maps were extracted from the parametric maps. Repeatability coefficients (%RC) were calculated from region of interest (ROI) and voxel-wise analysis of the parametric and feature maps in the tumour and benign tissues in the peripheral and non-peripheral (PZ and nPZ) zones. The repeatability of qMRI parameters from pharmacokinetic modelling of dynamic contrast enhanced (DCE) MRI were estimated by T1 error propagation. %RC between tumour and benign tissue types, and between PZ and nPZ regions were compared using the Student's t-test with 95% significance level.

Results: Table 1 summarises the %RC of qMRI parameters. The repeatability of DWI-derived qMRI parameters (all except f) and radiomic features were significantly different between the PZ and nPZ regions and between tumour and benign tissue types. Measurement uncertainties were larger when test-retest variations were assessed using voxel-wise analysis compared to the ROI measurements. The %RC of f, T1, R2*, and their radiomic features were not significantly different between the anatomical zones or between tumour and benign tissue types.

Conclusion: Thresholds of change required to distinguish true treatment-related changes from measurement uncertainties were formulated for the qMRI parameters investigated in this study. In DWI-derived qMRI parameters, such thresholds should be defined separately for the anatomical zones and tissue types to account for difference in uncertainty potentially due to proximity to rectum and size of ROI. DCE-derived qMRI parameters and T1 showed relatively higher precision and could be potentially more reliable as robust QIBs of treatment response. Higher uncertainties in voxel-wise measurements, likely due to lower SNR and image registration, could be a challenge in mapping of treatment response. The thresholds established in this study will be used to discriminate true treatment-related change from measurement uncertainties in the SI-BiRT clinical trial.

qMRI parameter	Tissue type	Region of interest		Voxel
		PZ	nPZ	WG
A) Regional				
ADC	Benign	16.3	6.8	30.1
	Tumour	31.2	13.8	43.9
D	Benign	17.0	6.9	30.1
	Tumour	28.1	12.1	40.2
HS	All	12.1	4.7	20.4
B) Whole gland				
f	All	35.1		140.5
*R2**	All	40.0		57.3
T1	All	10.5		24.9
Ktrans	All	10		34
ve	All	11		38
Kep	All	0.8		2.8

WG – whole gland, PZ – peripheral zone, nPZ – non-peripheral zone

Table 1. Threshold of percentage change required to distinguish measurement uncertainties from treatment-related change for qMRI parameters.

Acknowledgements:

This project was supported by NHMRC grant APP1126955, Sydney West TCRC – Partner Program 2019 and CI NSW Translational Program Grant TPG182165.

References:

1. Multiparametric MRI and radiomics in prostate cancer: a review (Y. Sun, et al.), *Australas Phys Eng Sci Med* **42**(1):3-25 (2019).

2. Artificial intelligence and imaging biomarkers for prostate radiation therapy during and after treatment (Y. F. Wang, et al.), *J Med Imaging Radiat Oncol* **65**(5):612-626 (2021).

3. Quantitative imaging biomarkers alliance (QIBA) recommendations for improved precision of DWI and DCE-MRI derived biomarkers in multicenter oncology trials (A. Shukla-Dave, et al.), *J Magn Reson Imaging* **49**(7):e101-e121 (2019).

AUS MRinRT

COMPARISON OF ADAPTIVE AND NON-ADAPTIVE RADIATION THERAPY PLANS USING DEFORMABLE DOSE ACCUMULATION

Maxwell Eastwood[1], Michael Jameson[2,3], David Crawford[2], Maddison Picton[2], Charlie Tran[2], Laura Mckenzie[2], Jeremy de Leon[2], Annette Haworth[1]

[1]Institute of Medical Physics, School of Physics, University of Sydney, Camperdown, meas2173@uni.sydney.edu.au
[2]GenesisCare, NSW
[3]School of Clinical Medicine, Medicine and Health, University of New South Wales, Darlinghurst

Introduction: Online adaptive treatment planning using an MR-Linac may improve dosimetric precision for prostate cancer and benefit patients with unfavourable anatomy, compared to conventional radiation therapy (RT)[1,2]. However, it requires significantly more time and cost compared to conventional treatment[1,3]. This study assessed the dosimetric differences between non-adapted plans and online adapted treatment plans, created using the adapt-to-shape process on the Elekta Unity (Elekta AB, Stockholm, Sweden).

Materials and Methods: Data from 12 prostate cancer patients treated on the Elekta Unity MR-Linac (Elekta AB, Stockholm, Sweden) at St Vincent's Hospital were included in this study. All patients were treated with online adapt-to-shape stereotactic body RT, delivered in 5 fractions. All patients were prescribed 36.25 Gy to the prostate PTV. At each fraction, pre-treatment imaging using T2 weighted MRI was acquired to verify alignment. The target volumes and OARs were contoured on the MRI and the plan was adapted to suit the daily anatomy using the adapt-to-shape process. Non-adapted plans were created by simulating the dose that would have been delivered had the plan not been adapted to the daily changes in shape and position of target volumes and OARs. The dosimetric benefit of applying the adapt-to-shape process was determined through a 2-stage process: Firstly, deformable image registration (DIR) methods were compared to determine the most suitable method for producing dose accumulation maps in the study. The DIR methods included: intensity-based DIR, contour-based DIR and hybrid DIR, available in MIM (MIM Software inc.). Intensity and contour metrics were used to measure the performance of each DIR method. Secondly, the optimal DIR method was used to accumulate the dose distributions from each fraction to calculate the total dose distribution. The differences in total accumulated dose between non-adaptive and online adaptive RT were assessed using clinical dose evaluation parameters and treatment planning objectives.

An exploratory study was also conducted with data from 4 pancreatic cancer patients using the same methods. All 4 patients were prescribed 40 Gy to the PTV.

Results: For both the prostate and pancreas studies, the intensity-based and hybrid DIR methods performed similarly well according to intensity metrics, while the contour-based method performed worse. The intensity-based method performed the best in contour metrics for most contours, while the contour-based method performed the worst for most contours.

For prostate cancer patients, there was a significant average increase in target coverage with online adaptive RT, compared to non-adaptive RT. The dose to most of the OARs, measured with a range of parameters, was decreased using online adaptive RT, although generally, the differences were smaller than 2 standard errors. Treatment planning objectives were fulfilled more often with online adaptive RT than non-adaptive RT for the CTV, PTV, rectum, bladder, urethra and penile bulb.

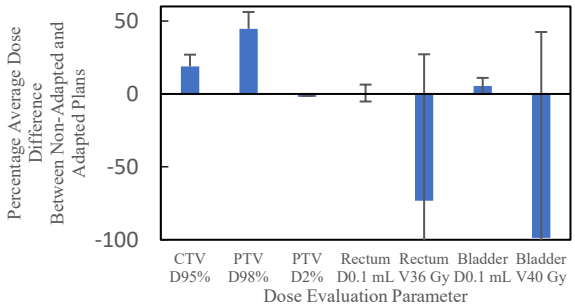

Figure 1. Average difference in dose evaluation parameters between non-adaptive and online adaptive RT, with the average values for non-adaptive RT as the baseline, for the CTV, PTV, rectum and bladder in prostate cancer patients. Error bars represent 2 standard errors.

Similar results were seen for pancreatic cancer patients, with increased average target coverage and an average reduction in most OAR dose evaluation parameters using online adaptive RT. Treatment planning objectives were fulfilled more often with online adaptive RT for the duodenum and jejunum and ileum, but less often for the stomach.

Conclusions: Online adaptive RT using the Elekta Unity (Elekta AB, Stockholm, Sweden) demonstrates a benefit to target coverage and a possible dosimetric benefit to OARs for prostate cancer and pancreatic cancer.

Acknowledgements: I would like to thank the GenesisCare team at St Vincent's Hospital for providing me with the data, tools and support necessary for the project.

References:

1. D. Winkel et al., *Clin. Transl. Radiat. Oncol.* **18**, 54–59 (2019).
2. A. Dunlop et al., *Clin. Transl. Radiat. Oncol.* **23**, 35–42 (2020).
3. L.-E. D. Schumacher et al., *Br. J. Radiol.* **93**, 0028 (2020).

AUS MRinRT

ADAPTIVE MR GUIDED RADIOTHERAPY FOR HEAD & NECK CANCER: FIRST GENESISCARE EXPERIENCE

M Picton[1], V Batumalai[1,2], D Crawford[1], C Pagulayan[1], C Tran[1], L McKenzie[1], U Jelen[1], N Dunkerley[1], S Sampaio[1], M Heinke[1], T Twentyman[1], M Jameson[1,2], J de Leon[1], D Forstner[1,2]

[1] GenesisCare, New South Wales, Australia
[2] School of Clinical Medicine, Faculty of Medicine and Health, UNSW Sydney, Australia

Introduction: MR-guided radiotherapy (MRgRT) is able to deliver adaptive RT in the online or offline setting. The treatment strategies of the Unity (Elekta AB, Stockholm, Sweden) MR-Linac system include Adapt-to-Position (ATP) and Adapt-to-Shape (ATS) [1]. The ATP workflow is a standard image-guided RT workflow and is able to be quickly executed, however restricted to a rigid translational registration and a limited optimizer that works to strictly reproduce dosimetric characteristics of the reference plan. In contrast, the ATS approach involve a full online adaptive workflow performed with deformable registration, target and organs at risk (OAR) delineation, and plan re-optimisation, therefore significantly more time consuming than the ATP approach. Recently, a novel simplified ATS strategy called ATS-Lite was introduced and provides adaptive RT without requiring daily online target and OARs delineation [2]. We present our early experience of adaptive MRgRT for head and neck cancer on a 1.5T MR-Linac.

Materials and Methods: One patient with unresected adenoid cyctic carcinoma of the hard palate (T4bN0M0) received radical RT on the MR-Linac. Primary tumour and high risk regions were treated with 3 dose levels (70, 60 and 54 Gy) in 35 fractions. For daily treatments, an automatic fusion between the rerefence image and daily MRI image was performed, where the patient contour, target and OAR volumes were assessed. The MR fusion was adjusted to provide a best fitting match of the volumes for that fraction. OAR constraints were prioritised over the planning target volume (PTV) coverage. Each fraction was adapted using the ATP workflow. If the OAR dose metrics were met and the volumes were within tolerance, the treatment was delivered. However, in the event of dose constraint violations, the plan was re-optimised (ATS-Lite).

Results: The patient received 6 fractions with the ATS-Lite workflow while the remaining fractions were treated with ATP workflow. The mean treatment time with the ATP and ATS-Lite workflow was 23.3 minutes (range 20-30 minutes) and 35.5 minutes (range 31-38 minutes), respectively. The patient's weight remained consistent throughout the course of RT. Median doses achieved comparing ATP and ATS-Lite fractions for PTVs and selected OARs are summarised in Table 1. All other OAR constraints assessed were met for all 35 fractions. The ATP fractions achieved better target coverage while the ATS-Lite fractions prioritised the OAR dose limits (Fig 1).

Table 1: Median dose achieved for ATP and ATS-Lite fractions

Structure	Criteria	ATP	ATS-Lite
PTV 70	D98% >65.1Gy	61.2	59.7
	D95% >66.5Gy	62.6	61.2
PTV 60	D98% >55.8Gy	55.4	54.0
	D95% >57Gy	57.3	56.0
PTV 54	D98% >50.2Gy	54.3	53.7
	D95% >51.3Gy	56.5	55.6
Left optic nerve	D0.1cm^3 <60Gy	59.9	58.7
Left cochlea	D0.1cm^3 <45Gy	45.5	44.3
Left lens	D0.1cm^3 <8Gy	8.4	8.0
Temporal lobe	D0.1cm^3 <70Gy	70.4	69.0

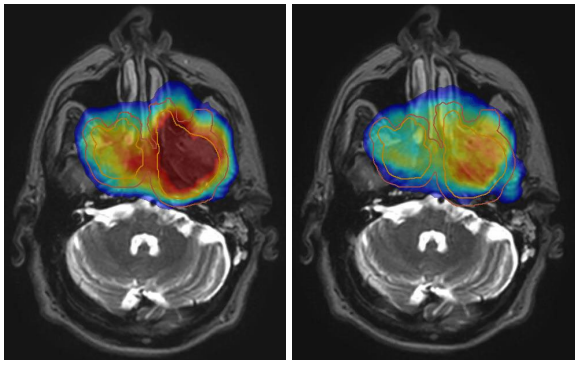

Figure 1: Example of ATP at fraction 3 (left) and ATS-Lite at fraction 4 (right) plans. Isodose is displayed from 54 to 70Gy.

Conclusion: Our early data show that the ATS-Lite workflow provided a robust online treatment planning approach to deliver adapted dose on the MR-Linac. The ATS-lite workflow provided an option to re-optimise the plan when dose constraint violations to OARs occurred, without the need for a full ATS approach. We plan to further utilise and develop the ATS-Lite technique for other clinical indications, e.g. liver.

References:

1. Winkel D et al. Adaptive radiotherapy: The Elekta Unity MR-linac concept. *Clin Transl Radiat Oncol*. 2019;18:54–9
2. Newbold et al. Online adaptive radiotherapy for head and neck cancers on the MR linear Accelerator: Introducing a novel modified Adapt-to-Shape approach. *Clin Transl Radiat Oncol*. 2022;32:48–51

AUS MRinRT

ASSESSING REAL-TIME LIVER MOTION MONITORING ON THE ELEKTA UNITY MR-LINAC

Parmoun Daghigh[1], MadelineCarr[2], TaniaTwentyman[2], David Crawford[2], Maddison Picton[2], Jeremy De Leon[2], Vikneswary Batumalai[2], Gerard Perera[3], Michael Jameson[1,2]

[1] Institute of Medical Physics, School of Physics, Sydney University, Sydney, Australia, pdag5970@uni.sydney.edu.au
[2] GenesisCare, New South Wales, Australia
[3] Elekta AB, Stockholm, Sweden

Introduction: The ability to monitor inter- and intra-fraction organ motion is provided by MR-Linac [1]. Currently, Elekta is using 2D balanced fast field echo (bFFE) orthogonal cine MRI to develop gating for the 1.5T Unity MR-Linac system [2]. The purpose of this study was to demonstrate the abilities of Elekta's updated pre-released gating motion monitoring research package (MMRP) to monitor liver tumour motion. This study was completed by quantifying the motion of three liver stereotactic body radiotherapy (SBRT) patients.

Material and methods: The data for three Unity SBRT liver patients were analyzed retrospectively, using MMRP. The software algorithm generates a template based on the initial T2/T1-weighted bFFE images. This is registered to the corresponding T2-weighted 3D navigated reference MR image and incoming cine images for target tracking. The internal target volume (ITV) was selected as the target structure and the gating envelope was set to the clinical planning target volume (PTV) (PTV = ITV + 0.5cm uniformly distributed) (figure 1).

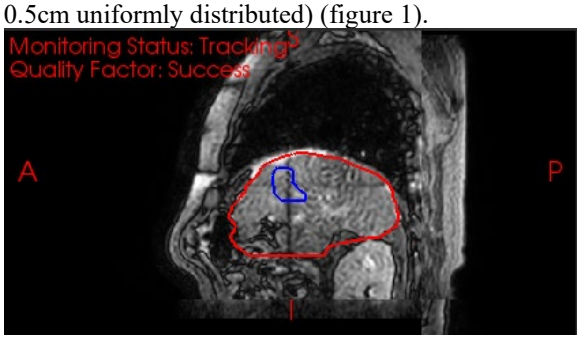

Figure 1. Modified screenshot from MMRP. The red contour represents the surrogate structure for tracking (liver) and the blue contour represents the ITV. PTV is not displayed.

The cine images were acquired with a temporal resolution of 0.2 s within the acquisition time (more than 7 minutes for each patient). The ITV displacement vector was tracked to investigate if it remained within the PTV thresholds and if the tracking quality was reported as successful.

Results: Qualitatively, tracking all target structures was achieved successfully by the MMRP. The quantitative average (SD) target displacement found over the three patients in the Right(R)-Left (RL), Anterior(A)-Posterior (AP) and Superior(S)-Inferior (SI) is reported as 0.43R (0.25), 1.23A (0.38) and 0.64S (0.47) mm respectively. Displacement plots can be found in figures 2 and 3. Additionally, the proportion of duration of the beam on time for each patient was reported as 89.7%, 79.2% and 94.1%. This demonstrates sufficient tracking during treatment and minimal target motion outside of the set threshold.

Figure 2. The target displacement vs image index (resolution = 0.2s) for one patient. Blue, orange, and grey represent average RL, AP, and SI displacement, respectively.

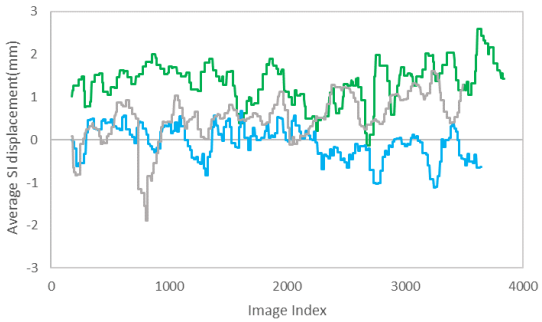

Figure 3. The target displacement in the SI direction vs image index (resolution =0.2s) for all three patients. Green, blue and grey, in this case, represent patient 1, patient 2 and patient 3.

Conclusion: Qualitatively, MMRP was able to successfully track all target structures. Targets remained within the PTV thresholds for at least 79.2% of the time. Such treatment tracking innovation could result in safely reduced treatment margins in the future. Further investigations would involve validating these findings on larger patient datasets, for multiple anatomical sites and over multiple fractions.

References:

1. Feasibility of real-time motion tracking using cine MRI during MR-guided radiation therapy for abdominal targets. (Keiper TD et al.). Medical physics (Lancaster) 47(8): 3554–3566 (2020).
2. Dosimetry impact of gating latency in cine magnetic resonance image-guided breath-hold pancreatic cancer radiotherapy. (Hu et al.), Physics in medicine and biology. 67(5):55008 (2022).

AUS MRinRT

MOTION EVALUATION FOR THE ABDOMEN IMAGING ON ELEKTA MR-LINAC.

Reza Alinaghizadeh[1], Jessica Lye[1], Leah McDermott [1], Felicity Height[1], Richard Khor[1], Sandra Fisher[1]

[1] Olivia Newton John Cancer Wellness and Research Centre, Austin Health, Reza.Alinaghizadeh@austin.org.au

Introduction: MRI provides great soft tissue contrast in the abdominal area [1]. Respiratory motion in the abdomen introduces uncertainties in target delineation, which will increase dosimetric uncertainty in patient treatment. The aim of this study was to evaluate the impact of respiratory motion on target delineation for upper abdomen patients at ONJ.

Method: The The Zeus MRgRT Motion Management QA phantom (CIRS) was used with different breathing waveforms (patient and synthetic) and imaged with the Elekta-recommended MRI T2 3D sequences for abdomen with and without a navigator. BFFE Cine mode was used to evaluate the imaging phase and shifts of the phantom [2]. All imaging evaluation was performed with MIM Maestro software (version 6 USA).

Results: The phantom images in Figure 1 showed that T2 3D Navigated images provide a clear image in exhale phase. For T2 3D imaging, with both the synthetic Cos6 waveform and slow breathing patient waveform, images are slightly noisier than no motion or the Navigated image (depending on the motion amplitude). However, they still show the target in the exhale phase. When the Sin waveform or saw-tooth patient breathing pattern was used, the T2 3D images became noisier with some blurring of borders, but were still similar to the exhale image. The noise reduction algorithm in the sequence reduced the motion artefact and made the image appear to be in exhale rather than the time weighted average position.

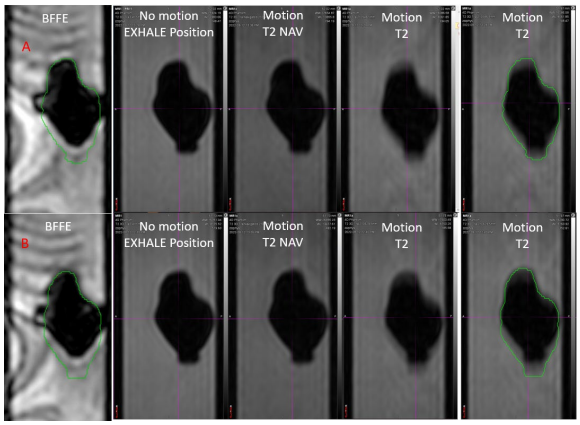

Figure 1: phantom target image with 2 different waveforms, with and without motion and navigator.

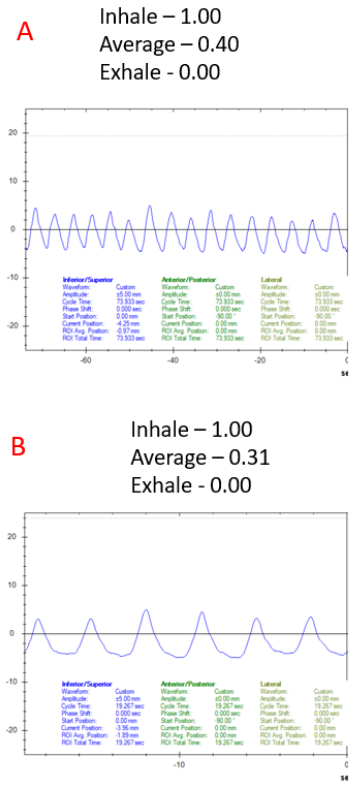

Figure 2: different patient waveforms used for the imaging.

Conclusion: This study showed the importance of performing a phantom study prior to a clinical study, to identify the sequence limitations and possible miss-guidance in target delineation and ITV expansion. Also, using the Cine imaging fused with 3D images is a great tool for checking the target motion, integrity and imaging phase for proper target delineation and expansion for ITV creation.

References:

1. Stanescu et al. MRI-Guided Online Adaptive Stereotactic Body Radiation Therapy of Liver and Pancreas Tumors on an MR-Linac System, Cancers 2022, 14, 716.
2. Yuichi Akinoa, Evaluation of potential internal target volume of liver tumors using cine-MRI, Med. Phys. 41 (11), November 2014

AUS MRinRT

PERSONALISED LIVER STEREOTACTIC BODY RADIATION THERAPY USING MAGNETIC RESONANCE IMAGING: THE PRISM CLINICAL TRIAL

Sirisha Tadimalla[1], Tim Wang[2], Val Gebski[3], Sheryl Foster[4,5], Vincent Lam[6], Jonathan Sykes[2], Robert Finnegan[1,7,8], Jacob George[9], Verity Ahern[2], Steven Sourbron[10], Annette Haworth[1]

[1] Institute of Medical Physics, The University of Sydney, Australia, sirisha.tadimalla@sydney.edu.au
[2] Sydney West Radiation Oncology Network, Western Sydney Local Health District, Australia
[3] NHMRC Clinical Trials Centre, University of Sydney, Australia
[4] Department of Radiology, Westmead Hospital, Australia
[5] Sydney School of Health Sciences, Faculty of Medicine and Health, The University of Sydney, Australia
[6] Acute Surgical Unit, Westmead Hospital, Australia
[7] Ingham Institute of Applied Medical Research, Liverpool, Australia
[8] Northern Sydney Cancer Center, Royal North Shore Hospital, Australia
[9] Department of Gastroenterology and Hepatology, Westmead Hospital, Australia
[10] Department of Infection, Immunity and Cardiovascular Disease, University of Sheffield, UK

Introduction: Stereotactic body radiation therapy (SBRT) is an emerging treatment option for patients with hepatocellular carcinoma (HCC). Baseline liver function, typically described by the Child-Pugh (CP) score determines dose constraints to the non-tumour liver, in turn limiting the dose delivered to the gross tumour volume (GTV)[1]. Therefore, for many patients with impaired liver function, SBRT is offered as a palliative option. However, patients with HCC can have a high degree of spatial variation in liver function due to underlying cirrhosis, providing a potential opportunity to optimize dose distributions to spare higher functioning sub-sections of the liver

In this study, **Per**sonalised **li**ver **S**BRT using **m**agnetic resonance imaging (**PRISM**) is proposed in which liver function will be spatially mapped using magnetic resonance imaging (MRI) to create function based SBRT treatment plans where radiation dose to high functioning regions of the liver is minimised, and low functioning liver is sacrificed to maximise the dose delivered to the GTV. The feasibility of a) identifying regions of high and low liver function using MRI, b) SBRT treatment planning guided by liver function maps and c) mid-treatment adaptation of dose plans using mid-treatment MRI will be investigated in the PRISM clinical trial.

Materials and Methods: In the pilot phase of this study, patients with HCC or liver metastases eligible for liver SBRT will be recruited. It is planned to recruit a total of 30 patients in three stages – Stage 1 will gather preliminary data from 5 participants to optimise the study design; Stage 2 will evaluate the potential of MRI to distinguish between high and low functioning regions of the liver and spatially define changes in liver function after irradiation on a further 10 patients; and Stage 3 where data will be collected for a further 15 participants. The number of patients with liver metastases will be limited to <1/3rd of study participants to include good and impaired baseline liver function. Participants will undergo pre-, mid-, and 3-month post-treatment MRI scans for liver function mapping. Indocyanine green (ICG) clearance test[3] will be performed prior to each MRI scan as surrogate measure of global liver function.

Results: The study has received ethics approval (WSLHD-HREC: 2022/ETH00203) and recruitment will commence in October 2022. Imaging protocols have been developed and will include diffusion-weighted imaging (13 b-values 0-800 s/mm2) for intravoxel incoherent motion (IVIM) modelling. Dynamic contrast enhanced (DCE) MRI in ***free breathing*** was added to a standard liver MRI protocol. A healthy volunteer was scanned without contrast injection. Example IVIM parametric maps (diffusion coefficient D, perfusion fraction *f*) and DCE-MRI frames (t=0, 7 and 14 sec) are shown in Figure 1.

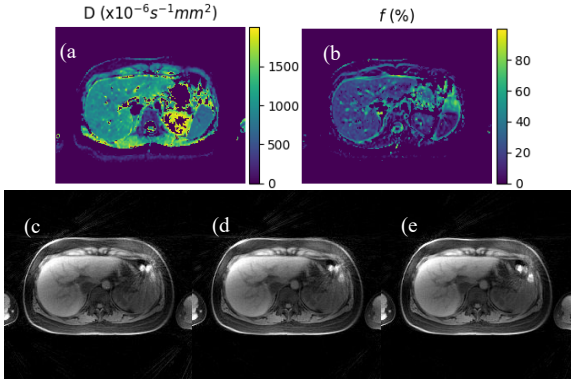

Figure 1. IVIM parametric maps a) D and b) f, and DCE time series at c) t=0 d) t=7sec and e) t=14sec.

Conclusions: An MRI protocol for liver function mapping has been developed for the PRISM clinical trial to establish the feasibility of personalised liver SBRT using MRI for patients with HCC.

Acknowledgements: We acknowledge the Sydney-West Radiation Oncology Network for supporting this work and funding Stage 1 of the study. We thank A/Prof. Tobias Block, Dr. Jonathan Goodwin, Ms. Kate Skehan, Ms. Yu-Feng Wang and Siemens Healthineers for their support on the MRI protocol.

References:

1. Stereotactic body radiotherapy in the management of hepatocellular carcinoma (H. Y. Liu et al.), *JMIRO*, **65**, 365–373 (2021).
2. Using Indocyanine Green Extraction to Predict Liver Function (K. Suresh et al.), *Int. J. Radiat. Oncol*. **100**, 131–137 (2018).

AUS MRinRT

INITIAL EXPERIENCE WITH DAILY ART FOR APBI ON UNITY

Sarah Elliott, Felicity Height, Jenna Dean, Sandra Fisher, Robert Behan, Reza Alinaghizadeh, Benjamin Harris, Rachel Farrell, Michael Chao, Farshad Foroudi, Sweet Ping Ng
ONJCWRC, Department of Radiation Oncology, Austin Health, Heidelberg, Victoria, sarah.elliott@austin.org.au

Introduction: An Elekta Unity 1.5T MRI Linac has been clinically operational at our centre since August 2021. Recruitment for breast cancer patients begun in April of 2022. This is a report of our initial experience with daily adaptive radiotherapy (ART) for breast cancer using the Unity in the adapt-to-position (ATP) workflow.

Materials and Methods: Patients with localised breast cancer meeting eligibility for accelerated partial breast irradiation (APBI) were enrolled on the prospective FIRM study.
Patients were simulated in a personalised cradle flat on the couch with arms raised above their head. CT and MRI scans were acquired in treatment position on the day of simulation. Individual treatment plans for the Unity and standard linac were created for each case using Monaco Treatment Planning System v5.51.11. Unity plans were designed with a range of Step and Shoot IMRT fields (6-15 fields) and optimised to meet the established local clinical guidelines. Treatments are scheduled across a 2-week period on the Unity. All patients currently have a Fraction 0, where the process of treatment is completed up to the point of treatment delivery to ensure reproducibility, highlight any changes in target size or position and patient tolerability of the procedure.
Treatment times are recorded from the patient entering the room and at different time points throughout each session.
In-vivo dosimetry was performed with Gafchromic EBT3 film for the first five patients to assess skin dose in the treatment field.
Daily setup variability was quantified by recording the isocentre shifts along the x (left/right), y (superior/inferior) and z (anterior/posterior) axes at each ART delivery, and assessed by calculating the average systematic error, standard deviation of the systematic error and standard deviation of the random error of the isocentre shifts using Van Herk's method (1).
Quality assurance was performed with an MR-compatible cylindrical diode array using 3%/3mm gamma criteria.

Results: Six APBI patients received daily ART using ATP. Four right-sided and two left-sided patients were treated with a prescription dose of 30 Gy in 5 fractions. The total number of adapted treatments delivered was 27, with one patient transferred to the conventional linac during their treatment due to a machine breakdown.
The online plan re-optimisation method was 'optimise weights' or 'optimise weights and shapes' for seven and twenty treatments respectively. Isodoses and dose constraints were reviewed online by the multidisciplinary team for each plan. Rescaling or changing optimisation parameters was utilised when necessary; the main variations observed were higher doses to targets, contralateral breast dose and skin dose. The mean monitor units for ATP plans was 996 (range: 890-1136), which is slightly lower than the mean for the reference plans of 1042. Prior to treatment delivery, an MRI bFFE sequence was acquired with the target structure displayed on the images, to observe patient breathing motion.

Treatment stage	Mean time (range) in minutes
Patient setup to beam on	37 (27-52)
Beam delivery	7 (4-17)
Total treatment time (Patient in to patient exit)	48 (37-63)

Figure 1. Approximate overall time data from treatments

In-vivo dosimetry showed skin dose in the high dose region of the planning target volume was between 60-90% of the prescription dose across all patients, and within the dose ranges calculated by Monaco.
The absolute mean systematic error of all isocentre shifts for this patient cohort was <1.5mm in all 3 orthogonal directions. Systematic and random errors were <4mm and <3mm respectively. The maximum absolute value isocentre shifts in any single fraction were 5.5, 9.6 and 6.8mm in the x, y and z directions respectively. Analysis of isocentre shifts indicates good reproducibility in patient positioning to date.
Intensity modulated radiation therapy quality assurance (IMRT QA) was performed for every reference and adapted plan following treatment, using ArcCHECK MR, with 3% dose/3mm distance to agreement gamma criteria, a threshold value of 10% and a tolerance limit of gamma ≥95%. All reference and daily fractions passed QA. Furthermore, the mean overall 2%/2mm pass rate was >94.6% (range: 91.2-100%).

Conclusions: The aim of this work was to describe our department's experience for treating APBI on the Unity through an analysis of six cases treated with an online ATP workflow to date. Adapted treatment plans showed consistency with clinical guidelines and reference plans. Total treatment times were under 50 minutes, all treatment plans passed IMRT QA, and patient immobilisation in the extended vac-bag showed good reproducibility.

References:

1. Errors and Margins in Radiotherapy (M. Van Herk), *Seminars in Rad Onc.* **14(1)**, 52-64 (2004).

AUS MRinRT

CLINICAL APPLICATIONS OF APTW CEST IMAGING IN BRAIN CANCER DIAGNOSIS AND TREATMENT

Marco Mueller[1], Patrick Liebig[1], Kieran O'Brien[1]
[1] Siemens Healthineers, marco.mueller@siemens-healthineers.com

Introduction: Magnetic resonance (MR) imaging is well known for its variety of image contrasts. MR spectroscopy imaging to probe for chemical compounds and metabolites related to the body's physiological function and pathological conditions can support cancer diagnosis and treatment [1]. This talk reviews the application of Chemical Exchange Saturation Transfer (CEST) imaging to brain tumour imaging in a clinical setting at 3T.

Materials and Methods: CEST imaging indirectly measures mobile protein and peptide content in tissue using a continuous process of re-saturation of biomolecules with attached protons that can undergo exchange with bulk water molecules [2]. CEST is based on common anatomical imaging sequences and can therefore benefit from well-known fast acquisition strategies, as well as improved spatial resolution over other MR spectroscopy techniques. Recently, technological advances enabled the transition of CEST imaging from advanced 7T MRI scanners to the common clinically available field strength 3T, paving the way for wide-spread clinical use.

Amide proton transfer-weighted (APTw) imaging is a CEST imaging technique that generates image contrast by radio frequency saturation labelling of the water-exchangeable backbone amide proton pool of proteins and peptides in tissue [3]. The amide protein content is higher in areas of elevated cellular density and proliferation, which are increased in aggressive tumours [4]. Studies world-wide have demonstrated that APTw imaging adds clinical value to the standard MRI procedures in brain cancer diagnoses, including the detection and grading of tumours [5], and prognosis related to tumour progression and survival [6]. APTw imaging can help to distinguish treatment effect from tumour recurrence in patients with glioma who underwent radiation treatment [7, 8], and to monitor the early radiation treatment effects [9], which results in the destruction of the cytoplasm, increasing the mobile protein content.

Despite the promising initial results, challenges remain for a widespread clinical implementation of APTw imaging [10]. APTw signal intensities depend on the APTw pulse sequence features and parameters, which may lead to differences in image contrast and in interpretation between sites and patients [3]. Large variations in imaging parameters as well as differences in image reconstruction, post-processing and analysis strategies complicate the reproducibility and comparability of results between studies in the literature.

This knowledge gap can be filled by creating and validating common guidelines to establish an optimised, reproducible, and standardized APTw imaging approach applicable to clinical 3T MRI scanners. One way clinical evidence can be collected is from multi-institutional clinical trials in collaboration between healthcare institutions and industry.

Conclusions: APTw CEST imaging has the demonstrated ability to enhance diagnostic specificity in brain tumour assessment. Reducing contrast variability across sites and patients will improve the clinical value of APTw imaging as a biomarker in the assessment of brain tumours at 3T. This will allow medical centres worldwide to routinely use APTw MRI in daily clinical practice in cancer diagnosis and treatment.

References:

1. Wu, B., et al., *An overview of CEST MRI for non-MR physicists.* EJNMMI physics, 2016. **3**(1): p. 1-21.
2. Van Zijl, P.C. and N.N. Yadav, *Chemical exchange saturation transfer (CEST): what is in a name and what isn't?* Magnetic resonance in medicine, 2011. **65**(4): p. 927-948.
3. Zhou, J., et al., *Review and consensus recommendations on clinical APT-weighted imaging approaches at 3T: Application to brain tumors.* Magnetic Resonance in Medicine, 2022.
4. Otazo, R., et al., *MRI-guided radiation therapy: an emerging paradigm in adaptive radiation oncology.* Radiology, 2021. **298**(2): p. 248-260.
5. Wen, Z., et al., *MR imaging of high-grade brain tumors using endogenous protein and peptide-based contrast.* Neuroimage, 2010. **51**(2): p. 616-622.
6. Regnery, S., et al., *Chemical exchange saturation transfer MRI serves as predictor of early progression in glioblastoma patients.* Oncotarget, 2018. **9**(47): p. 28772.
7. Chan, R.W., et al., *Quantitative CEST and MT at 1.5 T for monitoring treatment response in glioblastoma: early and late tumor progression during chemoradiation.* Journal of Neuro-Oncology, 2021. **151**(2): p. 267-278.
8. Zhou, J., et al., *Differentiation between glioma and radiation necrosis using molecular magnetic resonance imaging of endogenous proteins and peptides.* Nature medicine, 2011. **17**(1): p. 130-134.
9. Jones, K.M., et al., *Emerging magnetic resonance imaging technologies for radiation therapy planning and response assessment.* International Journal of Radiation Oncology* Biology* Physics, 2018. **101**(5): p. 1046-1056.
10. Zhou, J., et al., *APT-weighted MRI: Techniques, current neuro applications, and challenging issues.* Journal of Magnetic Resonance Imaging, 2019. **50**(2): p. 347-364.

AUS MRinRT

REPEATABILITY OF QUANTITATIVE MRI RADIOMICS IN GLIOBLASTOMA

Philip Martin[1,2], Peter Metcalfe[1,2], Caterina Brighi[2,5], Eng-Siew Koh[2,3,4], Edward Chan[6], Farhannah Aly[2,3,4], Lois Holloway[1,2,3,4]

[1] University of Wollongong, Wollongong, NSW pm603@uowmail.edu.au
[2] Ingham Institute for Applied Medical Research, Liverpool, NSW
[3] Liverpool and Macarthur Cancer Therapy Centres, Liverpool, NSW
[4] University of New South Wales, Sydney, NSW
[5] ACRF ImageX Institute, Sydney, NSW
[6] Department of Radiology, Liverpool Hospital, NSW, Australia

Introduction: Radiomics is a field which utilises quantitative features on medical images and correlates them to clinical endpoints. Radiomic features can be useful as a method for patient diagnosis, prognostication, stratification and clinical decision support for patients with Glioblastoma Multiforme (GBM). To build accurate and reliable radiomics models it is important to ensure that repeatable features are used. The importance of repeatability of quantitative features has been demonstrated in research with models developed on non-repeatable features from a single centre having a lower performance when applied to multicentre data [1].

Quantitative MRI (qMRI) techniques are used to investigate tissue physiological factors such as perfusion or diffusion characteristics. While incorporating qMRI into radiomics has been shown to produce high-performing radiomic models [2], there is a lack of comprehensive studies evaluating the repeatability of radiomic features obtained from qMRI.

Methods and Materials: This study used test-retest imaging to assess the repeatability of qMRI radiomics. qMRI imaging data from 43 patients from The Cancer Imaging Archive (TCIA) was utilised. Patients were scanned twice, less than a week apart without treatment intervention between the scans. Radiomic features were extracted from Diffusion Weighted (ADC) and Perfusion Weighted (DCE) MRI. Gross tumour volume (GTV) was manually contoured by a radiation oncologist. Image standardisation is an important step in the radiomics process where mathematical transformations are applied to make images more comparable. Image standardisation techniques including intensity standardisation (z-score, histogram matching and linear mapping) and noise filtering were applied to the images. Radiomic features were extracted using the PyRadiomics package, all feature classes and image transformations were enabled. The repeatability of individual features within the GTV was assessed by means of Intra-Class Correlation Coefficient (ICC) of features between the two timepoints. Redundancy was assessed by creating a correlation matrix of the extracted radiomic features for each standardisation method. The image standardisation methods were compared in terms of the repeatability and redundancy.

Figure 1 shows part of the process involved in this research. Histograms of ADC values within the GTV have been extracted from each image and are compared.

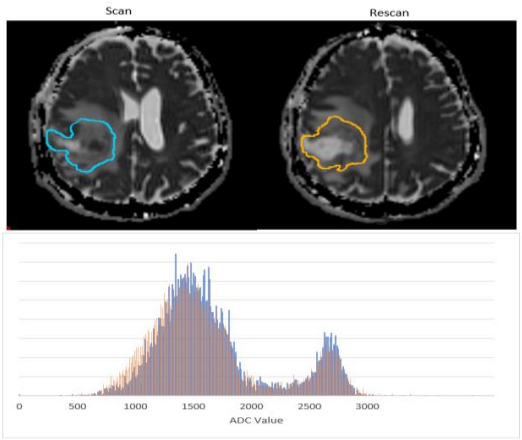

Figure 1 – ADC Images and overlaid GTV histograms (normalized) for scan (blue) and rescan (orange).

Results: No single standardisation method was universally effective for improving the repeatability of radiomics features, different types of standardisation were found to be effective at improving repeatability for different features.

Out of 299 features extracted from ADC images 93 were found to have an ICC greater than 0.95 without the application of standardisation. After z-score standardising 117 features were found to have an ICC above 0.95, these are features that can be considered 'highly-repeatable'.

Conclusion: Of the features extracted, without standardisation around 1/3 were found to be repeatable and as a result useful for a model. Applying image standardisation can increase the number of useful features and thus improve the model.

Implementing qMRI into radiomics models can improve their accuracy and usefulness. Image standardisation can improve radiomics models by allowing more features to be incorporated while maintaining repeatability.

References:

1. Suter et al. 2020, Radiomics for glioblastoma survival analysis in pre-operative MRI: exploring feature robustness, class boundaries, and machine learning techniques, *Cancer Imaging*
2. Park et al. 2020, Radiomics prognostication model in glioblastoma using diffusion- and perfusion-weighted MRI, *Scientific Reports*

AUS MRinRT

INTER-FRACTION T2/FLAIR VARIATION DURING MRI-GUIDED RADIOTHERAPY FOR GLIOBLASTOMA

Dominique Mathieu[1], Su Chen Fong[1], Jodie Tham[1], Morikatsu Wada[1], Richard Khor[1], Sandra Fisher[1], Benjamin Harris[1], Felicity Height[1], Sweet Ping Ng[1]

[1] Olivia Newton-John Cancer Wellness and Research Centre, Austin Health, Heidelberg, Victoria, Australia, dominique.mathieu@austin.org.au

Introduction: Recent progresses in linear accelerator (linac) technology has led to the incorporation of magnetic resonance imaging (MRI) in the radiotherapy (RT) treatment unit. This allows us to obtain updated MRI scans prior to each fraction, and to adapt the treatment plan to account for daily changes in anatomy and tumor. The aim of this study is to quantify the T2 weighted-Fluid-Attenuated Inversion Recovery (T2/FLAIR) inter-fraction variations in patients undergoing RT for glioblastoma (GBM).

Materials and methods: Patients with GBM treated with surgery or biopsy followed by chemoradiation were included. Patients were given daily fractions over 3 or 6 weeks on the Elekta Unity MR-linac using an adapt-to-position workflow. For this study, the T2/FLAIR images were reviewed at every 5th fraction and regions of hyperintensity were manually delineated. The T2/FLAIR hyperintensity volume was quantified as per volume in cubic centimeters (cc) and compared relative to a baseline reference MRI (fraction 0) acquired the day before radiation treatment initiation.

Results: The daily MRIs of 10 patients with GBM were reviewed. The median (range) age was 68 years (43 – 78 years) and 8 patients were men. Five patients were treated to 60 Gy in 30 fractions and 5 patients to 40 Gy in 15 fractions. Median T2/FLAIR hyperintensity volumes at fractions 0, 5, 10, 15, 20 and 30 were respectively 54 cc (12 – 159 cc), 52 cc (13 – 111 cc), 50 cc (12 – 87 cc), 48 cc (12 – 105 cc), 53 cc (34 – 116 cc) and 79 cc (40 – 114 cc). Five patients had ≥ 25% relative T2/FLAIR volume progression compared to fraction 0, with a maximum of 397%. Two patients had T2/FLAIR hyperintensity progression beyond the initial planning target volume (PTV). One patient had signal extension to the contralateral hemisphere via the corpus callosum. Two patients had offline replanning based on disease progression concerns identified on daily MRI.

Conclusion: Significant T2/FLAIR variations may be observed in GBM patient undergoing chemoradiation. MR-linac may be valuable for personalized treatment plan adaptation in patients with significant T2/FLAIR progression.

Acknowledgements: The authors thank Brayden Geary and Georgia Barjaktarovic for their valuable contributions.

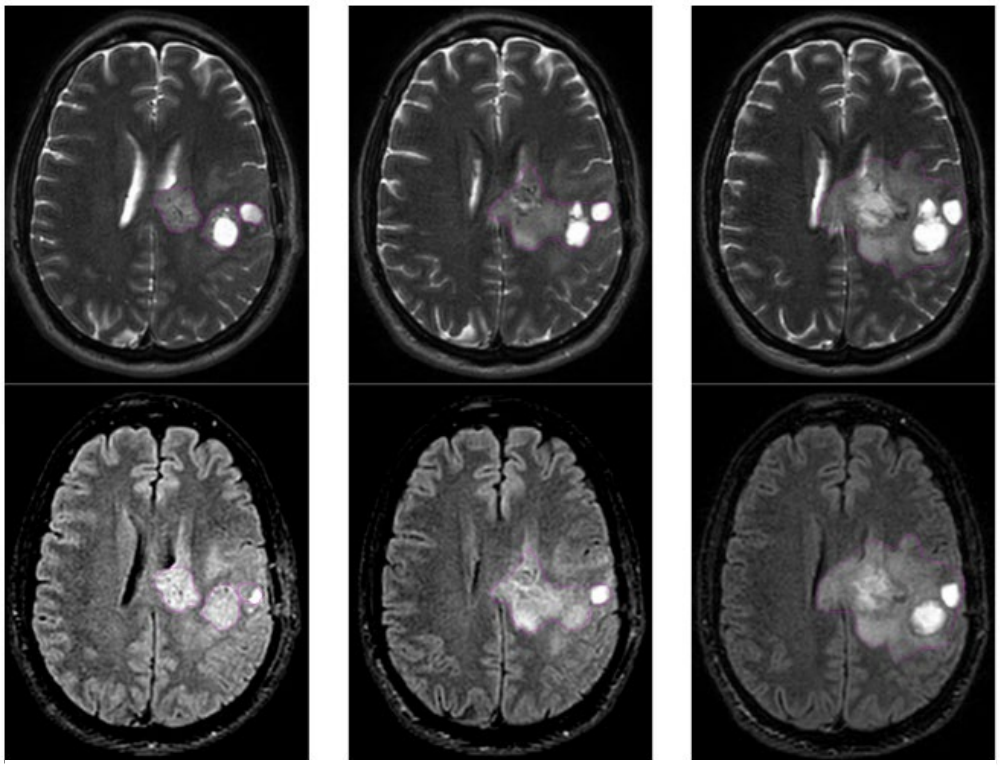

Figure 1: T2/FLAIR signal inter-fraction variations of a 43-year-old patient post biopsy of a left frontoparietal multifocal GBM, IDH1 wild-type, MGMT unmethylated. **Left**: Fraction 0 (volume of 18 cc). **Middle**: Fraction 15 (volume of 29 cc). **Right**: Fraction 30 (volume of 87 cc).

AUS MRinRT

AUTOMATIC SEGMENTATION OF SALIVARY GLANDS AND SKELETAL MUSCLES FOR MR-BASED DAILY ADAPTED HEAD AND NECK CANCER RADIOTHERAPY

Sweet Ping Ng[1], Tai Ermongkonchai[1], Daniel Xing[1], Benjamin Harris[1], Richard Khor[1], Zabed Iqbal[2], Andrew McDonald[2], Houda Bahig[3], Clifton D Fuller4, Carlos E Cardenas[2]

[1] Department of Radiation Oncology, Austin Health Victoria Australia. E-mail address: sweetping.ng@austin.org.au
[2] Department of Radiation Oncology, University of Alabama at Birmingham, USA
[3] Department of Radiation Oncology, Centre hospitalier de l'Université de Montréal, Quebec Canada
[4] Division of Radiation Oncology, The University of Texas MD Anderson Cancer Center, Houston Texas USA

Introduction: Contouring of normal structures for radiation adaptive planning and research remains one of the most time-consuming step. Here we aim to develop an MR-based auto-segmentation model for automated contouring of salivary glands and skeletal muscles in the head and neck for use in treatment toxicities and outcomes assessment. The hypothesis for this study is that high-quality MR-imaging allows for accurate auto-segmentation of these head and neck structures for automated dose response in daily online adaptive radiotherapy.

Materials and Methods: We used The Cancer Imaging Archive's (TCIA) collection from the "AAPM RT-MAC Grand Challenge 2019" to train our model. This collection includes T2-weighted MR images acquired prior to radiotherapy treatment commencement with patients setup in the treatment position. Scans from this collection were manually contoured by two trainees and all were checked by a subspecialized head and neck radiation oncologist to include 18 normal structures, including glands and skeletal muscles. This data was used to train a 3D U-net, using 50 patients for training and 5 for final contour evaluation. The quality of the contours were evaluated using the overlap (Dice Similarity Coefficient – DSC) and distance metrics (95th Hausdorff distance – 95HD), as well as via slice-by-slice evaluation by a radiation oncologist.

Results: The mean (± std. dev.) DSC and 95HD values for all structures across the 5 test patients were 0.85 ± 0.07 and 3.7 ± 3.0 mm, respectively. Radiation oncologist qualitative evaluation of the automatically generated contours deemed all contours within reasonable uncertainty and acceptable for quantitative treatment response assessment. The model were then used to generate structures on intra-treatment MR imaging. These were evaluated by a head and neck radiation oncologist and were deemed appropriate for use with no or minimal adjustments.

Conclusion: We generated a contour dataset and trained an auto-contouring model for comprehensive evaluation of doses delivered to head and neck salivary glands and skeletal muscles throughout the course of head and neck cancer radiotherapy. The accuracy of our model needs to be further validated with external image datasets prior to implementation for treatment response assessment studies are conducted.

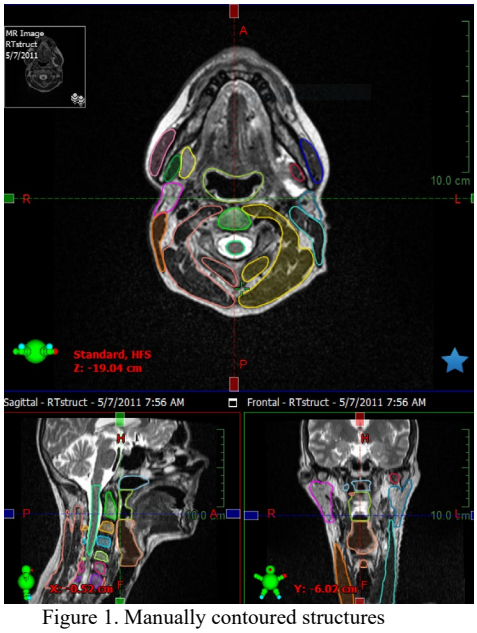

Figure 1. Manually contoured structures

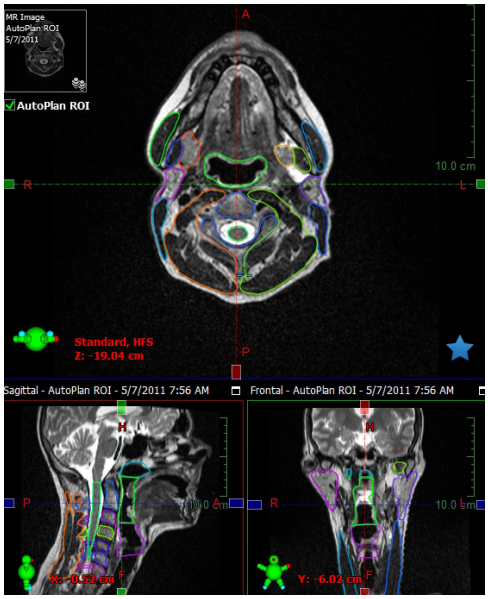

Figure 2. Auto-generated normal structure contours

AUS MRinRT

SEEING THE BEAM: FIRST-TIME IMAGING OF B_0 VARIATION DUE TO THE RADIATION BEAM ON AN MR-LINAC

Stephen Gibson[1], John Baines, Marcus Powers[1], Glenn de Vine[1], Panu Vesanen[2]
[1] Townsville Cancer Centre, Townsville University Hospital, QLD, Australia, stephen.gibson@health.qld.gov.au
[2] Philips Healthcare, Vantaa, Finland

Introduction: Clinical motion management imaging on the Elekta Unity MR-Linac utilizes the balanced fast field echo (bFFE) sequence, which is the Philips implementation of multi-stack balanced steady-state free-precession (bSSFP) cine imaging. This enables rapid, successive acquisition of 1, 2 or 3 orthogonal planes and thereby near real-time target monitoring with excellent soft tissue contrast. Unfortunately, bSSFP is known to be susceptible to a banding artefact which can result from insufficient time between frames for the steady state to be achieved.

The effect of Unity linac gantry angle on B_0 uniformity and of the radiation beam on image noise has been demonstrated [1,2], however until now the effect of the linac beam on B_0 has not been directly mapped.

Materials and Methods: A subtle change of the bFFE banding artefact was observed in a cylindrical water phantom during simultaneous delivery of a clinical IMRT plan. Comparison of cine modulus images with the linac log file confirmed the changes could be due to gantry rotation or x-ray beam on, prompting further investigation.

An unbalanced FFE sequence was used to generate both modulus and phase coronal cine images of the water phantom as FFE does not exhibit the banding artefact and permits a simple relation between phase and B_0. Time was allowed for the steady state to be reached after imaging was initiated, then a further 20 seconds before linac activities were initiated to allow a baseline image to be created, averaged over the whole 20 seconds.

The effect of beam-on and gantry motion were acquired separately in addition to beam limiting device (BLD)-only moves. A 10x10 cm^2 field at gantry 0° was given 100 MU 7 times at intervals of approximately 20 s (i.e. 20 s off, 20 s on, etc.) while coronal modulus and phase images were acquired. The effect of gantry position and movement was assessed by rotating the gantry by 40° every 30 s during coronal imaging without radiation. Similarly, the BLDs were exercised every 20 s during imaging with no beam to distinguish this condition from the beam state effect.

The mean phase across most of the phantom in each cine frame was converted to a mean ΔB_0 from that of the baseline image and correlated with linac state (i.e. beam state, gantry angle, BLD positions). This frame-wise analysis (i.e. single ΔB_0 value per frame) was then extended to voxel-wise for beam state to produce cine ΔB_0 maps, enabling spatial and temporal correlation between the radiation beams and the consequent changes in ΔB_0.

The 10x10 cm^2 field was then given a continuous 1000 MU for each of the 3 orthogonal imaging planes and analysed in the same manner as the 100 MU beams for comparison. Lastly, a chair or 'h' pattern was imaged to demonstrate the agreement between the coronal ΔB_0 maps and the beam aperture.

Results: Gantry movement and beam-on appeared to be correlated with changes in mean ΔB_0, however no discernible effect was seen with BLD-only moves.

The seven coronal ΔB_0 maps in Figure 1 are the average of the 20 seconds after each beam (i.e. beam off period) to illustrate the persistence of the effect. The square field was initially quite distinct, persisting between beams and building up to the third beam, but dissipated despite the further 4 beams.

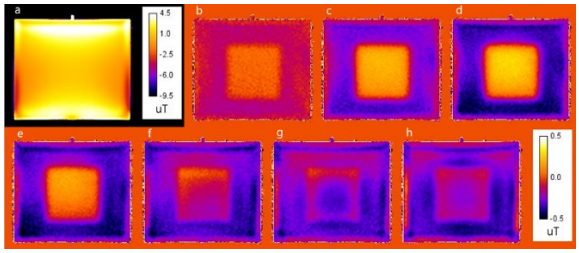

Figure 1. Coronal plane ΔB_0 after each of 7 100 MU beams

The 1000 MU coronal maps were similar to those in Figure 1, although the signal reversal was more pronounced. The images in the sagittal plane were expected to show the diverging beam seen in the transversal images, however no spatial information about the beam could be recovered; instead, a checkerboard-like pattern was seen to develop over the course of the sagittal acquisition.

Conclusions: MR imaging of the radiation beam has been demonstrated for the first time. In this analysis the change in B_0 is transient and does not appear to scale with dose. The magnitude of ΔB_0 attributable to the beam is typically less than 1 μT and therefore is not expected to effect modulus imaging geometric integrity. While it is unclear what physical processes are causing this effect, it is hoped that as they become better understood it may be harnessed for clinical application.

References:

1. MRI commissioning of 1.5T MR-linac systems – a multi-institutional study (R. Tijssen et al), *Radiotherapy and Oncology* **132**, 114-120 (2019).
2. Longitudinal Stability of MRI QA up to Two Years on Eight Clinical 1.5 T MR-Linacs (A. Wetscherek et al), *Frontiers in Physics* **10**, 526 (2022).

AUS MRinRT

OFFLINE AND ONLINE LSTM NETWORKS FOR RESPIRATORY MOTION PREDICTION AT MR-LINACS

Elia Lombardo[1,*], Yuqing Xiong[1], Moritz Rabe[1], Lukas Nierer[1], Davide Cusumano[2], Lorenzo Placidi[2], Luca Boldrini[2], Stefanie Corradini[1], Maximilian Niyazi[1], Michael Reiner[1], Claus Belka[1,3], Marco Riboldi[4], Christopher Kurz[1], Paul Z. Y. Liu[5,6], David E. J. Waddington[5,6], James Grover[5,6], Paul J. Keall[5,6] and Guillaume Landry[1]

[1] Department of Radiation Oncology, University Hospital, LMU Munich, Munich, Germany
[2] Department of Medical Physics, Faculty of Physics, Ludwig-Maximilians-Universität München, Garching, Germany
[3] German Cancer Consortium (DKTK), Munich, 81377, Germany
[4] Fondazione Policlinico Universitario Agostino Gemelli IRCCS, Rome, Italy
[5] ACRF Image X Institute, University of Sydney Central Clinical School, Sydney, NSW, Australia
[6] Department of Medical Physics, Ingham Institute for Applied Medical Research, Liverpool, NSW, Australia
* elia.lombardo@med.uni-muenchen.de

Introduction: Gated beam delivery based on cine MRI is clinically used on the MRIdian 0.35 T MR-linac (Viewray Inc, USA) to manage intra-fractional respiratory motion [1]. Gating has been shown to reduce healthy tissue dose, however, it comes with drawbacks such as increased treatment times and the need for patient compliance. Multileaf collimator (MLC)-tracking could address these limitations; however, the total system latency (≈ 350 ms) needs to be accounted for in real-time [2]. Long short-term memory (LSTM) networks are machine learning models which capture temporal dependencies of the input and are therefore ideally suited for motion prediction. We implemented LSTMs for the prediction of future tumor centroid positions based on clinically acquired 4 Hz sagittal 2D-cine MRIs and compared them with linear regression (LR) models.

Materials and Methods: We collected 556 cine MRIs from 88 patients treated with breath-holds and gating with a MRIdian MR-linac at the University Hospital of the LMU (lung, pancreas, heart, liver, mediastinum). Superior-inferior (SI) motion traces of the target centroid were extracted from the cine MRIs using in-house software. Breath-holds were excluded, and the traces were normalized and smoothed by performing outlier replacement and applying a moving average filter. These patients were sub-divided in training (60%), validation (20%) and testing (20%) sets. Additionally, 15 cine MRIs from 3 patients treated in free-breathing with a MRIdian MR-Co60 at the Fondazione Policlinico Universitario Agostino Gemelli were collected and used as a second testing set (lung and pancreas). Stateless LSTM networks were optimized with two different training schemes to predict the future centroid position in 250 ms, 500 ms, and 750 ms. For the *offline* LSTM, we iteratively optimized on the training set and applied the model unchanged to current motion. For the *offline+online* LSTM, we loaded the weights of an *offline* LSTM and re-optimized continuously on recent motion. We implemented a LR as baseline predictor and analytically solved it using two schemes. The *offline* LR is solved using data analogously to the *offline* LSTM while for the *online* LR we continuously solved from scratch based on recent motion.

Results: The *offline+online* LSTM performed best for all forecast times for both testing sets, achieving a RMSE (500 ms forecast) of 1.20 mm and 1.00 mm while the best performing LR model achieved a mean RMSE of 1.42 mm and 1.22 mm for the LMU and Gemelli testing set, respectively. Qualitatively, we found the LSTM to overshoot more but to more accurately predict steep inhalations and exhalations (Figure 1).

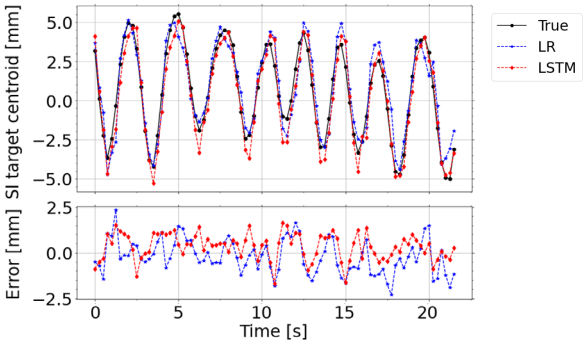

Figure 1. Comparison of ground truth motion (black), LSTM prediction (red) and LR prediction (blue) for a Gemelli testing set (MR-Co60) patient with baseline drift for the 500 ms forecast.

Conclusions: LSTM networks have potential as respiratory motion predictors and could be used to compensate for the system latencies present in MRgRT with MLC-tracking. An experimental validation of the implemented models on the Australian 1.0 T MR-linac is ongoing.

Acknowledgements: DFG research training group GRK 2274.

References:

1. First clinical implementation of real-time, real anatomy tracking and radiation beam control (O. Green et al.), *Med. Phys.* **45**, 3728-40 (2018).
2. Dosimetric evaluation of MRI-guided multi-leaf collimator tracking and trailing for lung stereotactic body radiation therapy (P. Uijtewaal et al.), *Med. Phys.* **48**, 1520-32 (2021).

AUS MRinRT

BEAM MATCHING FOR TWO 1.5T MR LINACS

A S Chhabra[1], K Y T Biggerstaff[1], U Jelen[2], M G Jameson[3,4], D Waterhouse[1]
[1] GenesisCare SJOG, Murdoch WA, Australia Amrinder.Chhabra@genesiscare.com
[2] GenesisCare, Darlinghurst NSW, Australia
[3] GenesisCare, Alexandria, NSW, Australia
[4] Faculty of Medicince & Health, The University of New South Wales, Sydney, Australia

Introduction: The concept of radiation beam matching applies to medical linear accelerators (LINACs) that have identical characteristics including model, radiation quality, and multileaf collimator features (1). We have performed a preliminary study to investigate the possibility of beam matching for two Elekta Unity MR LINACs, one installed at GenesisCare St. Vincent Hospital NSW and other at GenesisCare Murdoch WA.

Methods: As of now there is no vendor-defined ''fine beam-match'' criteria for Unity, Beam energy and wave guide angulation were modified to match beams during device acceptance testing and extended comparison was carried out during commissioning. St. Vincent Hospital machine is named as ACE and Murdoch one is named as K2. The beam matching criteria were based on the percentage depth dose (PDD), beam profile, output factors for field sizes 2x2, 3x3, 5x5, 10x10, 15x15, 22x22, 40x22 & 57x22 cm at Gantry angles 0 & 270 degree. Dosimetry measurements were carried out by using an PTW ionization chamber, farmer chamber of 0.125 & in 0.6 cm^3 volume and PTW microdiamond detector. An analysis of PDD and profile data was performed for different field sizes to evaluate beam matching. Beam profiles of both machines were analysed for γ-value with Monaco Commissioning Utility (MCU) software. Profiles at depth of dmax, 5cm and 10cm were analysed. Further γ passing and was point dose measurements evaluated for 5 plans for 4 different sites (Prostate, Liver, and Oligo Pelvic & Oligo Abdomen nodes) with SNC MR ArcCheck.

Results: The results indicated that the PDD10 of 7FFF photon beams for 10x10cm field size for both LINACs have excellent compatibility each other with a deviation of less than 0.5%. The TPR 20/10 for 10 × 10 cm^2 was well matched, showing energy differences pf 0.71%. γ-index passing rate for field sizes upto 20x22 shows excellent match with 100% passing at 1.0 % of DD, 1 mm of DTA. Profiles for Field sizes 40x22 and 57x22 passes with 2.0 % of DD, 3 mm of DTA. Output factor shows maximum difference of 0.4% (Table 1).

Table Below: Output factor for both Linacs

Table 1: Output Factor Comparison			
Field Size (cm)	ACE	K2	% Differnence
2x2	0.804	0.806	0.2
3x3	0.865	0.868	0.4
5x5	0.919	0.922	0.3
10x10	1.000	1.000	0.0
15x15	1.051	1.051	-0.1
22x22	1.105	1.104	-0.1
40x22	1.144	1.141	-0.3
57x22	1.159	1.155	-0.3

Below figure : a) shows PDD matching result for 10x10cm Field Size and b) shows profile comparison for 22x22 Field Size.

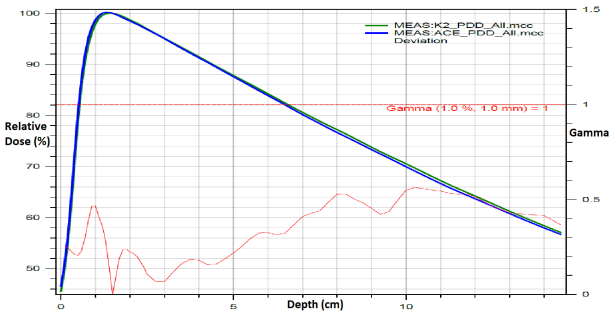

a) Gamma passing for 7FFF PDD for 10x10cm field size at SSD of 133.5cm at G0

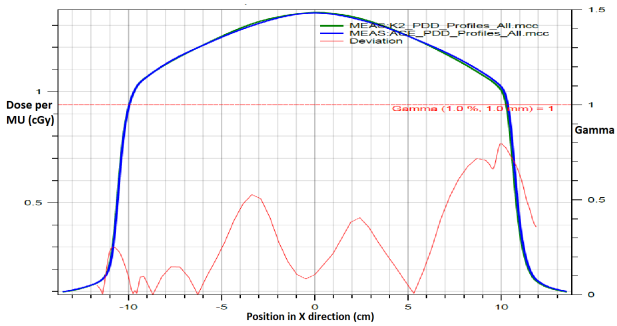

b) Gamma passing for 7FFF profile for 22x22cm field size at 5cm depth and SSD of 133.5cm at G0

Commissioning plan QAs were passed for gamma evaluation 3%/2mm above 95% and point dose difference within 2% for both machines.

Conclusion: Beam matching of Unity MR Linacs allows for the use of a single Radcalc model across both machines for the purpose of secondary MU checks. There are also benefits for routine QA, as the same tolerance values for beam flatness and symmetry can be used for both linacs. However, beam matching in this case does not allow for simple direct transfer of patients from one machine to another for several reasons. Cryostat characterisation, a gantry angle dependent output factor correction is unique to each machine and cannot be perfectly matchted. There are also safety checks built into the TPS, where the patient ID is tied to the machine ID, which would inhibit transfer of patients. Beam matching of Unity MR Linacs does have its benefits, though not to the same extent of a conventional linacs.

Acknowledgements: The authors acknowledge Jason Arts, Armia George and Elekta for providing the beam data for testing.

References: [1] A beam-matching concept for medical linear accelerators. David Sjöström, Ulf Bjelkengren, Wiviann Ottosson & Claus F. Behrens

AUS MRinRT

THE CURRENT STATUS OF MR-LINAC DOSIMETRY AUDITS: AN UPDATE FROM THE ACDS

Alex Burton[1,2], Rhonda Brown[1], Andrew Alves[1], Sabeena Beveridge[1]
[1] Australian Radiation Protection and Nuclear Safety Agency (ARPANSA), alex.burton@arpansa.gov.au
[2] RMIT University

Introduction: The Australian Clinical Dosimetry Service (ACDS) has conducted dosimetry audits of MR-linacs (MRLs) at four Australian radiation therapy facilities. 5 Level Ib (on-site reference dosimetry checks) and 3 Level III (end-to-end testing) audits have been performed since 2019.

Materials and Methods: ACDS auditors perform measurements on-site using ACDS' dosimetry equipment for both levels Ib and III audits. In Level 1b, the facility's 1D water tank is used to check the ouput under locally-defined reference conditions. An ARPANSA-calibrated PTW30013 Farmer-type ionisation chamber is used to measure beam output at Gantry 0˚ and Gantry 270˚/90˚, acknowledging the effect of helium levels in the cryostat and new reference recommendations from Elekta. A 10x10cm field size is used, and chamber readings are corrected for magnetic field-effect (k_b). Small field output factors are measured with a PTW60019 microDiamond aligned to the beam central axis as defined by MV imaging. IAEA TRS-483 corrections applied refer to nominal field sizes. Measurements made by the auditors are compared to the facility's own measurements under the same conditions and the tolerances applied are the same as for conventional linacs.

In Level III audits, the facility is sent a phantom in advance of the dosimetry audit for CT simulation and treatment planning. During this audit, dose is measured using seven IBA CC13 ionisation chambers for IMRT and compared to the adapted planned dosimetry. 3DCRT and IMRT plans are delivered during the audit with the phantom aligned within 1mm of the reference position. Adaptive workflows are tested for both positional shifts (Case 18), and a geometric deformations (Case 20). In both adaptive cases, the final planning target structure and dosimetry goals are identical to Case 7, hence, similar measurement results from all three cases are expected. Indicative outcomes are provided using the the tolerances applied for conventional linacs.

Results: All Level Ib audits have achieved a passing result within ACDS tolerances. The median (and range) dose difference is -0.5% (-0.9% to +0.5%) (see Fig 1). This is comparable to the mean (and standard deviation) dose difference on conventional linacs, which range from -0.3% to +0.1% (±0.6% to ±0.7%) across the available energies.

Two Level III audits returned indicative Out of Tolerance outcomes resulting in changes to clinical workflows being implemented prior to patient treatment. The median dose difference (and range) across all in-volume measurement points in passing Level III cases 7, 18 and 20 is +1.5% (-2.9% to +4.7%), +1.2% (-3.7% to +4.5%), and +0.8% (-3.5% to +4.2%). Overall, outcomes in these cases for MRLs are comparable to outcomes in Case 7 on conventional linacs, where mean (and standard deviation) dose differences across all points and energies range from -0.1% to +1.5% (±0.6% to ±2.1%) (see Fig 2).

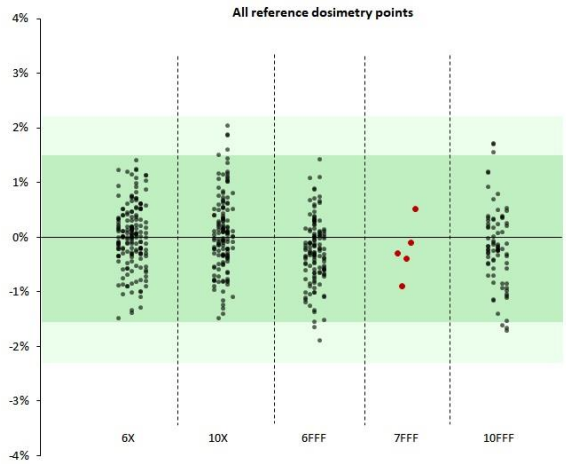

Figure 1. All Level Ib dose differences (conventional linacs in black, MRL in red). Action level = 1.4%, Tolerance = 2.1%)

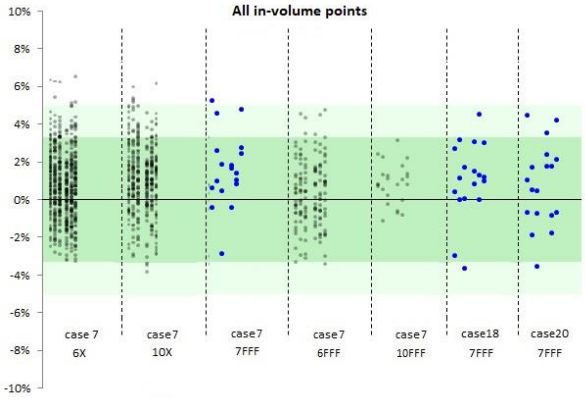

Figure 2. All Level III dose differences excluding indicative OT deliveries (conventional linacs in black, MRL in blue). Action level = 3.3%. Tolerance = 5% .

Conclusions: The presence of the magnetic field and unique workflows required to perform irraditions on the MRL present a challenge for both auditors and end-users in performing accurate dosimetry measurements. Level III end-to-end tests have successfully identified necessary changes to clinical workflows. The ACDS audits conducted thus far have indicated that MRL audit outcomes are comparable to conventional linacs.

AUS MRinRT

OPEN SOURCE TOOLKIT FOR QUANTIFACTION, REPORTING, AND CORRECTION OF GEOMETRIC DISTORTION IN MRI

Brendan Whelan[1, 2], Paul Liu[1, 2], Shanshan Shan[1, 2], David Waddington[1, 2], Bin Dong[1, 2], Michael Jameson[3,4], Paul Keall[1,2]

[1] ACRF Image-X Institute, School of Health Sciences, FMH, University of Sydney, brendan.whelan@sydney.edu.au
[2] Ingham Institute for Applied Medical Research, Liverpool NSW
[3] GenesisCare, Sydney, Australia
[4] Faculty of Medicine and Health, University of New South Wales, Australia

Introduction: Geometric distortion is present in MR images primarily due to gradient non-linearities and B_0 inhomogeneity. The use of MRI in radiotherapy requires that these distortions are quantified, and – if exceeding some threshold – corrected. Existing tools are generally expensive, black box, and not suitable for general purpose sequences.

In this work, we present an open-source and parametric distortion phantom which can be constructed for around 1000 AUD. We also present open-source software for the analysis of data acquired with this phantom, covering quantification of distortion, characterisation of magnetic fields via spherical harmonics, automated reporting via interactive html, and distortion correction in both the image and k-space domains (Figure 1).

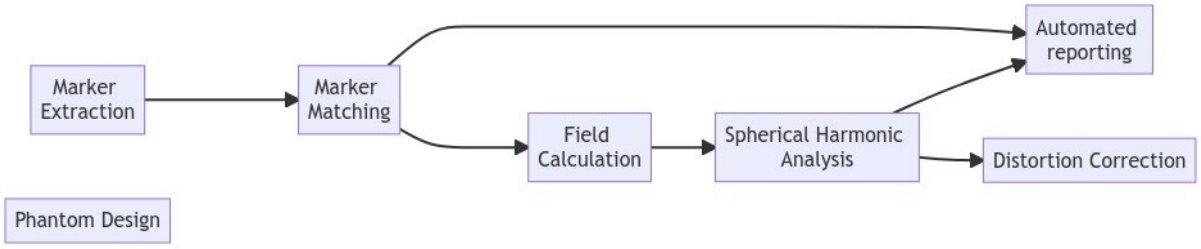

Figure 1: Modules/workflow of the open-source mri distortion toolkit

Materials and Methods: The distortion phantom was constructed from laser cut foam. 531 fish oil capsules were embedded in a spherical volume of 300 mm diameter. This phantom was imaged with CT to provide a zero-distortion ground truth, on the Australian MRI-Linac magnet, and an Elekta Unity system. For the Australian MRI-Linac, FLASH gradient echo images with a bandwidth of 260 Hz were acquired; for the Elekta Unity a 3D spin echo with a bandwidth of 740 Hz was used and vendor supplied distortion correction was applied. Our open-source software was used to extract the marker centroids, match the MR centroids to the CT, calculate the gradient encoding fields, and characterise these fields with spherical harmonics. Using the spherical harmonics, high resolution distortion maps were reconstructed, and the images corrected with two different distortion correction algorithms, image-domain, and k-space-domain.

Results: The open-source distortion phantom performed well, with markers clearly visible on all images. Our software extracted the correct number of markers from all three images and was able to generate 1:1 matches even in the presence of large distortions. For the Australian MRI-Linac, undistorted data over a DSV of 300 mm had mean distortion of **6.1±2 mm (max 10.7).** Following distortion correction, the total distortion on the Australian MRI-Linac was **0.8±0.4 (max 2.2 mm)**. For the Elekta Unity over the same DSV with vendor distortion correction, these values **0.6±0.2 mm (max 1.3 mm).** Both the k-space and image-domain distortion correction algorithms performed equally well at correcting distortion.

Conclusions: We have developed an open-source hardware/software solution for the measurement, characterisation, reporting, and correction of geometric distortion in MRI. We tested marker extraction/ distortion quantification for Elekta Unity and further tested distortion correction on MRI-Linac.

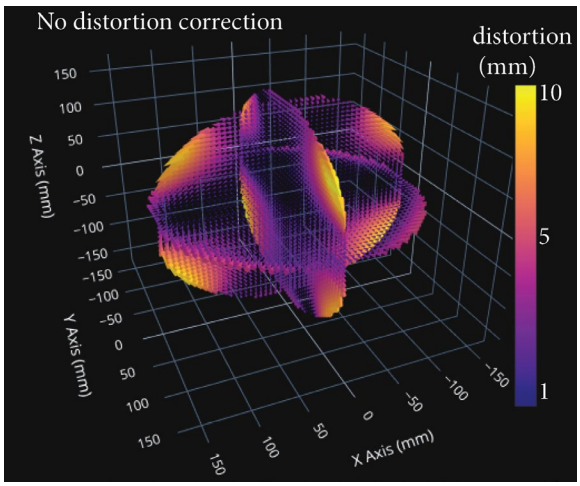

Figure 2: Distortion map on the Australian MRI-Linac magnet pre distortion correction.

AUS MRinRT

EARLY EXPERIENCE OF MR-GUIDED RADIOTHERAPY FOR BRAIN, HEAD AND NECK AND BREAST CANCERS

Sweet Ping Ng[1], Richard Khor[1], Michael Chao[1], Sandra Fisher[1], Felicity Height[1], Sarah Elliott[1], Drew Smith[1], Rob Behan[1], Kym Rykers[1], Nigel Anderson[1], Morikatsu Wada[1], Farshad Foroudi[1]

[1] Department of Radiation Oncology, E-mail address: sweetping.ng@austin.org.au

Introduction: The optimal utilisation of MR-guided radiotherapy in brain, head and neck, and breast cancer is currently being investigated. Here we aim to illustrate and evaluate the implementation and early experience of MR-guided radiotherapy for patients with brain, head and neck, and breast cancers at a single Australian public hospital.

Methods and Materials: Staff involved in the program underwent credentialing processes and training in MR safety and MR-Linac workflows. Site specific implementation considerations including patient immobilization, planning techniques and dosimetry differences due to the MR environment, image sequence testing and development of robust quality assurance (QA) methodologies were investigated during commissioning. Patients were enrolled on a Feasibility of Imaging and Radiation Treatment Delivery on the MR-Linac (FIRM) trial. The FIRM trial has 2 stages: Stage 1: end-to-end workflow testing, and Stage 2: Interventional treatment with standard of care fractionation. The Adapt to Position (ATP) online workflow was selected for all patients with brain, head and neck, and breast tumours. Workflow and different stages of treatment times were recorded.

Results: We have successfully treated 17 brain, 8 head and neck, and 6 breast patient on Phase 2 of the FIRM study since November 2021. More than 550 fractions were adapted, delivered and QA performed successfully. Prior to opening phase 2 of the study 2 brain patient, 3 head and neck, and 3 breast cancer patients were enrolled to Phase 1 of FIRM to facilitate and inform our development and site rollout process. 5 patients required replan between simulation and fraction zero due to disease progression. Four patients required replan during treatment course. The average treatment time for brain, head and neck, and breast cancer patients were 30, 42 and 40 minutes, respectively. Patient and QA pathways have been streamlined with a reduction in post treatment QA. Initial dosimetric/ dose delivery testing confirmed appropriate and acceptable dose delivery as predicted in treatment plan. Cumulative (treated) plans were compared to reference plans and showed relatively similar dosimetry, within acceptable uncertainties. The target dose coverage adjacent to the critical organs at risk was marginally improved in some treated plans compared to reference plan.

Conclusion: The use of MR-Linac ATP workflow is feasible and was established in patients with brain, head and neck, and breast cancers in an Australian setting.

AUS MRinRT

NEW KIDS ON THE BLOCK: WINNING AND LEARNING – THE PAH MRI SIM SERVICE

Tamara Barry[1], Clinton Gould[1]

[1] Princess Alexandra Hospital, Tamara.Barry@health.qld.gov.au

Introduction: February 2022 saw the culmination of years of work with the clinical start to a new dedicated MRI Simulation service in Radiation Oncology Princess Alexandra Hospital, Ipswich Road Campus. The simulator is conveniently located within the ROPAIR Radiation Oncology department, immediately adjacent to both existing CT simulators and the Gamma Knife Centre of Queensland.

Materials and Methods: From the outset, the MRI Simulator team were acutely aware of potential benefits to be gained from the service and were heavily focussed on maximising the clinical output with efficient, integrated workflows. Members from medical, radiography, radiation therapy, physics, nursing and administrative teams worked together to create a safe and functional MRI Suite, which subsequently allowed for the development of safe and efficient workflows. A Siemens Magnetom Vida 3T with XT gradients was installed and commissioned.

Results: During the first 6 months of operation, 472 patients were scanned. Of these, 220 were for the Gamma Knife Centre of Queensland and the remainder were for Linac-based Therapy Planning, predominately composed of brain, head and neck, abdomen, prostate and spine cases.

A significant clinical change has been the ability to confidently and accurately contour spinal cord and brachial plexus for head and neck patients, enabling improved dosimetry where planning target volumes are in close proximity to these organs. For the prostate cancer cohort, the MRI Sim team work to match bladder and bowel filling with the CT simulation scan, improving target delineation by providing near-perfect images with minimal translations and rotations of data sets required for registration. Workflow efficiency has been enhanced by upskilling Radiation Therapist staff to perform cannulations for contrast procedures. The unit continues to scan an average of 20 patients per week, including a small number of interhospital patients from ROPART Radiation Oncology, located at Mater Hospital, Raymond Terrace, South Brisbane. Practice improvements are continually evolving and implemented clinically.

The XT gradient is optimal for MR Therapy Planning, with this latest gradient technology allowing decreased scan times, excellent spatial resolution and minimal geometrical distortion. Our system has achieved a mean and maximum definition error of 0.3mm and 0.6mm respectively for a small grid phantom (for brain imaging) and the largest deviation detected at 2.8mm, 18 cm from the isocentre on the CIRS large distortion phantom[1].

Evaluation: The hybrid MR/RT imaging team and optimised MRI technology ensures examinations add valuable planning information, increasing RO confidence in margins, whilst reducing overall planning time, especially regarding time for image registration and contouring of targets and organs at risk. The ability to provide improved dosimetry has also been a significant benefit. Patients have indicated that they tolerate the MRI Sim process well, with the focus on optimal scan times to allow for various treatment positions. To date, usable planning images have been achieved for every single patient.

Additionally, the new MRI Simulator has allowed improved overall access to dedicated MRI planning for ROPAIR patients. The service is provided at no additional cost to the patients, who were previously paying out-of-pocket costs at nearby private providers.

Conclusion: There have been many benefits following the implementation of the MRI Simulator. Thus far the focus has been on clinical implementation; however, the team has commenced research projects and aim to accelerate this aspect of the MRI Simulator workload over the coming months.

References:

1. MR Sim Commissioning Executive Summary (P.Hanlon, C.Jones) Internal departmental document February 2022

AUS MRinRT

PROSTATE CANCER TREATMENT: VALIDATION OF AIR COILS AND SYNTETIC CT IMAGES FOR USE IN DOSE PLANNING

Yosef Al-Abasse[1], Tova Roman Rung[1], Peter Larsson[1], Dan Josefsson[1], Lena Lundkvist[2], Kristina Redelius[2], Kristina Hultman[2], Maria Medin[2], Maria Nilsson[2], Jan Rzepecki[2], Peter Lundberg[1,3]

[1] *Radiation Physics, and Department of Health, Medicine and Care, Linköping University, Linköping Sweden*

[2] Department of Oncology, and Department of Biomedical and Clinical Sciences, Linköping University, Linköping, Sweden

[3] *Center for Medical Imaging and Visualization (CMIV), Linköping University, Linköping, Sweden*

E-mail: Yosef.al-abasse@regionostgotland.se

Introduction: By generating a so called 'synthetic CT image' (sCT) directly from the MR images, the CT examination can be excluded and the uncertainties in the registration of MR- and CT-images are eliminated. Basing the radiation treatment process solely on MR images is called 'MRI-only' and is beneficial for the patient due to less CT examinations and more accurate target delineation.

One aim of this project was to develop and validate a software tool for MRI-only in a clinical workflow. A second aim was to investigate the difference between calculated radiation doses based on sCT and CT prostate images, respectively. We also aimed at examining if an AIR™ coil positioned directly on the skin of the patients would affect the body contours and the associated calculated doses.

Materials and Methods: Comparisons of radiation dose calculations based on sCT versus CT from 10 prostate patients were performed using the dose-volume histogram statistics in *Eclipse* dose planning system (Varian Medical Inc.). The sCT-images were generated from T2W images using locally installed software called *MRI Planner* (Spectronic Medical AB). A method for calculating the 'gamma index' was implemented in *MICE Toolkit, aka HERO* (NonpiMedical). For the evaluation of the AIR coil (GE Medical) three different similarity comparison methods were used, Hausdorff distance, Dice similarity coefficient (DSC) and Surface Dice similarity coefficient (SDSC).

Results: Fig. 1 shows that nine out of ten gamma indexes had values above 96.5% for 2%/2 mm. Fig. 2 shows a box diagram of mean absorbed dose deviation for PTV, CTV, bladder, rectum and femoral heads. CTV had the largest difference, but still within 2,5%. In general the doses calculated on sCT were higher than those calculated on CT.

The SDSC values for the skin contour using AIR coil are shown in Fig. 3. The maximum Hausdorff distances were within 5 mm and the impact on the dose calculation were negligible, less than 1% for the patient with the largest deviation (no 5 in Fig.3).

Conclusions: The main purpose of this project was to develop a software tool to validate an MRI-only clinical workflow, and to investigate if the radiation dose calculation based on sCT data differed from calculations based on actual CT data. An implementation for gamma analysis in MICE toolkit has been proposed. The gamma index analysis showed good agreement between sCT and CT for the included prostate patients. Moreover, a software tool to evaluate the AIR Coil effect on the skin contour has been developed.

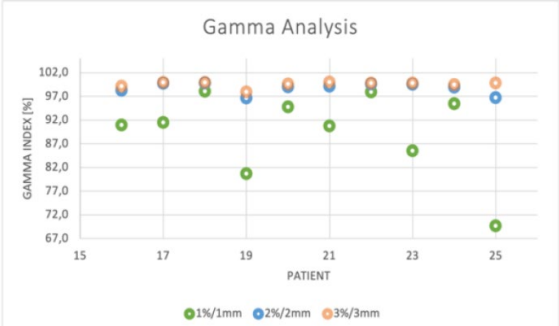

Figure 1. Gamma analysis for criterion 1%/1 mm(green), 2%/2 mm(blue) and 3%/3 mm(orange).

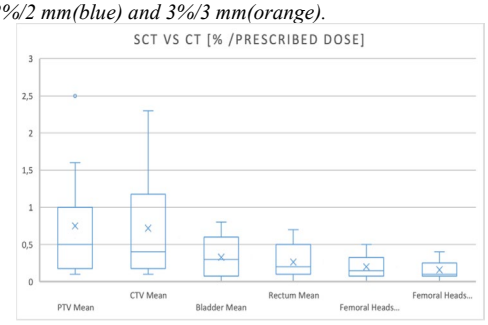

Figure 2. Deviations between sCT and CT mean doses (percentage of prescribed dose) for planning target volume (PTV), clinical target volume (CTV), femoral heads, bladder and rectum.

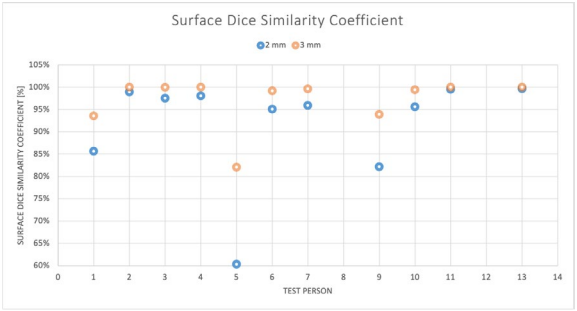

Figure 3. The Surface Dice Similarity Coefficient,SDSC, [%] for tolerance criterion 2 mm and 3 mm for the skin contour.

References:

1. Clinical feasibility of a prostate MRI-only radiotherapy treatment workflow and investigation of acceptance criteria (E. Persson et. Al), *Radiation oncology. 77, Vol. 15, 1 (2020).*

AUS MRinRT

SUSCEPTIBILITY BASED DETECTION OF GOLD SEED FIDCUCIAL MARKERS FOR MRI ONLY TREAMENT PLANNING OF PROSTATE CANCER

Jonathan Goodwin[1, 2], Ashley Stewart[3,4], Matthew Richardson[1], Kieran O'Brien[4,5], Steffen Bollmann[3,4]

[1] Calvary Mater Newcastle, Department of Radiation Oncology, Jonathan.Goodwin@calvarymater.org.au
[2] University of Newcastle, School of Information and Physical Sciences (SIPS)
[3] School of Information Technology and Electrical Engineering, The University of Queensland
[4] ARC Training Centre for Innovation in Biomedical Imaging Technology, The University of Queensland
[5] Siemens Healthcare Pty Ltd, Brisbane

Introduction: One of the current constraints of MRI only workflows for radiation planning and daily image guidance for prostate cancer therapy, is the ambiguity in identifying gold seed fiducial markers in the presence of prostate calcifications. Similar diamagnetic properties and size can result in visual uncertainty in T1 weighted images, and poor conspicuity in T2 weighted images. With accurate identification of gold seeds critical for consistent patient positioning during treatment, we investigated the use of a quantitative susceptibility mapping post processing pipeline (QSMxT) (1) for improving identification of gold seed markers in the presence of prostate calcifications.

Materials and Methods: 10 patients undergoing MRI in addition to CT simulation for prostate treatment planning, were scanned with an in-phase multi echo T2*, 3D VIBE acquisition with 1.4mm isotropic resolution, to generate phase and magnitude images for post processing. QSMxT v1.1.13 (2) was used for offline processing. Phase-based masking was performed with a threshold of 25% phase matching quality. A two-pass reconstruction was performed with all echoes reconstructed independently and combined by weighted averaging. Susceptibility values across manually segmented calcifications, gold seeds, and prostate tissue were assessed. Segmented regions confirmed by the patient CT were then overlayed onto a magnitude image to demonstrate the potential workflow with a QSM based image processing pipeline.

Results: Group level analysis of susceptibility values measured from manually segmented voxels in gold seed, prostate tissue and calcification, demonstrated similar susceptibility values for most voxels in gold seed and calcification (Fig. 1). Voxels located central to the segmented gold seed were found to have notably lower susceptibility than the equivalent central voxels extracted from calcification. Using an automated mask clean up, we were able to identify susceptibility values two standard deviations below the mean, and overlay these regions onto a magnitude image for clear gold seed identification (Fig. 2).

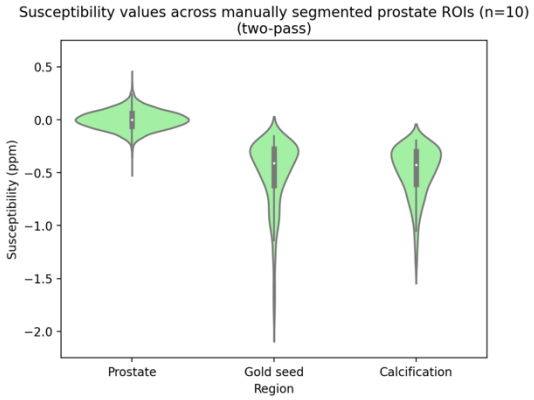

Figure 1. Voxel level analysis of susceptibility across 10 prostate patients

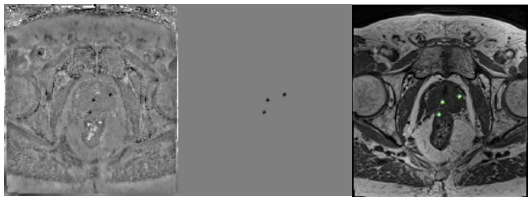

Figure 2. QSM image (left) with susceptibility based seed masking (centre) and magnitude image overlay (right)

Conclusions: While susceptibility values measured in fiducial gold seeds and prostate calcification largely overlap, we observed a greater spread of values in gold seed, with voxels central to the gold seed displaying larger negative susceptibility than calcifications. We are currently developing a deep learning model to further improve the accuracy of this technique, using additional information such as seed shape.

References:

1. Stewart, Ashley Wilton, Simon Daniel Robinson, Kieran O'Brien, Jin Jin, Georg Widhalm, Gilbert Hangel, Angela Walls, et al. "QSMxT: Robust Masking and Artifact Reduction for Quantitative Susceptibility Mapping." Magnetic Resonance in Medicine 87, no. 3 (2022): 1289–1300. https://doi.org/10.1002/mrm.29048.
2. github.com/QSMxT/QSMxT
3. S. Agostinelli et al., *Nucl. Instrum. Meth. Phys. Res*. A **506**, 250-303 (2003).

AUS MRinRT

MRI-ONLY RADIATION THERAPY FOR PROSTATE CANCER: EXPLORATION OF THE IMPACT OF SYNTHETIC-CT UNCERTAINTIES ON DOSE CALCULATION

Hilda Chourak[1,2], Dowling Jason[1], Peter Greer[3,4], Anais Barateau[2], Safaa Tahri[2], Renaud de Crevoisier[2], Jean-Claude Nunes[2], Oscar Acosta[2]

[1] Australian eHealth Research Centre, CSIRO Health and Biosecurity, Brisbane, QLD, Australia, hilda.chourak@csiro.au
[2] Univ Rennes, CLCC Eugène Marquis, INSERM, LTSI - UMR 1099, Rennes, France
[3] School of Mathematical and Physical Sciences, University of Newcastle, Newcastle, NSW, Australia
[4] Department of Radiation Oncology, Calvary Mater Newcastle Hospital, Newcastle, NSW, Australia

Introduction: Synthetic-Computed Tomography (sCT) generation is a critical component of MRI-only radiation therapy workflows. Quality of the sCT is currently assessed by comparing its Hounsfield Units (HU) to their ground truth[1], resulting in global or organ-wise values, but local error may have an impact on treatment delivery and might not be highlighted with global scores. The aim of this study is to investigate the correlation between local errors (in terms of HU number, volume and distance to the prostate) and dose delivered at the isocenter. This is the first step to the definition of thresholds of acceptability of HU errors in sCT for safe MRI-only radiation therapy practice.

Method: Spearman correlation coefficient (SCC) between HU errors and dose were computed. A SCC close to -1 or 1 denotes a strong correlation, while a SCC close to 0 illustrate a weak relationship.

A sensitivity analysis (SA) was then performed, following the Morris screening method[2]. A SA is designed to quantify the effect of parameters on the output; in this study the effect of intensity, size and distance of a volume of error on dose calculation. This aimed to define which parameter has the highest impact on the dose. It calculates the mean $\mu*$ and the standard deviation σ of the absolute values[3] of the elementary effects of the parameters. Low $\mu*$ and σ indicate an insignificant factor and high $\mu*$ and σ stand for significant impact, and a non-linear effect on the output or a significant interaction with other factors.

Data: *Reference CT*: 39 patients with localised prostate cancer aged 58 to 78 years were used in this study. For each patient, a CT scan was acquired on a GE LightSpeed RT or a Toshiba Aquilion, (256 x 256 x 128 matrix with a voxel size of 1.17 mm x 1.17 mm x 2.5 mm or 2.0 mm).

Modified CT: To simulate local HU error, an artefact of 50mm centered on the isocenter was added to the 39 planning CTs. The following parameters were assessed:

- HU variation (from -400HU to +400HU, with a step of 25 HU)
- Distance to the isocenter (from 0 to 100 mm, step of 10mm , with an error fixed at 200HU). This displacement followed a beam axis.
- Size (diameter from 50mm to 2mm, error of 200HU, located at 30mm from the isocenter)

2147 images were thus used to compute the SCC.

Morris screening: 3692 images were generated. The features values and results presented Fig1 were obtained using the sensitivity R package. (https://cran.r-project.org/web/packages/sensitivity/index.html)

Dose planning: Intensity-modulated radiation therapy (IMRT) was planned on reference CT images using a dose grid resolution of 3 mm (39 fractions, 2 Gy by fraction) with MatRad, an open-source software for radiation treatment planning developed for research purposes. The beam parameters used to compute the dose on the reference CT were used to calculate the dose on the modified CT.

Results: With an SCC of 0.99, and high $\mu*$ and σ (Fig1), the error in term of HU is the most deterministic factor for dose calculation, following by the the size and distance (Fig1) (SCC of 0.52 and -0.74 respectively).

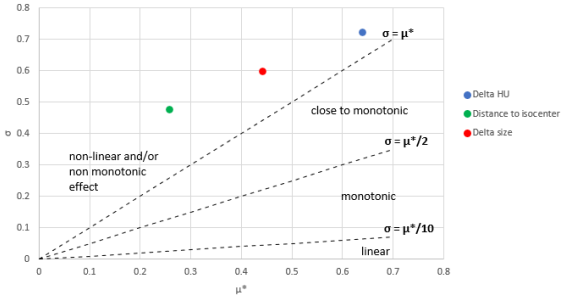

Figure 1.Morris screening results, identifying the most influential factor. The 3 factors (HU in blue, distance in green and size in red) has a non-linear and/or non-monotonic effect on the dose.

Conclusion: For sCT, special attention should be paid to the presence of gas in the rectum: the sCT error can reach 1000 HU while being located close to the prostate. This can lead to a severe impact on the dose. This confirms the necessity to locally assess each generated sCT prior to its used in a clinical workflow.

References:

1. Deep learning methods to generate synthetic CT from MRI in radiotherapy: A literature review (M. Boulanger et al), *Phys Medica*. **89**:265-281(2021).
2. Factorial Sampling Plans for Preliminary Computational Experiments (MD. Morris). *Technometrics*. **33**(2):161-174 (1991).
3. Enhancing the Morris method (Campolongo F etal.). http://library.lanl.gov/

AUS MRinRT

THE NINJA MRI-ONLY IMPLEMENTATION SUBSTUDY-PRELIMINARY RESULTS

Peter Greer[1,2], Jason Dowling[3], Jae Choi[2], Parnesh Raniga[3], Mark Sidholm[4], Tony Young[4], Dean Wilkinson[5], Laura O'Connor[1,2], Kate Skehan[1], Lee Wilton[1], Perry Hunter[1], Jarad Martin[1,2]

[1] Calvary Mater Newcastle Hospital, Newcastle, Australia, peter.greer@newcastle.edu.au
[2] University of Newcastle, Newcastle, Australia
[3] CSIRO Australian e-Health Research Centre, Herston, Queensland, Australia
[4] Liverpool Hospital, Liverpool, Australia
[5] Illawarra Cancer Centre, Wollongong, Australia

Introduction: The NINJA TROG18.01 clinical trial is comparing two schedules of stereotactic prostate treatments throughout Australia and New Zealand. A technical sub-study was incorporated to the trial to implement MRI-only treatment workflow in a multi-centre setting.

Methods: A comprehensive implementation and evaluation guide for MRI-only was developed as part of the trial RT QA guidelines. A staged three-phase implementation was developed:1) conventional treatment workflow with additional synthetic CT (sCT) evaluation against conventional CT dose (5 patients); 2) MRI-only workflow with quality assurance CT scan acquired for comparison of sCT dose to QA-CT dose (10 patients); 3) fully MRI-only workflow with QA of sCT dose using MRI-based bulk anatomical density (BAD) map calculation (1) shown in Figure 1. Isocentre doses ($\Delta Diso$) were compared along with 3D Gamma evaluation with 3%/3mm, 2%/2mm, 2%/2mm and 1%/1mm criteria. PTV D98, D95, D50 and D2) and Rectum D50 were compared.

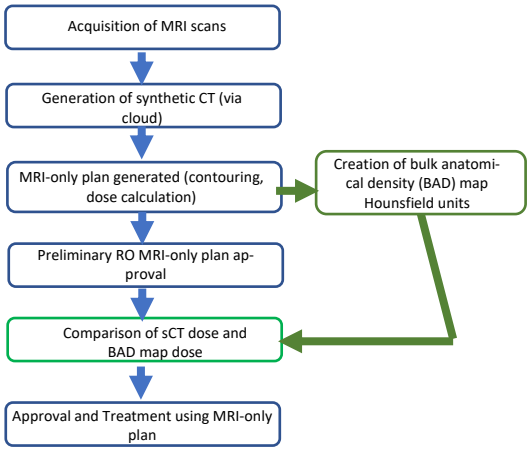

Figure 1. Phase 3 Full NINJA workflow for the MRI-only study

Results: To date four centres are participating and two further centres are in development. At least 56 patients have received MRI-only workflow at three centres (Phase 3). While all patients had differences within 2.5%, only one patient had greater than 2% difference (-2.2%) between the sCT and BAD map isocentre dose calculations. Overall, the mean ±1 SD $\Delta Diso$ between the scans was -0.95 ± 0.56%. All PTV dose differences were within 2.5% and the greatest difference was -2.3% for D2. The mean difference in Rectum D50 was -0.04 ± 0.62% and only one patient had greater than 2% difference (2.03%) (Figure 2). Overall, the mean gamma pass rates at 3%/3mm, 2%/2mm, 2%/1mm and 1%/1mm criteria were 100.0 ± 0.1%, 100.0 ± 0.1%, 99.9 ± 0.1% and 96.8 ± 2.5% respectively (Figure 3).

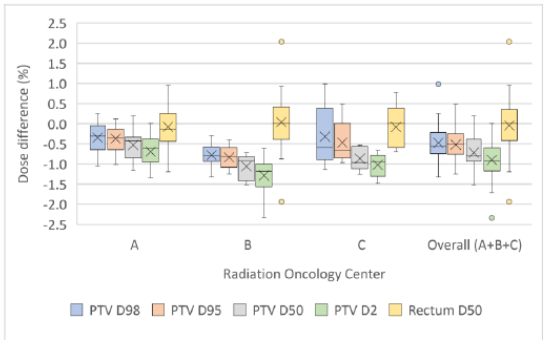

Figure 2. DVH metric differences between sCT dose and BAD dose

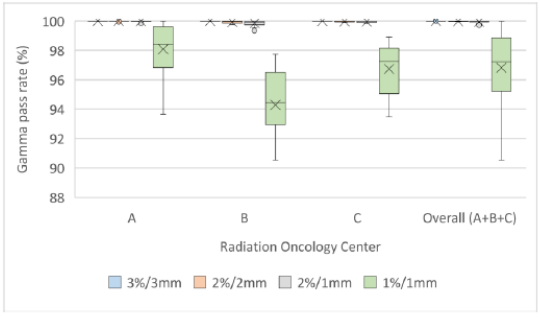

Figure 3. Gamma metric differences between sCT dose and BAD dose

Conclusion: For MRI-only workflows sCT dose calculations were in close agreement to optimised bulk density calculations. MRI-only prostate workflow can be implemented in a multi-centre setting with appropriate quality assurance to validate sCT dose calculations.

References:

1. Bulk anatomical density based dose calculation for patient-specific quality assurance of MRI-only prostate radiotherapy (J. Choi et al.), *Frontiers in Oncology*. **9**, (2016).

AUS MRinRT

COMPARISON OF POPULAR SCT GENERATION METHODS FOR MRI ONLY DEFINITIVE PELVIC RADIOTHERAPY

Laura M O'Connor[1,2], Jae Hyuk Choi[1,3], Jason A Dowling[4], Helen Warren-Forward[2], Jarad Martin[1], Peter Greer[1, 3]
Correspondance:Laura.O'Connor@calvarymater.org.au

[1] Calvary Mater Hospital, Newcastle, NSW, Australia, E-mail address
[2] School Health Sciences, University of Newcastle, Callaghan, NSW, Australia
[3] School of Mathematical and Physical Sciences, University of Newcastle, Newcastle, NSW, Australia
[4] CSIRO Australian E-Health Research Centre, Herston, QLD, Australia

Introduction: To move away from the conventional use of CT in radiation therapy treatment planning, a synthetic CT (sCT) is created from the MRI, to facilitate MRI based treatment planning. The sCT is an estimation of the electron densities of the tissues in the body, which allows for dose calculation in the radiation therapy treatment planning systems. Several method of sCT creation have been reported on in the literature, which can be summarised into essentially four popular methods; bulk density assignment, tissue class segmentation, atlas based and computer learning [1]. Each of these methods have their advantages and trade-offs in their accuracy, time and ease of conversion. sCT methods have been predominantly developed to date for prostate and brain treatment sites. Reviews of sCT generation methods in the literature have compared the commonly used techniques for brain and limited pelvic sites, not on the same cohort of patients.

This work applied four of the most popular methods of sCT creation for MRI only radiation therapy treatment planning for male and female rectum, anal canal, cervix and endometrium neoplasms. The sCT methods are validated against conventional CT, in regards to Hounsfield Unit estimation and plan dosimetry.

Materials and Methods: Paired MRI and CT scans of 40 patients (20 male and 20 female), treated for a range of pelvic malignancies was used for sCT generation and validation. Bulk density assignment, tissue class segmentation, hybrid atlas and deep learning sCT generation methods were applied to all 40 patients. Each sCT creation method used was based on successfully applied methods in the literature [2-4]. Dosimetric accuracy assessed by dose difference at ICRU reference point, DVH parameters and 3D gamma dose comparison. Hounsfield Unit estimation assessed by mean error and men absolute error in HU value between each sCT and CT. Statistical significance was determined using a Mann-Whitney U-test with a significance level of 0.05.

Results: The median percentage dose difference between the CT and sCT was <1.0% for all sCT methods (Table 1). The highest agreement in median percentage dose difference was for the deep learning method, and the lowest agreement was for the bulk density assignment. For the bulk density sCT, there was a statistically significant difference in the median percentage dose difference at the ICRU reference point between the male and female cohort (p=0.002) of -0.89% (interquartile range (IQR) of -1.15, -0.72), and -0.09% (IQR of -0.83, 0.09) respectively. The mean 3D gamma dose agreement at 3%/2mm amongst all sCT methods was 99.8%. The highest agreement at 1%/1mm was 97.3% for the deep learning method and lowest was 93.6% for the bulk density method.

Conclusion: Bulk density assignment, tissue class segmentation, hybrid-atlas and deep learning methods of sCT generation all result in similarly high dosimetric agreement for MRI only planning of male and female cancers of the rectum, anal canal, cervix and endometrium. Choice of sCT generation technique can be guided by department resources available and image guidance considerations, with minimal impact on dosimetric accuracy.

Table 1 ICRU median percentage dose difference and median DVH dose difference by sCT method

	ICRU %DD			DVH %DD	
	Median	**IQR**	**p-value**	**Median**	**IQR**
Deep learning	-0.03	-0.31, 0.13	1.00	0.18	-0.05, 0.40
Hybrid-Atlas	-0.30	-0.57, -0.02	0.82	-0.27	-0.77, 0.12
Tissue Class	-0.48	-0.85, -0.28	0.68	-0.48	-0.66, 0.11
Bulk Density	-0.73	-1.01, -0.10	0.64	-0.33	-0.67, 0.185

References:

1. Johnstone, E., et al., Systematic Review of Synthetic Computed Tomography Generation Methodologies for Use in Magnetic Resonance Imaging-Only Radiation Therapy. *Int J Radiat Oncol Biol Phys*. **100**(1), 199-217 (2018)
2. Choi, J.H., et al., Bulk Anatomical Density Based Dose Calculation for Patient-Specific Quality Assurance of MRI-Only Prostate Radiotherapy. *Front Oncol.* **9**, 997 (2019).
3. Dowling, J.A., et al., Automatic Substitute Computed Tomography Generation and Contouring for Magnetic Resonance Imaging (MRI)-Alone External Beam Radiation Therapy From Standard MRI Sequences. *Int J Radiat Oncol Biol Phys*. **93**(5), 1144-53 (2015).
4. Maspero, M., et al., Deep learning-based synthetic CT generation for paediatric brain MRonly photon and proton radiotherapy. *Radiotherapy and Oncology*. **153,** 197–204 (2020).

AUS MRinRT

TOWARDS SIMULATION-FREE MR-LINAC TREATMENT PLANNING

Urszula Jelen [1], Madeline Carr [1], Maddison Picton [1] , Vikneswary Batumalai [1,2], David Crawford [1], Valery Peng [1], Tania Twentyman [1], Jeremy de Leon [1], Michael Jameson [1,2]

[1] GenesisCare, New South Wales, Australia, Urszula.jelen@genesiscare.com
[2] School of Clinical Medicine, Medicine and Health, University of New South Wales, Australia

Introduction: In the current Elekta Unity MR-Linac (MRL) radiotherapy workflow, a simulation-CT provides reference anatomical and voxelised electron density (ED) information for treatment planning. Each contoured organ is then assigned an average bulk-density value, which is later used to assign densities to structures contoured on the daily MR scans (Figure 1). An MRL provides opportunities to explore novel MR-only workflows [1] and accurate ED estimates are required without simulation-CT [2-4]. This MRL-based study investigates the dosimetric impact of using an individual- and population-based bulk-density override.

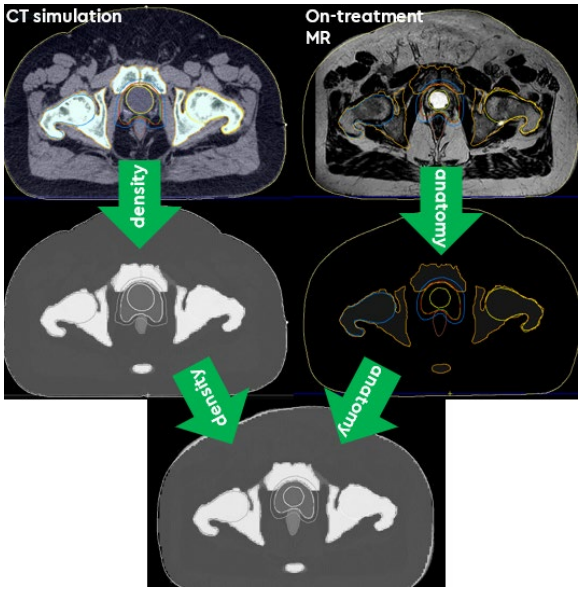

Figure 1. In a standard MRL adaptive workflow, CT simulation data is used to generate the required ED information for each structure. These EDs are then assigned to the contours of the patients' anatomy, of which are created from the daily on-treatment MR-scan.

Materials and Methods: Datasets of 74 male-pelvis patients treated on the St Vincent's Unity MRL were analysed retrospectively. Their individual-EDs were extracted and the population value was calculated for several organs (bladder, rectum, sigmoid colon, patient outline, bone, femurs and GTV). 10 patients with outlying organ ED values had their reference plans recalculated to find an Individual-ED Dose (IndD) and Population-ED Dose (PopD). Percentage differences in mean dose were calculated between these plans and the voxelised simulation-CT Dose (sCTD).

Results: The individual-EDs of all selected patients remained within 5% of the population average for solid soft tissue organs, and within 8% for bony structures. The largest residual variation was observed for hollow organs (rectum, sigmoid) due to variable amounts of gas included in the contour. The differences in maximum and mean doses, and also in minimum doses for target structures only, between sCTD and IndD/PopD plans remained $\leq \pm 1.9\%$, $\pm 2.9\%$ and $\pm 3.7\%$ for soft tissue organs, target organs, and bony structures, respectively. The average of the 10 patients mean dose differences between these noted plans is presented in Figure 2. No clear correlation was observed to occur between structures with larger differences in their individual-ED values compared to the population, and %differences in dose indices between the 3 calculated plans.

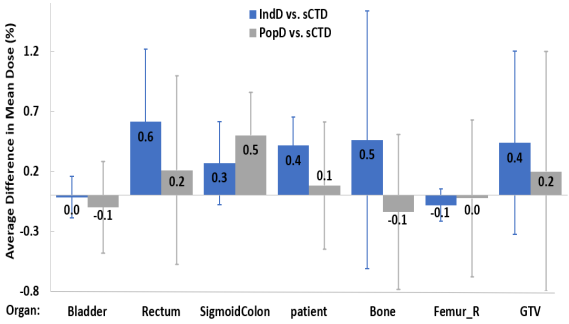

Figure 2. The average of all 10 patients' percentage difference in mean dose; when calculated between both sCTD and IndD, and sCTD and PopD. The average dose difference calculated for each organ is presented, with error bars representing the standard deviation found between all patients.

Conclusions: Given the comparable dose differences observed between PopD and IndD (current clinical method), using a population-based ED was deemed feasible in an MRL workflow.

References:

1. Advances in MRI-guided precision radiotherapy (C. Lui et al.), *Precision Radiation Oncology*. **6**, 75-84 (2022).
2. Comparison of bulk electron density and voxel-based electron density treatment planning (A. Karotki et al.), *Journal of Applied Clinical Medical Physics*. **12**, 97-104 (2011).
3. Towards abdominal MRI-based treatment planning using population-based Hounsfield units for bulk density assignment, (SH. Hsu et al.), *Physics in medicine and biology*. **63(15)**, 155003 (2018).
4. MRI-based IMRT planning for MR-linac: comparison between CT- and MRI-based plans for pancreatic and prostate cancers (P. Prior et al.), *Physics in medicine and biology*. **61(10)**, 3819-3842 (2016).

AUS MRinRT